The Non-canonical Function and Regulation of TBK1 in the Cell Cycle

Swagatika Paul

Dissertation submitted to the faculty of the Virginia Polytechnic Institute and State University in partial fulfillment of the requirements for the degree of

Doctor of Philosophy
In
Biomedical and Veterinary Sciences

Alicia M. Pickrell, Chair
Michelle H. Theus, Co-Chair
Daniela Cimini
Paul Morton

August 31st, 2023
Blacksburg, Virginia

Keywords: Mitosis, cell cycle, Tank Binding Kinase1, NAK Associated Protein1

The Non-canonical Function and Regulation of TBK1 in the Cell Cycle

Swagatika Paul

Abstract

Protein kinases play essential roles in orchestrating almost every step during mitosis. Aberrant kinase activity often leads to errors in the cell cycle progression which consequently becomes the underlying cause for developmental defects or abnormal cell proliferation leading to cancer. Tank Binding Kinase 1 (TBK1) is overexpressed in certain cancer types and is activated on the centrosomes during mitosis. Loss of TBK1 impairs cell division resulting in growth defects and the accumulation of multinucleated cells. Therefore, proper activation and localization of TBK1 are essential for mitotic progression. Yet, the upstream regulation of TBK1 and the function of activated TBK1 on the centrosomes is unknown. Also, the cause and consequences of overexpression of TBK1 in cancers remain to be explored. Activation of TBK1 depends on its binding to an adaptor protein which induces a conformational change leading to trans autophoshorylation on serine 172 of its kinase domain. We identified that an established innate immune response protein, NAK Associated Protein1 (NAP1/AZI2), is the adaptor required for binding and activating TBK1 during mitosis. Loss of either NAP1 or TBK1 results in the accumulation of binucleated and multinucleated cells, possibly due to several mitotic and cytokinetic defects seen in these knockout (KO) cells. We establish NAP1 as a cell cycle regulated protein which colocalizes with activated TBK1 on the centrosomes during mitosis. Furthermore, by performing an unbiased quantitative phosphoproteomics analysis during mitosis, the substrates discovered reveal that TBK1 also regulates other known cell cycle regulating kinases such as Aurora A and Aurora B. TBK1 is also an established autophagy protein and since the autophagy machinery is often impaired or remodeled to facilitate rapid cell division, we evaluated the underlying connection between TBK1 activation and autophagy. The data shows that cells lacking the essential autophagy proteins FIP200 or ATG9A exhibit overactivation and mislocalization of TBK1. By using both genetic and pharmacological inhibition of autophagy processes, we found that impaired autophagy leads to a significantly higher number of micronuclei – a hallmark for tumorigenesis that correlates with defects in mitosis and cytokinesis. Taken together our work has uncovered a novel function for the NAP1-TBK1 complex during mitosis and establishes that overactivation and mislocalization of TBK1 is a direct consequence of impaired autophagy which causes micronuclei formation.

The Non-canonical Function and Regulation of TBK1 in the Cell Cycle

Swagatika Paul

General Audience Abstract

Defective cell division is the underlying cause for many human health maladies such as birth defects and cancer. Investigation into the proteins that are abnormally expressed in cancer can help us identify their physiological roles in regulating the cell cycle. Tank Binding Kinase 1 (TBK1) is often overexpressed in several types of cancer such as glioblastomas, breast, and lung cancers. It has also been extensively studied in the process of removing damaged cytosolic components from cells called autophagy. During cancer progression, cells often hijack the autophagy machinery to their advantage for abnormal cell proliferation. However, we do not completely understand the role of TBK1 in cancer pathogenesis or during normal cell division.

Each cell duplicates its genomic contents and divides its organelles and cytosolic components during cell division. Centrosomes organize microtubules to attach to the duplicated genomic material to equally segregate the DNA between two daughter cells. Previous studies have shown that TBK1 is active on the centrosomes during mitosis, and the loss of TBK1 leads to reduced cell proliferation. However, the function of TBK1 and what regulates its activation on the centrosomes are unknown. Using a combination of genetic, biochemical, and molecular biology techniques, we found that an immune response protein Nak Associated Protein 1 (NAP1/AZI2) binds to TBK1 and activates it on the centrosomes during cell division. Furthermore, our study demonstrates that the loss of either NAP1 or TBK1 exhibits a multitude of different types of defects in the process of cell division. We further identified TBK1 substrates in a phosphoproteomic screen indicating that TBK1 regulates the activity of other major cell division kinases. We show that defects in autophagy machinery result in the mislocalization and overactivation of TBK1 resulting in defects during chromosome segregation, and in the formation of micronuclei. Together our study shows that an established immune response protein NAP1 regulates the function of TBK1 during cell division and there exists a connection between TBK1 activity and disrupted autophagy.

Dedication

To my parents, for their unconditional love, support, and encouragement all along!!

Acknowledgments

I would like to thank my entire family for their endless love and support throughout my career. I would not have reached so far without the immense love from my grandparents, the encouragement from my parents and the guidance from my brother. Thank you, Aja, Aai, Maa, and Papa for always inspiring me to follow my dreams and showing me the importance of hard work through your lives. Bhai, I would not have pursued my career in life sciences without your life altering suggestion. You are the reason that I am enjoying my career in life science. A special thank you to my husband, Sandeep, who has been the tower of strength throughout my grad school. I do not think I can express just how much you have enriched my life with your solution-oriented approach and helped me grow as a researcher. Papa and Sandeep, I appreciate your patience, and enthusiasm to understand my research projects even though you have different backgrounds than mine. Riddhi, you have come to my life as a blessing. You have no idea about your contribution to your Paa's mental health through your quirks and fascinating questions. Thanks to all my friends and especially Pratikshya, for our long random conversations that have made it easier for me to sustain my life as a graduate student in a different country so far away from home.

My sincere gratitude to my Ph.D. advisor Dr. Alicia Pickrell, whose passion for scientific research and invaluable guidance has made this project possible. Thank you so much for believing in me and always encouraging me to follow my scientific goals. I am honored that you have trained me not only to perform experiments but also to design scientific projects and think like a scientist. I have been immensely influenced by your optimism and work ethics, which I am sure is going to help me further my scientific career.

I would like to thank all my committee members, Dr. Michelle Theus, Dr. Daniela Cimini, Dr. Paul Morton, who have guided me throughout this project and helped me grow as a researcher. I am grateful for all your suggestions and constructive criticisms that have improved not only my research project but also my scientific writing skills. A special thank you to Dr. Cimini for guiding me with the scientific protocols and experimentations to improve my project. This research would not have shaped the way it has without your expert opinion and suggestions in the field of mitosis.

I will forever be grateful to all my teachers since childhood who have trained me to come so far in my career. Thank you all my Guruji and Guruma at Saraswati Shishu Vidya Mandir for enriching my life with all the fundamental values and teachings that have shaped my thought process to take better decisions in life. A special thank you to my master's mentor Dr. Bibha Choudhary to whom I owe most of my technical and experimental skills to become a researcher in the field of life sciences.

I thank all my past and present lab mates who have made my Ph.D. life easier with their help and cooperation. I am grateful to the previous undergraduate intern Leila Zavar, and our lab technician Nicole DeFoor who helped me all throughout this project. Thank you, Colin, Sammi, and Sahitya, for keeping the lab environment lively and filled with fun. I am also grateful to Dr. Cimini's wonderful graduate student Mathew Bloomfield for his help in setting up experiments and guidance in analyzing data for my project.

I appreciate the help from all staff in Life Science 1, the BMVS graduate program, and the School of Neuroscience for their help and support in the administrative work. Annette, you have been amazing in helping all the researchers in Life Science 1 with your management skills.

Contents

List of Figures

Chapter 1

Introduction

Introduction

Mitosis is a tightly coordinated, dynamic, and the shortest phase of the cell cycle. While the mitotic phase only persists for a brief amount of time, dramatic biochemical and structural events take place in a timely manner to ensure successful transition from one mitotic stage to another. Although many proteins are well characterized within the various mitotic signaling cascades, several other proteins involved in different cellular processes have been identified to be playing key roles in mitosis. Interestingly, most of these newly characterized multifunctional proteins act at the crossroads of mitosis and immune signaling pathways (Zhong et al. 2020; Zhang et al. 2013; Zeng and Yin 2023; Huang, Wan, et al. 2021). Entry into mitosis is marked by the highest number of protein phosphorylation events catalyzed by several protein kinases which regulate the transition from one mitotic phase to another (Dephoure et al. 2008; Olsen et al. 2010). Recently, an established innate immune kinase, Tank Binding Kinase 1 (TBK1), has been identified to be activated on the centrosomes during mitosis (Sarraf et al. 2019; Pillai et al. 2015). While overexpression of TBK1 is related to several types of cancer progression (Runde et al. 2022; Revach, Liu, and Jenkins 2020), its functional loss or mislocalization impairs mitosis (Sarraf et al. 2019; Onorati et al. 2016; Kodani et al. 2022). The goal of this work was to understand 1) the upstream mechanisms that determine the activation and localization pattern of TBK1 during mitosis, and 2) the mechanism by which TBK1 modulates mitotic progression.

TBK1 is an IKK family serine/threonine kinase whose role in various innate immune signaling pathways have been well established (Goncalves et al. 2011; Ikeda et al. 2007; Sharma et al. 2003; Tojima et al. 2000; Pomerantz and Baltimore 1999). TBK1 also participates in the process of mitophagy (Ravenhill et al. 2019; Boyle, Ravenhill, and Randow 2019; Lazarou et al. 2015; Heo et al. 2015) and xenophagy (Richter et al. 2016; Thurston et al. 2009). Recently, it has become appreciated that TBK1 functions during mitosis where its activation on the centrosome is necessary for cell division (Sarraf et al. 2019; Pillai et al. 2015; Maan et al. 2021). As a multifunctional kinase, it is essential for TBK1 to be activated at the correct subcellular location, only when it is needed. Therefore, it is imperative to understand the upstream regulation of TBK1 in different cellular contexts.

Previous studies have revealed that TBK1 associates itself with multiple binding partners during each different stimulus in innate immune signaling (Goncalves et al. 2011; Morton et al. 2008; Ryzhakov and Randow 2007; Sasai et al. 2006; Fujita et al. 2003) and during selective autophagy (Heo et al. 2015; Stolz, Ernst, and Dikic 2014; Matsumoto et al. 2011; Thurston et al. 2009; Morton et al. 2008), several of which competitively bind to activate TBK1 (Boyle, Ravenhill, and Randow 2019; Fu et al. 2018; Richter et al. 2016; Shu et al. 2013; Goncalves et al. 2011). The crystal structure of TBK1 with its binding partners has identified that TBK1 activation is a two-step process. First, an adaptor protein with a TBK1 binding motif binds to the

inactive TBK1 monomer at its C' terminus adaptor binding domain. This adaptor binding event facilitates the oligomerization of TBK1 to form an adpator-TBK1 dimer complex. Next, this oligomerization of the adaptor-TBK1 complex brings about a conformation change in its kinase domain to autophosphorylate TBK1 at serine 172, which activates TBK1 (Li et al. 2016; Larabi et al. 2013). The adaptors are responsible for linking TBK1 activation with the upstream signaling events and possibly determine the localization of TBK1 activation for different downstream signaling cascades (Fu et al. 2021).

Multiple studies have shown that sequestration of activated TBK1 away from the centrosomes can impair mitosis and lead to growth defects (Sarraf et al. 2019; Onorati et al. 2016). One physiological consequence of TBK1 mislocalization is evident during Zika virus infection, where activated TBK1 is localized on the viral particles and on the mitochondria driving abnormal mitosis in radial glia cells and neural stem cells causing microcephaly (Onorati et al. 2016). Additionally, either functional or genetic loss of TBK1 leads to slower cell growth, mitotic defects, and accumulation of multinucleated cells (Sarraf et al. 2019). Broadly, this work focuses on gaining the mechanistic insights into how TBK1 loss or mislocalization leads to the observed phenotypic consequences by identifying the unknown TBK1 mitotic adaptor(s) responsible for its activation on the centrosomes and by curating the possible downstream substrates of TBK1 during mitosis (Chapter 3). Furthermore, this work shows that there are abnormal TBK1 activation patterns and mislocalization of the protein upon the loss of autophagy. This abnormal TBK1 activation negatively influences mitosis, cell growth, and correlates with the accumulation of micronuclei (Chapter 4). Together, this work establishes the upstream regulation of TBK1 during mitosis and underscores the importance of TBK1 activity by identifying downstream targets of TBK1 that ensure proper cell division (Chapter 5).

Chapter 2

Review of Literature

Adaptor mediated regulation of TBK1 in diverse cellular processes

Abstract:
The serine/threonine kinase Tank Binding Kinase 1 (TBK1) plays crucial roles driving distinct cellular processes like innate immune signaling, selective autophagy, and mitosis. It is suggested that translocation and activation of TBK1 at different subcellular locations within the cell downstream of diverse stimuli is driven by TBK1 binding partners/adaptors and TBK1 associated proteins which form a complex with TBK1. Various TBK1 adaptors and associated proteins like NAP1, TANK, SINTBAD, p62, OPTN, TAX1BP1, and NDP52 have been identified in the innate immune and selective autophagy pathways, while the unknown adaptor(s) facilitating TBK1 activation and recruitment during mitosis remain to be identified. This review focuses on what is known between the binding interactions between TBK1 with each of its adaptors and functional consequences of these associations. We shed light on the importance of these TBK1 binding partners to explain how TBK1 contributes to several diverse signaling processes.

Introduction:
TBK1 mediates diverse cell signaling pathways including the innate immune response (Tojima et al. 2000; Pomerantz and Baltimore 1999; Fitzgerald et al. 2003), selective removal of damaged and superfluous mitochondria called mitophagy (Heo et al. 2015; Moore and Holzbaur 2016; Wong and Holzbaur 2014; Lazarou et al. 2015; Richter et al. 2016; Vargas et al. 2019), selective removal of invading cytosolic pathogens called xenophagy (Wild et al. 2011; Thurston et al. 2009), selective removal of damaged lysosomes called lysophagy (Eapen et al. 2021), and mitosis (Onorati et al. 2016; Pillai et al. 2015; Sarraf et al. 2019; Ravenhill et al. 2019) by its selective activation at distinct subcellular locations. The first functional role ascribed to TBK1 was in the context of innate immune signaling (Pomerantz and Baltimore 1999; Tojima et al. 2000) and has paved the way for immunobiologists to explore its role in pathogen-associated inflammation extensively. It has been established to play regulatory roles in both NF-κb and Type I interferon signaling cascades triggered by a wide variety of immunogenic stimuli (Bakshi et al. 2017; Fitzgerald et al. 2003; Thurston et al. 2009; Wild et al. 2011). Subsequently, TBK1 has been found to play key roles during selective autophagy. TBK1 is recruited at the ubiquitinated cargo by its direct or indirect binding of autophagy receptors like p62, OPTN, NBR1, TAX1BP1 and NDP52 during selective autophagy, (Vargas et al. 2019; Ravenhill et al. 2019; Fu et al. 2018; Richter et al. 2016; Lazarou et al. 2015; Heo et al. 2015; Eapen et al. 2021). and this association of TBK1 with autophagy receptors is essential for the recruitment of proteins to initiate autophagy at this cargo (Heo et al. 2015; Boyle, Ravenhill, and Randow 2019; Ravenhill et al. 2019; Fu et al. 2021). The newest function attributed to TBK1 were discovered

in cell division where its activation and localization on the centrosomes is necessary for proper mitotic progression (Pillai et al. 2015; Sarraf et al. 2019; Kim et al. 2013). However, its upstream regulation and downstream substrates during mitosis is mostly unknown.

The crystal structure of TBK1 indicates that an adaptor protein is required for its activation (Larabi et al. 2013; Zhang et al. 2019; Li et al. 2016; Fu et al. 2018). Binding of an adaptor protein induces a conformational change of TBK1 resulting in its autophosphorylation and activation of the kinase domain after dimerization (Larabi et al. 2013; Li et al. 2016; Fu et al. 2021) (Figure 2.1). This binding of the adaptor protein also can drive subcellular localization (Thurston et al. 2016; Goncalves et al. 2011; Heo et al. 2015). Multiple adaptors like NAP1/AZI2, TANK, SINTBAD, and OPTN contain a common TBK1 binding domain which competitively bind to the C-terminal domain (CTD) of TBK1 during mitophagy and innate immune signaling (Fu et al. 2018; Li et al. 2018; Ryzhakov and Randow 2007). Therefore, it is essential to explore the nature and consequences of the binding between TBK1 and adaptor/associated proteins to better understand how the kinase participates in such a diverse number of cellular processes.

Discovery of TBK1:

TBK1 was first discovered in 1999 in a study which aimed to understand the mechanism by which TANK and TRAF2 modulated NF-kB activation, and by pulling down the NFkB complex; this complex contained TBK1 (Pomerantz and Baltimore 1999). Subsequently, another group isolated and cloned the cDNA of TBK1 and demonstrated that it activated both IkB and NF-kB pathways (Tojima et al. 2000). To understand its role *in vivo*, the generation of TBK1 knockout (KO) mice soon followed (Bonnard et al. 2000) and while TBK1 heterozygous mice had no apparent phenotype, TBK1 KO mice resulted in embryonic lethality around E14.5 caused by massive liver degeneration and cell death. (Bonnard et al. 2000). TBK1 protein consists of one N' terminus kinase domain necessary for its catalytic activity (KD; aa 1-307), one regulatory C' terminus adaptor binding domain (CTD; aa 659-729), two accessory ubiquitin like domains (ULD; aa308-384), and a dimerization domain (DD; 385-657) (Ikeda et al. 2007; Shu et al. 2013).

Two independent studies reported that, TBK1 parallel to its homolog IKKε, could induce the Type 1 interferon response by activating IRF-3 to trigger defense against viral infection downstream of TLR-3 (Fitzgerald et al. 2003; Sharma et al. 2003). Since then, multiple groups have corroborated the fact that TBK1 is necessary for the transcription of several Type I interferon genes (ISGs) in the context of both viral and bacterial infection (McWhirter et al. 2004; Ishii et al. 2008; Thurston et al. 2009; Gu et al. 2016). In each of these immune response pathways, TBK1 has multiple binding partners/adaptors crucial for its activation like TANK, SINTBAD, NAP1/AZI2, Optineurin (OPTN), and STING (Clark, Takeuchi, et al. 2011; Gatot et al. 2007; Tanaka and Chen 2012; Bakshi et al. 2017; Goncalves et al. 2011; Fujita et al. 2003; Zhang et al. 2019; Ryzhakov and Randow 2007; Gleason et al. 2011). TBK1-adaptor complexes phosphorylate downstream targets such as IRF-3 and IRF-7, transcription factors that control the

ISG response (Fitzgerald et al. 2003; Liu et al. 2015; Hemmi et al. 2004; Iwamura et al. 2001) inducing a specific immune response.

The selective autophagy regulatory role of TBK1 was first identified in a study examining the host cell response to invading cytosolic bacteria where autophagosome engulfment and lysosomal degradation called xenophagy reduces bacterial load. During Salmonella infection, the TBK1-adpator complex is recruited at the sites of ubiquitinated bacteria by autophagy receptors NDP52 and TAX1BP1 (Thurston et al. 2009). TBK1 was also found to play an essential role during PINK1/Parkin-mediated mitophagy (Heo et al. 2015; Vargas et al. 2019). During selective autophagy pathways like mitophagy and xenophagy, the autophagy receptors, optineurin, TAX1BP1, and NDP52 are phosphorylated by TBK1 upon their recruitment to the ubiquitinated cargo, thus enhancing their binding to both ubiquitin chains on outer mitochondrial membrane proteins and LC3 autophagy proteins driving mitophagy (Heo et al. 2015; Lazarou et al. 2015; Moore and Holzbaur 2016; Richter et al. 2016). Therefore, loss of these autophagy receptors or impairment of their binding to TBK1 impairs selective autophagy (Heo et al. 2015; Lazarou et al. 2015; Moore and Holzbaur 2016; Richter et al. 2016; Vargas et al. 2019; Wong and Holzbaur 2014).

Recently, TBK1 was found to be necessary for proper progression through mitosis (Pillai et al. 2015; Sarraf et al. 2019; Kim et al. 2013) where it was found to be activated at the centrosomes of dividing cells (Pillai et al. 2015). Loss of TBK1 impairs mitosis leading to aberrant cell division and the accumulation of multinucleated cells (Pillai et al. 2015; Sarraf et al. 2019). In this case, the adaptors(s) required are yet to be fully evaluated.

In its role as an upstream regulatory protein of distinct signaling pathways, activated TBK1 is sequestered to different organelles or regions of the cell in a seemingly exclusive manner dictated by its binding to the autophagy adaptors. For example, active mitophagy – in which autophosphorylated TBK1 is localized to mitochondria - impedes mitosis due to the unavailability of pTBK1 (S172) at the centrosomes (Sarraf et al. 2019). Similarly, infection by Zika virus sequesters activated TBK1 away from the centrosomes to mitochondria and Zika viral particles (Onorati et al. 2016). In this review, I will evaluate what is known about each adaptor and its interaction with TBK1.

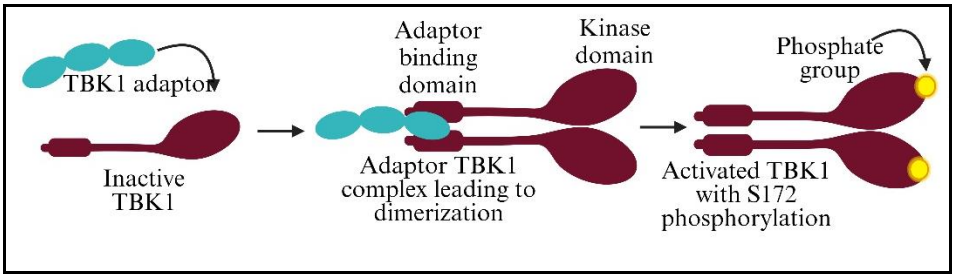

***Figure 2.1**: Illustration of TBK1 activation upon adaptor binding to its C' terminus domain.*

TANK:

TANK was originally discovered to be involved with NF-kB activation signaling as an TRAF binding protein and hence name, TRAF family member associated NF-kB activator (TANK)

(Cheng and Baltimore 1996). However, its role as TBK1 adaptor was first evident in a yeast two hybrid screen for TBK1 binding proteins (Pomerantz and Baltimore 1999), which also discovered TBK1 as an innate immune signaling kinase. Although TANK plays a role in activating TBK1 downstream of various types of immune stimuli *in vitro*, this view was challenged as TANK was found to be dispensable for IFN production via both TLR and RLR signaling pathways *in vivo* (Kawagoe et al. 2009). (Kawagoe et al. 2009). Two independent studies investigating the physiological relevance of TANK found that TANK KO mice exhibited fatal autoimmune glomerular and osteoporosis due to heightened activation of immune cells and osteoclasts which is fatal at around 3 months-of-age (Kawagoe et al. 2009; Maruyama, Kawagoe, et al. 2012). It is still unclear whether TBK1 activation and its function is affected due to loss of TANK.

After, the discovery of other TBK1 adaptors like NAP1 and SINTBAD, sequence homology and mutagenesis experiments identified that three of these adaptors have a common TBK1 binding domain (TBD) in their protein structure (Fujita et al. 2003; Ryzhakov and Randow 2007). All three of these adaptors use their TBD and compete to bind with the CTD of TBK1 constitutively *in vitro* (Goncalves et al. 2011); however, due to the dispensable nature of TANK in innate immune signaling there has been less focus on understanding TANK mediated TBK1 activation.

NAP1/AZI2

Nak Associated Protein 1 (NAP1) was first identified when its cDNA was isolated in 1999 from a library prepared after stimulating mouse embryonic fibroblasts (MEFs) with a potent methyltransferase inhibitor, 5-azacytidine, and it is alternatively known as AZI2 (Miyagawa et al. 1999). Although this study initially characterized the 48kD cytoplasmic protein, its function in the innate immune response as a TBK1 binding protein was discovered in 2003 using yeast two hybrid screening with TBK1 as a bait (Fujita et al. 2003). It was then renamed to NAK associated protein 1 considering its function as a NAK (TBK1) binding protein. The findings of this study established key characteristics of NAP1 mRNA and protein. NAP1 mRNA was found to be ubiquitously expressed in all major human tissues with the highest expression levels in pancreas and testis. *In vitro* binding assays and mutagenesis experiments found that amino acid sequence between 150-270 was the region necessary for TBK1 binding and this binding enhanced the activity of NF-kB activity in a dose dependent manner (Fujita et al. 2003). Thereafter another study discovered that endogenous NAP1 binds to TIR containing adaptor molecule 1 (TICAM-1) and participates in TLR3 mediated IRF-3 activation pathway post poly-I:C stimulation in HeLa cells. This binding facilitated TBK1 mediated INFβ promoter activation, which was abolished in case of truncated NAP1 lacking the TBK1 binding domain (aa 150-270). However, TANK, another adaptor of TBK1, did not precipitate with TICAM-1 either endogenously or overexpressed (Sasai et al. 2005), suggesting TANK cannot replace NAP1 to induce TICAM-1 mediated IFNβ. This group again reported a year later that both full length and truncated NAP1 can bind to the double stranded RNA pattern recognition receptors RIG-1 and

MDA5 to promote the IFN response, suggesting this binding is not always dependent on the TBK1 binding domain of NAP1 (Sasai et al. 2006). NAP1 can induce transcription of INFβ by both the transmembrane receptor TLR3 pathway and cytoplasmic pattern recognition receptors RIG-1 & MDA5 pathways (Sasai et al. 2005; Sasai et al. 2006).

Upon Salmonella infection, NAP1 has been shown to participate in xenophagy. The NAP1-TBK1 complex gets recruited on the ubiquitin coated bacteria by a constitutive binding between the highly conserved N' terminus coil coiled domain of NAP1 (aa 33-75) and the SKICH domain of an autophagy receptor NDP52 (aa 10-126). (Thurston et al. 2009; Fu et al. 2018). Another study shows that xenophagic removal of cytosolic bacteria activates ULK-1 mediated autophagy where the conserved N' terminus coiled coil domain of both the TBK1 adaptors SINTABD and NAP1 can form trimer complex with NDP52 and FIP200 on the bacterial surface in response to cytosol-invading Salmonella (Ravenhill et al. 2019; Fu et al. 2021). This direct interaction between the C' terminus of FIP200 (aa 1401-1591) and the N' terminus coil coiled domain of NAP1(aa 33-75) was reported by a subsequent study which characterized the non-canonical role of a core autophagy protein FIP200 in tumor progression (Okamoto et al. 2020). Loss of FIP200 correlated with NAP1 mediated overactivation of TBK1 resulting in a heightened Type I IFN response and recruitment of infiltrating T cells at the site of mammary tumor restricting tumor growth in mice. However, in the presence of FIP200, binding between FIP200 and NAP1 restricted TBK1 activation (Okamoto et al. 2020).

NAP1 KO mice displays severe osteoporosis due to enhanced accumulation of osteoclasts during development (Maruyama et al. 2015). While NAP1 KO impairs the TLR and RLR mediated IFN production in the bone marrow derived dendritic cells cultured in the presence of the differentiation factor GM-CSF (GM-DC), it was dispensable in macrophages isolated from NAP1 KO mice. It was found that GM-DCs lacking NAP1 had impaired differentiation with significantly lower number of mitotic cells in comparison to the WT due to lack of activation of TBK1 and this phenotype could not be rescued by the NAP1 mutant lacking TBK1 binding domain suggesting that NAP1-TBK1 binding is necessary for GM-DCs proliferation and growth (Fukasaka et al. 2013; Fu et al. 2021). Although NAP1 is an established innate immune response protein, some of the studies show it also regulates cell survival and proliferation suggesting it could be involved in cell cycle regulation.

SINTBAD/TBKBP1

Large-scale proteomics identified SINTBAD as an innate immune signaling protein that participated in the TNF-α /NF-kB pathway naming it TBK1 binding protein 1 (TBKBP1) based on protein structure homology and protein-protein interaction map (Bouwmeester et al. 2004). Further validation found a direct interaction between the C' terminus adaptor binding domain of TBK1 and the TBK1 binding domain of SINTBAD (aa 280-330) by affinity purification (Ryzhakov and Randow 2007). SINTBAD, NAP1, and TANK competitively bind to TBK1 to facilitate its activation after an innate immune stimulus for this TBK1 binding domain. (Goncalves et al. 2011; Ryzhakov and Randow 2007; Lee et al. 2013). Only NAP1 and

SINTBAD have a homologous N' terminus coil coiled region (CC1 and CC2) (Ryzhakov and Randow 2007). These homologous domains facilitate their binding with the SKICH domain of the autophagy receptors NDP52 and TAX1BP1 to form a higher order complex in case of xenophagy (Fu et al. 2021; Ravenhill et al. 2019; Fu et al. 2018; Thurston et al. 2009).

Germline SINTBAD KO mice are born with a significantly reduced number of natural killer T c ells (NKT) in the thymus, liver, and spleen with a predominant loss of stage 3 NKT cells with little to no effect on the number of stage 1 and stage 2 NKT cells. Further investigation showed that conditional NKT KO mice led to IL-15 mediated NKT cells survival and maturation, explaining the loss of stage 3 cells (Zhu et al. 2018). SINTBAD has also been described in acting in the autophagy machinery by forming a complex with ULK1 and FIP200 (Zhu et al. 2018; Ravenhill et al. 2019). SINTBAD was also found to be a part of cell cycle regulation and cell proliferation as lack of SINTBAD inhibited the growth factor stimulated TBK1 activation and downstream mTORC1 activation(Zhu et al. 2019). Mice with conditional lung epithelial cell SINTBAD KO mice corroborated the *in vitro* data where TBK1 mediated EGF stimulated mTORC1 signaling was impaired. Further crossing these conditional SINTBAD KO mice with oncogenic KRAS LA2 mice demonstrated that the loss of SINTBAD reduced lung tumor growth and increased survival (Zhu et al. 2019). Like NAP1, SINTBAD is another potential candidate to further investigate its role in cell cycle regulation.

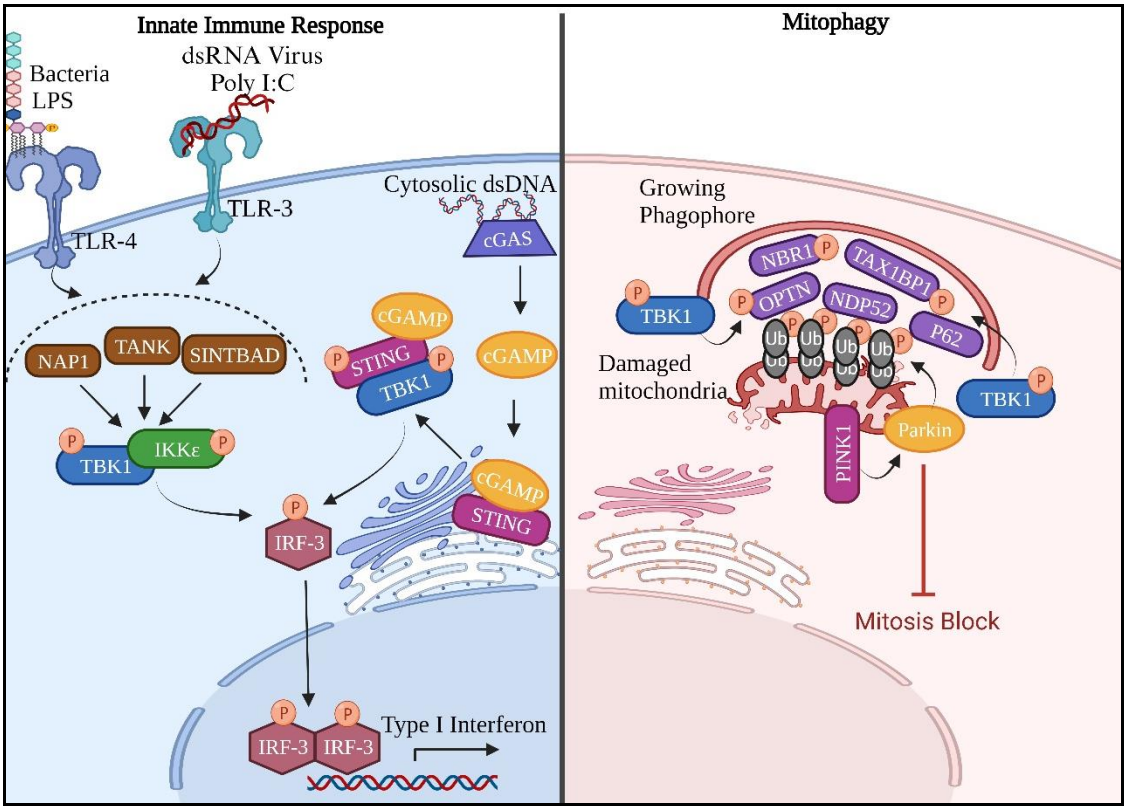

Figure 2.2: *Illustration of TBK1 activation in various innate immune signaling pathways and during mitophagy.*

Interaction of TBK1 and autophagy receptors NDP52 and TAX1BP1

Nuclear Dot Protein 52 (NDP52) is named after its protein distribution pattern in the nucleus (Sternsdorf et al. 1997; Dos Santos et al. 2023); however, due to its interaction with TBK1 which is found in the cytoplasm, this review will focus its cytoplasmic roles (Thurston et al. 2009). TAX1BP1 was first discovered as an interacting protein of human T cell leukemia virus type 1 (Tax1) in a yeast two hybrid screen and hence named as Tax1 Binding Protein 1 (Gachon et al. 1998). Although TAX1BP1 is ubiquitously expressed in all tissues (Verstrepen et al. 2011), it is highly expressed in the brain essential for the autophagic removal of protein aggregates to eliminate proteotoxic stress (Sarraf et al. 2020).

Both NDP52 and TAX1BP1 are essential ubiquitin binding autophagy receptors which share similar protein domain structures (Vargas et al. 2019). Their association with TBK1 has been reported in basal autophagy (Newman et al. 2012), xenophagy (Thurston et al. 2009; Newman et al. 2012; Tumbarello et al. 2015; Bell et al. 2021; Budzik et al. 2020) and mitophagy (Lazarou et al. 2015; Furuya et al. 2018) . During xenophagy, NDP52 and TAX1BP recruit the TBK1 adaptors NAP1 and SINTBAD using their SKICH domain and form a higher order complex with TBK1 (Ravenhill et al. 2019; Thurston et al. 2009; Fu et al. 2018; Furuya et al. 2018; Minowa-Nozawa et al. 2017). During mitophagy, activated TBK1 recruited on the depolarized mitochondria then directly phosphorylates NDP52 (Heo et al. 2015); however, phosphophorylation of TAX1BP1 by TBK1 has not been reported yet. NDP52 has been shown to directly bind with a core autophagy protein FIP200 using an unbiased yeast two hybrid approach. During both xenophagy and mitophagy, the SKITCH domain of NDP52 recruits the autophagy initiation ULK1 complex by binding with the Leucine zipper domain of FIP200 (aa 800-1591) (Ravenhill et al. 2019; Vargas et al. 2019; Fu et al. 2021; Boyle, Ravenhill, and Randow 2019). This recruitment of ULK1 complex on the ubiquitinated cargo was found to be cooperated by the availability of activated of TBK1 due to the formation of a stable higher adaptor-TBK1-NDP52 complex(Vargas et al. 2019; Heo et al. 2015; Fu et al. 2021; Ravenhill et al. 2019). Similarly, in lysophagy, the SKICH domain of TAX1BP1 also was found to interact with FIP200, driven by activated TBK1 recruitment at the site of damaged lysosomes in HeLa and induced neuron cells (Eapen et al. 2021). From the above findings, it is suggestive that TBK1 recruitment at the site of autophagy occurs due to the binding between the SKICH domain of autophagy receptors NDP52 and TAXBP1 and TBK1 adaptors NAP1 and SINTBAD. This TBK1 complex with NDP52 and TAXBP1 then further promotes the recruitment of autophagy initiation ULK1 complex.

Consequences of interaction between OPTN and p62 with TBK1

OPTN was first discovered to interact with TBK1 in a yeast two hybrid screen where they found that OPTN binding activates TBK1, and is enhanced by a mutant version of OPTN E50K (Morton et al. 2008). OPTN uses its N' terminus Tank binding domain homologous with other TBK1 adaptors NAP1, SINTBAD and TANK to interact with TBK1 (Morton et al. 2008). p62

alternatively known as sequestosome1 (SQSTM1) originally got its name because of its propensity to form aggregates (Joung, Strominger, and Shin 1996). It was initially found to be a part of inclusion bodies containing polyubiquitin coated protein aggregates in the context of neuropathology and liver proteinopathies (Kuusisto, Salminen, and Alafuzoff 2002; Zatloukal et al. 2002; Kuusisto, Salminen, and Alafuzoff 2001; Strnad et al. 2008). Later, it was reported that p62 simultaneously binds with ATG8 proteins and the ubiquitin chains during autophagy (Johansen and Lamark 2011; Kirkin and Rogov 2019).

OPTN mediated TBK1 activation in innate immune response pathway was studied in a polyubiquitin binding defective mutant of OPTN knock in mouse model where OPTN was replaced with $OPTN^{D477N/D477N}$. Bone marrow derived macrophages from this mutant mouse showed that although binding between TBK1 and OPTN was not affected by this OPTN mutation, TBK1 mediated INFβ activation and IRF3 phopshorylation was severely compromised post LPS and poly I:C stimulation (Gleason et al. 2011). Another study corroborated the function of OPTN-TBK1 complex by reporting the bone marrow derived macrophages and bone marrow derived dendritic cells isolated from the mice lacking the UBAN and ZF domain of OPTN had significantly lower TBK1 mediated activation of INFβ and IRF3 (Munitic et al. 2013).

During autophagy, both p62 and OPTN associate with ATG8 proteins with the help of the LC3 interacting region (LIR) necessary for the linking between the cargo and the growing autophagophore (Weidberg and Elazar 2011; Stolz, Ernst, and Dikic 2014; Pankiv et al. 2007). Interestingly this binding is promoted by the phosphorylation of OPTN on serine 177 and phosphorylation of p62 on serine 403 by TBK1 (Matsumoto et al. 2011; Matsumoto et al. 2015; Wild et al. 2011). In the case of Salmonella infection, TBK1 is recruited by the UBAN domain of OPTN to facilitate phosphorylation of xenophagy proteins to restrict bacterial growth in host cells (Wild et al. 2011). Several studies have reported that both OPTN and p62 function redundantly during mitophagy where they get phosphorylated by TBK1 on several residues (Nguyen et al. 2023; Heo et al. 2015; Richter et al. 2016).

Discussion:

Activation of TBK1 is reliant upon binding to adaptor proteins, which initiates higher order oligomerization of the TBK1-adaptor complex and leads to trans-autophosphorylation at serine 172 (Fu et al. 2018; Larabi et al. 2013; Ma et al. 2012). Multiple adaptors like NAP1/AZI2, TANK, SINTBAD, and OPTN contain a common TBK1 binding domain which competitively bind to the C-terminal domain (CTD) of TBK1 during mitophagy and innate immune signaling (Fu et al. 2018; Li et al. 2018; Ryzhakov and Randow 2007). These adaptors in different cell signaling contexts may also be redundant. For example, OPTN binding to TBK1 during viral infection drives Type I interferon production (Outlioua, Pourcelot, and Arnoult 2018), and it also activates TBK1 for mitophagy at the outer mitochondrial membrane (Richter et al. 2016). Loss of either TBK1 or these adaptors/associated proteins have revealed that the mechanism by which TBK1 drives different cellular processes at different subcellular locations (Figure 2.2). However, considerable compensation for the loss of an adaptor by other adaptors in innate immunity and

selective autophagy pathways occurs. Therefore, identifying the unknown activator(s) of TBK1 during mitosis can help us understand the mechanisms by which TBK1 drives cancer progression and if there exists crosstalk across innate immunity, mitosis, and mitophagy.

The sequence of events for TBK1 activation and localization is unclear. Whether an adaptor first binds to TBK1 to activate it, and this TBK1-adaptor complex gets recruited at the site of necessity or the adaptor arrives at the required site which recruits TBK1 to facilitate phosphorylation of the substrates is ambiguous (Helgason, Phung, and Dueber 2013). It is known that the TBK1 adaptor OPTN and the associated autophagy proteins NDP52, p62, TAX1BP1, and NBR1 get phosphorylated on various residues at the site of xenophagy and mitophagy (Heo et al. 2015; Lazarou et al. 2015; Matsumoto et al. 2015; Richter et al. 2016; Ravenhill et al. 2019; Nguyen et al. 2023). However, the precise spatial temporal organization of these complex events are obscure.

Chapter 3

NAK associated protein 1/NAP1 activates TBK1 to ensure accurate mitosis and cytokinesis

This work is under revision in the Journal of Cell Biology. The preprint version of this work can be found at https://doi.org/10.1101/2022.03.09.483647

NAK associated protein 1/NAP1 activates TBK1 to ensure accurate mitosis and cytokinesis

Short title: NAP1 activates TBK1 during cell division

Authors

Swagatika Paul[1], Shireen A. Sarraf[2], Ki Hong Nam[3], Leila Zavar[4], Sahitya Ranjan Biswas[5], Lauren E. Fritsch[5], Nicole DeFoor[4], Tomer M. Yaron[6,7], Jared L. Johnson[6], Emily M. Huntsman[6,7], Lewis C. Cantley[6,8,9], Alban Ordureau[3], and Alicia M. Pickrell[4,*]

Affiliations

[1]Graduate Program in Biomedical and Veterinary Sciences, Virginia-Maryland College of Veterinary Medicine, Blacksburg, VA 24061 USA.

[2]Biochemistry Section, National Institutes of Neurological Disorders and Stroke, National Institutes of Health, Bethesda, MD 20892 USA.

[3]Cell Biology Program, Sloan Kettering Institute, Memorial Sloan Kettering Cancer Center, New York, NY 10065 USA.

[4]School of Neuroscience, Virginia Tech, Blacksburg, VA 24061 USA.

[5]Translational Biology, Medicine, and Health Graduate Program, Virginia Tech, Roanoke, VA 24016 USA.

[6]Meyer Cancer Center, Weill Cornell Medicine, New York, NY 10065 USA.

[7]Englander Institute for Precision Medicine, Institute for Computational Biomedicine, Weill Cornell Medicine, New York, NY 10021 USA.

[8]Department of Cell Biology, Harvard Medical School, Boston, MA 02115 USA.

[9]Dana-Farber Cancer Institute, Harvard Medical School, Boston, MA 02215 USA

[*]Correspondence should be addressed to:

Alicia M. Pickrell, Life Science I Room 217, 970 Washington Street SW, Blacksburg, VA 24061

Tel: 540-232-8465; Email: alicia.pickrell@vt.edu

Abstract
Subcellular location and activation of Tank Binding Kinase 1 (TBK1) govern precise progression through mitosis. Either loss of activated TBK1 or its sequestration from the centrosomes causes errors in mitosis and growth defects. Yet, what regulates its recruitment and activation on the centrosomes is unknown. We identified that NAK Associated Protein 1 (NAP1) is essential for the binding mediated activation of TBK1 on the centrosomes to ensure proper mitosis. Loss of NAP1 causes several mitotic and cytokinetic defects due to inactivation of TBK1. Our quantitative phosphoproteomics identified numerous TBK1 substrates that are not only confined to the centrosomes but also are associated with microtubules. Substrate motifs analysis indicates that TBK1 acts upstream of other essential cell cycle kinases like Aurora and PAK kinases. We also identified that NAP1 is phosphorylated on serine 318 by TBK1 which promotes NAP1's degradation by ubiquitin proteasomal system acting as a negative regulatory step. These data uncover an important distinct function for the NAP1-TBK1 complex during cell division.

Summary
NAP1 is a cell cycle protein necessary for binding mediated activation of TBK1 on the centrosomes which regulates key mitotic and cytokinetic proteins to ensure proper cell division.

Introduction
Successful cell division is dependent on the precise and timely transition between different cell cycle phases, which is regulated by dynamic changes in protein phosphorylation. Thus, protein kinases play a vital role in orchestrating almost every step of cell cycle including DNA replication, centrosome maturation, chromatin condensation, spindle assembly formation, sister chromatid segregation, and cytokinesis (Nasa and Kettenbach 2018; Nigg 2001; Seki et al. 2008; Enserink and Kolodner 2010). Entry into mitosis is marked by the highest incidences of protein phosphorylation and kinase activity (Dephoure et al. 2008; Olsen et al. 2010). Therefore, impaired or aberrant kinase activity often leads to errors in all these cell cycle events which consequently become the underlying cause for developmental defects (Colas 2020; Schneider and Ellenberg 2019) or abnormal cell proliferation leading to cancer (Huang, Scott, et al. 2021; Singh et al. 2017). Tank Binding Kinase 1 (TBK1) is one such kinase, which is known to be activated on the centrosomes during mitosis (Pillai et al. 2015; Sarraf et al. 2019) and is also often overexpressed in certain cancer types (Chen et al. 2017; Uhlen et al. 2017; Wei et al. 2014). Genetic loss of TBK1 leads to embryonic lethality in mice (Bonnard et al. 2000), and its loss results in mitotic defects in cancer cell lines (Pillai et al. 2015; Sarraf et al. 2019; Maan et al. 2021). Interestingly, sequestration of activated TBK1 away from the centrosomes also disrupts mitosis in neural epithelial stem cells and radial glia during Zika virus infection (Onorati et al. 2016). Our previous work has shown that sequestration of TBK1 to the mitochondria during the selective degradation of mitochondria known as mitophagy, also blocks mitosis due to the unavailability of activated TBK1 on the centrosomes (Sarraf et al. 2019). Thus, both proper

activation and subcellular localization of TBK1 are essential for mitotic progression. Yet, the upstream regulation of TBK1 during mitosis is unknown, and we do not completely understand the function of activated TBK1 on the centrosomes.

Activation of TBK1 depends on its binding to an adaptor protein which induces a conformational change leading to trans-autophosphorylation on serine 172 of the kinase domain of TBK1 [27, 36, 37, 39]. Interaction with the adaptor protein not only activates the TBK1 kinase domain but may drive its subcellular localization to different organelles to regulate distinct signaling pathways (Thurston et al. 2016; Goncalves et al. 2011; Heo et al. 2015). From extensive studies examining its regulation during innate immune signaling, autophagy, and mitophagy, we know that TBK1 has multiple binding partners/adaptors for each of these cellular processes. While TANK, SINTBAD, NAP1/AZI2, optineurin (OPTN), and STING (Clark, Takeuchi, et al. 2011; Gatot et al. 2007; Tanaka and Chen 2012; Bakshi et al. 2017; Goncalves et al. 2011; Fujita et al. 2003; Zhang et al. 2019; Ryzhakov and Randow 2007; Gleason et al. 2011) are the major TBK1 adaptors during innate immune signaling, OPTN, TAX1BP1, and NDP52 (Heo et al. 2015; Lazarou et al. 2015; Moore and Holzbaur 2016; Richter et al. 2016) can activate TBK1 during mitophagy. However, the adaptor or adaptors required for TBK1 activation and recruitment during mitosis are unknown.

Along with activation, localization of TBK1 on the centrosomes is also essential for mitosis (Onorati et al. 2016; Sarraf et al. 2019). This localization brings activated TBK1 in the proximity of microtubules as centrosomes are the microtubule organizing center. Past studies have identified a few of the TBK1 substrates on the centrosomes (Maan et al. 2021; Pillai et al. 2015; Kim et al. 2013). Whether TBK1 functions only to phosphorylate centrosomal proteins during mitosis or also regulates microtubule binding proteins remains to be determined. The complete landscape of the proteins targeted by TBK1 during mitosis remains unclear. Identifying all the mitotic substrates would offer mechanistic insight into pathways modulated by TBK1 to ensure proper chromosomal segregation.

We show that NAP1/AZI2, whose function has only been described in innate immunity to trigger Type I interferon or NF-κB signaling (Fujita et al. 2003; Sasai et al. 2005; Sasai et al. 2006) is necessary for TBK1 activation during mitosis. We discovered NAP1 to be a centrosomal protein which regulates proper cell division by binding and activating TBK1 during mitosis. Loss of either NAP1 or TBK1 results in the accumulation of binucleated and multinucleated cells, due to the several mitotic and cytokinetic defects observed across several cell lines. We also describe a new function for both proteins, as our data suggests that they are also implicated in cytokinesis. Interestingly, NAP1 levels during mitosis are tightly regulated by TBK1. Activated TBK1 phosphorylates NAP1 on serine 318 flagging it for ubiquitin proteasomal degradation (UPS). Through unbiased quantitative phosphoproteomics analysis during mitosis, we also uncovered unidentified TBK1 substrates, which implicate its upstream effects on other cell cycle kinases such as Aurora A and Aurora B. This NAP1-TBK1 signaling axis during mitosis is distinct from to its function in innate immunity.

Results

NAP1/AZI2 is required for TBK1 activation during mitosis.

Activation of TBK1 is reliant upon its binding to adaptor proteins, which initiates higher order oligomerization of the TBK1-adaptor complex, leading to trans-autophosphorylation at serine 172 (p-TBK1) (Fu et al. 2018; Larabi et al. 2013; Ma et al. 2012). Previous identification of these adaptor proteins for TBK1 activation in other cellular contexts displayed overlap and redundancy. For example, during mitophagy, TAX1BP1, optineurin, and NDP52 have been found to be necessary for TBK1 activation (Heo et al. 2015; Lazarou et al. 2015; Moore and Holzbaur 2016; Richter et al. 2016). Optineurin and NDP52 are also the bound adaptor for TBK1 during certain innate immune stimuli (Li et al. 2016; Thurston et al. 2009; Morton et al. 2008; Fu et al. 2018). Despite these observations, the adaptor or adaptors required for TBK1 during miosis are unknown. Therefore, we screened known TBK1 adaptors to determine whether any of these proteins were responsible for its activation during mitosis.

First, we investigated TBK1 adaptors restricted to innate immune signaling, TANK, SINTBAD, and NAP1, by generating cell lines in which these proteins were stably knocked down (KD) at the mRNA and protein level in HeLa cells (**Figure 3.1A-F**). Reductions in TANK and SINTBAD did not alter TBK1 activation during mitosis (**Figure 3.1D-E**). However, NAP1 KD cells displayed a reduction of p-TBK1 during mitosis, indicating NAP1 could be required for TBK1 activation (**Figure 3.1F**). We also assessed p-TBK1 levels in an NDP52/OPTN double KO (DKO) HeLa cell line as both adaptor proteins have been implicated in TBK1 activation during mitophagy, xenophagy, and innate immunity (Ravenhill et al. 2019; Wild et al. 2011; Thurston et al. 2009; Heo et al. 2015; Vargas et al. 2019; Richter et al. 2016; Lazarou et al. 2015; Wong and Holzbaur 2014; Moore and Holzbaur 2016; Pourcelot et al. 2016), but found no difference between p-TBK1 levels in the synchronized mitotic cell population(**Figure 3.1G**). This was also true for a cell line lacking five autophagy related adaptors that TBK1 either binds or phosphorylates: NBR1, TAX1BP1, OPTN, p62, and NDP52 (**Figure 3.1H**).

To confirm that TBK1 activation during mitosis was dependent on NAP1, we generated two independent NAP1 CRISPR knockout (KO) clones targeting exon 4 (**Figure 3.2A**). Both NAP1 KO HeLa clones displayed decreased p-TBK1 levels during mitosis (**Figure 3.2A**). To confirm this result, we performed immunocytochemical experiments to detect p-TBK1 staining on centrosomes, which was significantly reduced in NAP1 KO cells (**Figure 3.2B-C**). This result was specific to NAP1 because p-TBK1 levels were restored during mitosis upon stable reintroduction of the protein (**Figure 3.2D**).

NAP1 KO cells have mitotic and cytokinetic defects like those lacking TBK1.

Previously, we and others have shown that loss of TBK1 led to slowed cell growth, decreased number of mitotic cells in asynchronous conditions, and an increased prevalence of

multinucleated cells (Pillai et al. 2015; Sarraf et al. 2019; Onorati et al. 2016; Kim et al. 2013). However, a more thorough analysis of the defects in cell division that led to these observations have not been performed. Therefore, we characterized cell division defects in NAP1 and TBK1 KO HeLa cells to compare whether these lines phenocopied each other. In asynchronous conditions, NAP1 KO cells exhibited slower growth rates, fewer number of mitotic cells, an increase in the number of bi- and multinucleated cells, and an increased number of cells displaying abnormal mitotic division (**Figure 3.2E-I**). We further characterized the types of abnormal mitotic defects between these KO lines. Both genotypes had a significant prevalence of monopolar spindles and splayed/unfocused spindle poles, but TBK1 KO had a significantly higher percentage of acentric fragments, while NAP1 KO cells had a higher percentage of cells with multipolar spindles (**Figure 3.2J-K**).

To further characterize how NAP1 and TBK1 regulate the progression of cell division, we also evaluated if cytokinetic defects were present. Both KO lines had a significantly higher percentage of cytokinetic cells in asynchronous conditions and display a higher percentage of cytokinetic defects (**Figure S3.1A-B**). Both KO lines exhibited unequal cytokinesis, as well as multipolar cytokinesis at a higher percentage than the parental line (**Figure S3.1C-D**).

We attempted to use the non-transformed near diploid RPE-1 and DLD-1 cell lines to confirm our findings in HeLa cells but were unable to generate either knockout or stable shRNA-mediated knockdown of NAP1 in both cell lines due to excessive cell death. Using a transient viral mediated transduction of NAP1 shRNA over 36 hours, we could generate a transient reduction of NAP1 (**Figure 3.3A**). These transient NAP1 KD in DLD-1 cells had reduced p-TBK1 levels during mitosis (**Figure 3.3A**). From the mitotic analysis on transient NAP1 KD DLD-1 cells, we observed a decrease in the mitotic index and increased percentage of multinucleated cells in transient (**Figure 3.3B-E**). However, there were an insufficient number of mitotic cells found in the KD cells to perform an in-depth mitotic defect analysis (**Figure 3.3F**). The high number of binucleated cells (**Figure 3.3D**), along with the significantly skewed frequency distribution compared to scramble shRNA KD (**Figure 3.3F**), suggested cells underwent cytokinetic failure over the 36-hour time period.

Considering that the KD DLD-1 cells had NAP1 disrupted over a span of two cell divisions, we utilized the degradation tag system (dTAG) (Nabet et al. 2018; Nabet et al. 2020) for target-specific protein degradation to generate a $FKBP^{F36V}$-NAP1 DLD-1 cell line to allow for immediate and selective manipulation of NAP1 instead of relying on the temporal time scale required for KD efficiency to occur with viral transduction. This would allow us to characterize mitotic defects caused due to NAP1 loss within one mitotic division period and minimize cell death. The $FKBP^{F36V}$ variant allows for selective recognition by a dTAG ligand, like dTAG-13 or $dTAG^{V}$-1, to induce dimerization of the $FKBP^{F36V}$ fused NAP1 to the CRBN or VHL E3 ligase for ubiquitin proteosome degradation (UPS) (Nabet et al. 2018; Nabet et al. 2020) (**Figure 3.3G**). After the addition of $dTAG^{V}$-1, NAP1 degradation occurred in both asynchronous and synchronized mitotic cells, and p-TBK1 activation was dampened as compared to untreated mitotic lysates (**Figure 3.3H**).

To observe the consequences of NAP1 loss in DLD-1 cells over one cell division period in an asynchronous population, we treated the dTAG^{V}-1 to FKBP^{F36V}-NAP1 cell line for 20 hours (**Figure 3.3I**). In line with our results when NAP1 was knocked down for 36 hours, we observed a decline in mitotic index and an accumulation of binucleated cells, but multinucleated cell accumulation did not differ (**Figure 3.3J-L**). The lack of multinucleated cells was not completely unexpected as only one round of cell division occurred. The stress of the sudden degradation of NAP1 did lead to an increase in the number of dead cells present after dTAG^{V}-1 treatment (**Figure 3.3M**). dTAG^{V}-1 treated FKBP^{F36V}-NAP1 cells had a significantly higher percentage of abnormal mitotic cells (**Figure 3.3N**) with many more mitotic defects (**Figure 3.3O-P**) than seen in the NAP1 KO HeLa cell line (**Figure 3.2J-K**). This result extended again into cytokinesis where dTAG ^{V}-1 treated FKBP^{F36V}-NAP1 cells had a higher percentage of cytokinetic cells that were abnormal with significant unequal and multipolar cytokinetic cells (**Figure 3.3Q-U**). These data suggest NAP1 is required for both mitosis and cytokinesis most likely through the activation of TBK1.

TBK1 selectively interacts with and binds NAP1 during mitosis.

RNA-seq and northern blotting data demonstrated that NAP1 is expressed ubiquitously in multiple different tissue types (Fagerberg et al. 2014; Fujita et al. 2003). To check the level of protein expression in these tissues, we probed a human tissue blot for NAP1, and found it to be expressed in all human tissues, except for small intestine, in which there was little detectable NAP1 protein(**Figure 3.4A**). , This NAP1 protein level corroborates with the previously reported NAP1 mRNA levels in the small intestine (Fujita et al. 2003). These data confirm NAP1 is a ubiquitously expressed protein most likely important for a wide range of tissue and cell types, supporting the evidence it has a critical function like in cell division.

Next, we wanted to determine if there was an interaction between NAP1 and TBK1 during mitosis, as the literature suggests that adaptor binding must occur for TBK1 activation (Larabi et al. 2013; Ma et al. 2012). We performed co-immunoprecipitation (co-IP) experiments by transiently overexpressing either full length NAP1 (N' EGFP FL NAP1) or NAP1 lacking the TBK1 binding domain (N' EGFP NAP1 Δ230-270) in HEK293T cells (Ryzhakov and Randow 2007)(**Figure 3.4B**). As our previous data indicated that TBK1 levels are tightly regulated in the cell, we performed the reciprocal co-IP by stably expressing two different TBK1 rescue constructs, N' FLAG HA FL TBK1 and N' FLAG HA Δ TBK1 (**Figure 3.4C**) in TBK1 KO HeLa cells(Sarraf et al. 2019). Phosphorylated endogenous TBK1 was enriched upon the immunoprecipitation of N' EGFP FL NAP1 with significantly increased binding during mitosis (**Figure 3.4D-E**). Binding of p-TBK1 was abolished in both asynchronous and mitotic conditions when NAP1 lacked its TBK1 binding domain (**Figure 3.4D**). Endogenous NAP1 was enriched upon immunoprecipitation of full length TBK1 (N'FLAG-HA FL TBK1) during mitosis (**Figure 3.4F-G**). This binding did not occur in rescue lines when the known C-terminal TBK1 adaptor binding site was deleted (N'FLAG-HA TBK1ΔC') (**Figure 3.4C, H**). Additionally, we verified

the enriched binding between NAP1 and TBK1 during mitosis by performing immunoprecipitation of endogenous TBK1 in DLD-1 cells (**Figure 3.4I-J**).

Next, we sought to corroborate our IP data with experiments to detect the subcellular location of NAP1 during mitosis. Due to the unavailability of antibodies suitable to detect endogenous NAP1 by immunofluorescence, we transiently expressed N'EGFP NAP1 in HeLa cells. We found that NAP1 colocalized with p-TBK1 on the centrosomes of mitotic cells (**Figure 3.4K-L**). To verify if NAP1 localization on the centrosomes is dependent on TBK1 binding, we stably rescued NAP1 Δ230-270 lacking its TBK1 binding domain in NAP1 KO cells. We failed to observe GFP-NAP1 Δ230-270 localization on the centrosomes during mitosis, and the intensity of p-TBK1 signal in these cells was significantly decreased (**Figure 3.4M-O**). These data suggest that activation of TBK1 during mitosis is dependent on NAP1 binding.

Although our data suggest that NAP1 has a separate function in regulating TBK1 during mitosis, previous studies of NAP1 have been limited to understanding its role during innate immunity (Fujita et al. 2003; Ryzhakov and Randow 2007; Goncalves et al. 2011; Sasai et al. 2005). It is possible that the binding of NAP1 to TBK1 during the cell cycle could aberrantly activate innate immune pathways. NAP1 is an adaptor for TBK1 during innate immune response, in which TBK1 on the endoplasmic reticulum phosphorylates the transcription factor, interferon regulator factor 3 (IRF3), causing its translocation to the nucleus, which in turns results in the stimulation of the Type I interferon response (Goncalves et al. 2011; Ryzhakov and Randow 2007; Fitzgerald et al. 2003; Sharma et al. 2003; Sasai et al. 2005).

Using a human monocytic cell line that is highly responsive to immunogenic stimuli, we first confirmed that this cell line displayed TBK1 activation during mitosis (**Figure S3.2A**) and after exposure to innate immune responsive stimuli (LPS and poly I:C) (**Figure S3.2B**). We then assessed the expression of a few select cytokine genes, Il10, Il6, TNF-α, whose expression is known to be upregulated upon LPS and poly I:C treatment (**Figure S3.2C-D**). During mitosis, the expression of these genes was either downregulated or only slightly upregulated, in the case of TNF-α, but not reaching the upregulation levels seen during immune stimuli (**Figure S3.2C-E**), indicating that TBK1 activation during mitosis does not trigger a robust innate immune response. Phosphorylation of either IRF3 or an alternative innate immune kinase (IKKε) that works in conjunction with TBK1 and shares high sequence homology (Tojima et al. 2000), occurred only in response to immunogenic stimuli (LPS and poly I:C) and not during mitosis (**Figure S3.2F**). Together, these data suggest there exists a distinct mitotic NAP1-TBK1 signaling axis at centrosomes.

NAP1 protein expression is cell cycle regulated.

We consistently observed a reduction in NAP1 protein during mitosis across four different cells lines (HeLa, DLD-1, THP1, and RPE-1, an additional near-diploid cell line), independent of the method of synchronization (**Figure 3.1F, 3.2A, 3.2D, 3.3A, 3.3H, 3.5A-B**). This reduction in NAP1 during mitosis also occurred at the mRNA level (**Figure 3.5C-D**). However, this was not

surprising as global transcription is repressed during mitosis (Taylor 1960; Prescott and Bender 1962). Inhibition of protein synthesis with cycloheximide over 6 hours did not disrupt NAP1 protein levels in asynchronous conditions (**Figure 3.5E-G**). Also, the inhibition of lysosomal fusion with chloroquine, which blocks autophagy, showed no change to NAP1 levels in asynchronous conditions (**Figure 3.5H-J**). From these data we conclude that NAP1 is a relatively stable protein except during mitosis.

To better define when and how NAP1 levels decreased during mitosis, we synchronized cells using the CDK1 inhibitor RO-3306 at G2 and released cells into mitosis. NAP1 was significantly reduced 10 minutes after release across cell lines (HeLa, RPE-1, and DLD-1), but the protein level mostly recovered during cytokinesis 60 minutes after release (**Figure 3.5K-M, lanes 1-3**). However, NAP1 levels did not degrade 10 minutes after release from G2 with the addition of the proteasome inhibitor, MG132 (**Figure 3.5K-M, lanes 4, 5)**. This indicates that the UPS was involved in this reduction of NAP1 during mitosis. To better characterize the exact time-point at which NAP1 levels degrade during mitosis and return to levels seen during asynchronous-G1 conditions, we used the RPE-1 cell line. Using p-PLK1 T210 and p-CDK1 Y15 as markers to indicate different stages during mitosis, we saw that NAP1 levels continuously degrade up to 40 minutes (anaphase) after G2 release (**Figure 3.5N, lane 8**). Levels began to increase and recover at the 50- and 60-minute time points (cytokinesis), and 90-minute time point (asynchronous, G1) (**Figure 3.5N, lanes 9-11**). We treated another set of cells with the E3 activating enzyme inhibitor TAK243 as an alternative method to inhibit the UPS (Hyer et al. 2018) and saw that NAP1 levels were stabilized throughout the time points collected after G2 release (**Figure 3.5N**). These data indicate that levels of NAP1 are tightly regulated during mitosis by the UPS.

Quantitative phospho-proteomics pipeline identifies the mitotic downstream substrates of TBK1.

The complete landscape of proteins targeted by TBK1 during mitosis is unidentified, and the substrates that have been identified do not fully explain the diverse array of mitotic and cytokinetic defects displayed due to the loss of TBK1 or NAP1 (**Figure 3.2, 3.3, S3.1**), nor do they provide insight into the regulation of these proteins (Kim et al. 2013; Pillai et al. 2015; Maan et al. 2021). Therefore, using unbiased quantitative phospho-proteomics, we sought to identify additional targets of TBK1 during mitosis. We synchronized WT HeLa and two independently created TBK1 KO HeLa cell lines from our previous work (Sarraf et al. 2019) into mitosis. Additionally, to account for off-target gene-editing effects, we also blocked TBK1 pharmacologically with a specific inhibitor, MRT67307 (Clark, Peggie, et al. 2011) (**Figure 3.6A**). Thus, phosphopeptides of interest should not be regulated with the small molecule inhibitor in either condition lacking functional TBK1 activity. While some previous studies (Dephoure et al. 2008; Olsen et al. 2010) have quantitatively detailed the global cell cycle and

mitotic phosphorylation landscape, to our knowledge, an in-depth, focused quantitative analysis of TBK1-dependent changes in the phosphoproteome during mitosis has not been performed.

To broadly understand how the phosphoproteome is remodeled and to search for potential mitotic TBK1 substrates, we performed quantitative proteomics on synchronized and released total cell extracts using 16plex TMTpro (**Figure 3.6A**). Tryptic peptides from whole-cell extracts were subjected to phosphopeptide enrichment, and samples were analyzed using 16plex TMTpro workflow (Li et al. 2020), with phosphopeptide intensities normalized with total protein abundance measured in parallel. In total, we quantified 8,650 proteins and 49,986 phosphopeptides in 7150 phosphoproteins from the phosphopeptide enrichment. Total proteomics carried out in parallel to normalize phosphopeptides revealed no major stabilization or degradation of protein upon TBK1 loss of function (**Figure S3.3A**). Principal component analysis revealed reproducible replicate data, with 39.7% of the variance being driven by cell genotype and 27% driven by the small molecule inhibitor treatment (**Figure S3.3B**). Given that both CRISPR editing and small molecule inhibitors can independently result in off-target effects, we set to compare the four different experimental conditions such that only variations that are abolished in both the CRISPR edited cells and cells treated with MRT67307 would be enriched in our TBK1-focused analysis. From the ~50,000 unique phosphorylation sites quantified; we identified 63 sites in 56 proteins whose abundance was statistically increased by >2-fold ($p < 0.01$, 1%FDR) (**Figure 3.6B**). Several significant studies have previously reported bona fide substrates of TBK1 (e.g., SQSTM1, TAX1BP1), thus validating our experimental approach. Further analysis revealed several enriched sites linked to the mitotic cell cycle gene ontology term, which led us to consider them strong TBK1 substrate candidates.

Considering that the disruption of one kinase can have many subsequential changes to other kinases, phosphoproteomics data although informative, cannot always be traced back to one particular kinase. In this case, we compared our phosphoproteomics data and the motifs surrounding our identified substrates to data generated from the Cantley laboratory that screened all 303 kinases with a synthetic peptide library to determine their motifs (Johnson et al. 2022). This would enable us to identify if other kinases were potentially affected by the loss of TBK1 as well as sort out which potential substrates were directly TBK1 dependent. Performing a motif analysis using this methodology to determine any enrichment at the sequence level for sites statistically increased by >2-fold ($p<0.05$, 5%FDR), found that Aurora, PAK, and TBK1/IKKε kinase motifs were predominately represented from our substrate list (**Figure 3.6B-D, S3.3C, S3.4A**).

To further evaluate the global effect of impairing TBK1's activity upon mitosis, we performed functional enrichment analysis based on Gene Ontology (GO) annotations for Biological Processes (**Figure 3.6E, S3.4B**), Molecular Function (**Figure S3.4C**), and Cellular Component terms (**Figure S3.4D**). This analysis revealed strong enrichment of many biological processes linked to mitotic cell cycle and chromosome segregation (**Figure 3.6E, left panel**) and visualized as enrichment map networks (**Figure 3.6E, right panel**). Taken together, these data

assert a role for TBK1 activity in mitotic progression, and we highlight a list of phosphorylation sites and possible TBK1 substrates or indirect substrates (**Figure 3.6B, Data file S3.3, S3.4A**).

We then experimentally validated if Aurora A and B kinases were regulated by TBK1. In DLD-1 and RPE-1 cells treated with TBK1 pharmacological inhibitors, the trans-autophosphorylation sites (T288 AurA, T232 AurB) indicative of activity for Aurora A and B were abolished as well as the downstream p-HistoneH3 S10 site, which is directly downstream of Aurora B (Hirota et al. 2005) (**Figure S3.4E-F**). It is possible that TBK1 pharmacological inhibitors display off-target effects *in vitro* (Clark et al. 2012), so we also tested our TBK1 KO cells. TBK1 KO HeLa cells displayed a less prominent reduction, but also displayed a decrease in p-AurA T288 and p-AurB T232 (**Figure S3.4G-H**). To our knowledge, this is the first time TBK1 has been implicated in regulation of Aurora and PAK kinases. In addition to the effects that TBK1 can have on direct substrates during mitosis, this dysregulation of Aurora kinases would cause defects not only in mitosis but also during cytokinesis, which may better explain the diverse cell division defects we found.

Our GO analyses indicated that microtubule polymerization and function were highly represented. Performing immunofluorescence staining for p-TBK1, the signal colocalized to centrin and γ-tubulin foci during mitosis across two independent cell lines (**Figure S3.5A-B**) reconfirming that TBK1 is activated on centrosomes. However, the p-TBK1 signal also appeared to be localized to the spindle assembly during metaphase (**Figure S3.5A-B**). When we compared the coverage area of the p-TBK1 signal, the area is significantly reduced upon the loss of NAP1 or in the TBK1 binding deficient NAP1 rescue line compared to WT cells (**Figure S3.5C-D**). These results indicate that TBK1 is involved in both centrosomal organization and function, and microtubule processes as indicated by the substrates found in our phosphoproteomics screen.

TBK1 phosphorylation of NAP1 at S318 impacts its stability during mitosis.

Our phosphoproteomics data indicated that NAP1 is phosphorylated at serine 318 during mitosis by TBK1 (**Figure 3.6B**). Although, the NAP1 sequence motif at this serine residue did not perfectly match the preferred *in vitro* TBK1 sequence motif (**Figure 3.6D, S3.3C**), our data suggested it was a bona fide substrate. First, TBK1 and NAP1 are bound, colocalizing at the centrosomes during mitosis (**Figure 3.4**). Second, TBK1 phosphorylates its own adaptors to modulate their function in other contexts (Richter et al. 2016; Wild et al. 2011; Heo et al. 2015). Third, when comparing the NAP1 sequence motif around S318 against all other 303 kinases, NAP1 still had a high 82.43% kinase preference probability. Therefore, we decided to further investigate the connection between NAP1 and TBK1.

First, we tested whether TBK1 affected NAP1 levels. We collected DLD-1 cells at different stages of the cell cycle and checked for NAP1 levels with or without MRT67307 treatment (TBK1 inhibitor). As expected, the control cells had a significant reduction of NAP1 during mitosis compared to asynchronous conditions; however, MRT67307 treated cells had significantly increased levels of NAP1 **(Figure 3.7A-B)**. Next, we sought to validate NAP1

phosphorylation during mitosis by Phos-tag gel analysis. A higher molecular weight band indicating the presence of a phosphorylated form of NAP1 appeared, which was missing from either TBK1 inhibitor treated or phosphatase treated mitotic cell lysates **(Figure 3.7C)**. NAP1 stability was also significantly increased during mitosis in a TBK1 kinase dead mutant (K38A) rescue line **(Figure 3.7D-E)**. The mitotic lysates from TBK1 K38A cells displayed a reduced higher molecular weight NAP1 banding pattern indicating TBK1 K38A was not able to phosphorylate NAP1 (**Figure 3.7F**). We then generated S318A phospho-deficient NAP1 rescue line to test whether TBK1 phosphorylation affected NAP1 stability during mitosis. NAP1 S318A resulted in a significantly higher amount of NAP1 during mitosis as compared to asynchronous conditions (**Figure 3.7G-H**). We also confirmed this result in our TBK1 KO line where NAP1 appeared less degraded during mitosis (**Figure 3.7I**). Together, these data suggest that activated TBK1 phosphorylates NAP1 on serine 318, which regulates NAP1 degradation **(Figure 3.7J)**.

Discussion

Our work demonstrates that NAP1/AZI2 is a mitotic and cytokinetic regulatory protein required for normal cell cycle progression. Mechanistically, NAP1 binds to TBK1 at centrosomes to activate TBK1, which subsequently phosphorylates several mitotic and cytokinetic proteins which we identified. NAP1 protein levels during mitosis are tightly regulated by the ubiquitin proteasome system where TBK1 phosphorylation of NAP1 at S318 influences its stability, thus acting as a possible feedback regulatory mechanism (**Figure 3.7J**).

Previous studies including our own have not extensively characterized all the consequences to cell division upon loss or pharmacological inhibition of TBK1, although these studies reported an increase in the number of multinucleated cells (Maan et al. 2021; Pillai et al. 2015; Sarraf et al. 2019). Previous experiments treating different cancer cell lines with TBK1 inhibitors or siRNAs showed an increase in the presence of supernumerary centrosomes and unfocused spindle poles (Maan et al. 2021; Pillai et al. 2015). However, our results find that these defects are more extensive than previously thought, affecting every stage of mitosis and cytokinesis. Mitotic and cytokinetic analyses with cells lacking either TBK1 or NAP1 displayed many of the same phenotypes, which we would expect if NAP1 and TBK1 acted within the same pathway.

The plethora of mitotic and cytokinetic defects found in both NAP1 and TBK1 KO cells led us to perform phosphor-proteomic analysis to unbiasedly discover additional TBK1 substrates to explain these diverse types of defects. Comparing the phosphorylation sites to the kinome substrate specificity motifs defined by synthetic peptide libraries (Johnson et al. 2022), substrates identified indicated that TBK1 either directly or indirectly affects Aurora A/B and PAK kinase activity as their motifs were highly represented. This was in addition to substrates that are direct TBK1 substrates. In DLD-1 and RPE-1 cells treated with TBK1 pharmacological inhibitors, Aurora A and Aurora B kinase activity was abolished. However, HeLa cells lacking TBK1 did not have such a dramatic reduction in p-Aurora A T288 and p-Aurora B T232, likely due to its state of aneuploidy compensating in some unknown manner. These results also provide an explanation as to why we were unsuccessful in generating a NAP1 KO or stable KD cell line and

instead had to generate the FKBP^{F36V}-NAP1 knock in line to characterize mitotic defects in cells that were near diploid. The choice to utilize different TBK1 KO clones with and without the TBK1 pharmacological inhibitor was to increase stringency in our experimental design to avoid the detection and identification of non-specific phosphorylation sites. However, the generation of an inducible conditional TBK1 knockout diploid cell line may better distinguish phosphor-sites in substrates that are compensated for in other cell lines. In this case, the balance between temporal timing of the loss of the protein with the concern for cell death need to be considered. This also may explain whyPlk1 (Kim et al. 2013), which was identified, in an asynchronous TBK1 KD screen in A549 cells, did not appear as a major hit nor did Plk1 activity appear disrupted in our DLD-1 MRT67307 treated cells.

Regardless, to our knowledge, this is the first time TBK1 has been implicated in Aurora A and B kinase activity and does explain how loss of TBK1 and NAP1 is so detrimental. Previously reported substrates, NuMa, CEP170, Plk1, Cdc20, Cdh1, all function during different stages of mitosis (Kim et al. 2013; Pillai et al. 2015; Maan et al. 2021), but these substrates do not explain all of the cytokinetic defects observed or the increase in binucleated cells in NAP1 and TBK1 KO cells, which can be indicative of cytokinetic failure. Aurora B is important in the formation of the contractile ring and cleavage furrow during cytokinesis (Steigemann et al. 2009; Ozlu et al. 2010; Carmena, Ruchaud, and Earnshaw 2009), and its disruption alone may explain these defects upon the loss of TBK1 and NAP1. Future work will be required to determine the mechanism by which TBK1 affects these other kinases and the careful dissection between bona fide TBK1 substrates and those of other kinases regulated by TBK1.

The *drosophila* orthologue of TBK1, ik2, is associated with the minus ends of microtubules (Bitan et al. 2010). *ik2* mutant flies display bristle and oocyte abnormalities due to defects in microtubule and cytoskeletal organization due to the inability of mutant ik2to phosphorylate spn-F and correctly localize ik2 to microtubules (Bitan et al. 2010; Shapiro and Anderson 2006; Abdu, Bar, and Schupbach 2006; Dubin-Bar et al. 2008; Lin et al. 2015). Microtubule disruption activates ik2, but dominant negative ik2 reduces microtubule polymerization suggesting its role in increasing microtubule stability (Barros and Bossing 2021). We observed p-TBK1 enriched at the spindle poles, as evidenced by its co-localization with gamma-tubulin and centrin. However, p-TBK1 was also visible along the spindle microtubules, in the region between the spindle poles and the chromosomes. TBK1 phosphorylating NuMa by way of its interaction with CEP170 may be responsible for its association to the spindle poles and correct microtubule tethering (Pillai et al. 2015). However, another paper in the context of Zika infection suggested that CEP63 is involved in TBK1 recruitment to centrosomes identified by γ-tubulin and centrin (Kodani et al. 2022). Considering that there is no mammalian orthologue to *spn-F* and our analysis revealed several microtubule-associated proteins largely represented in our proteomics data, more work is required to determine specifically where TBK1 is active or inactive on microtubules in different cellular contexts and what downstream consequences this may have to microtubule stability.

We attribute the ability for NAP1 to regulate TBK1 due to its ability to bind to the C' terminal of TBK1. These results are not surprising as it has previously been shown that multiple

adaptors bind to this region of TBK1 to facilitate dimerization and trans-autophosphorylation of the S172 site to activate kinase activity (Larabi et al. 2013; Ma et al. 2012). However, surprisingly, our data suggests that NAP1 localization to the centrosomes is dependent on TBK1 binding, which is opposite of previous findings. TBK1 adaptors are thought to facilitate TBK1 translocation and localization to target damaged mitochondria, bacteria, or exogenous innate immune triggering stimuli (Ravenhill et al. 2019; Richter et al. 2016; Goncalves et al. 2011; Moore and Holzbaur 2016). In our observations, NAP1 no longer localizes to centrosomes when lacking its TBK1 binding domain (NAP1 D230-270) nor is TBK1 mis localized upon the loss of NAP1. The area and intensity of p-TBK1 signal is weaker but activated TBK1 is still localized at the centrosomes. This indicates that TBK1 may translocate in a manner independent of its adaptors during cell division. Another possibility is that there is another adaptor not yet identified that can also activate TBK1 during mitosis and participate in regulating its localization or an adaptor that normally does not participate in mitosis can compensate to activate TBK1 in response to the loss of NAP1. TBK1 KO mice are embryonic lethal at day 14.5 (Bonnard et al. 2000). However, the NAP1 knockout mouse is viable, but does display proliferative defects in GM-dendritic cells (Fukasaka et al. 2013). We observed other TBK1 adaptors being phosphorylated during mitosis, but their role is unknown. How TBK1 localizes to centrosomes in the first place is quite intriguing and requires future study.

TBK1 expression is tightly regulated, and our previous data showed abnormal activation and subcellular localization upon overexpression of TBK1 (Sarraf et al. 2019). Elevated expression of TBK1 has been reported in many different types of cancer with high expression correlated with negative patient outcomes (Chen et al. 2017; Uhlen et al. 2017; Wei et al. 2014) This may explain our data showing the tight regulation of NAP1 expression which displays UPS dependent degradation from prophase to anaphase, but expression begins to increase and normalize to baseline in the late phases of mitosis and cytokinesis. The regulation of NAP1 protein levels during mitosis may ensure that TBK1 is not abnormally activated or overactivated, nor persists longer than necessary. To understand how the degradation of NAP1 affects TBK1 activation and function during mitosis, manipulation of the E3 ligase responsible for the ubiquitination and degradation of NAP1 is necessary. Future studies for E3 ligase screens are warranted to identify this protein.

We characterized the role of NAP1 and TBK1 during mitosis; other reports indicate that genetic influence and external environmental signaling/stimuli also influence cell division in a TBK1-dependent manner. TBK1's role in cell proliferation was originally described in KRAS mutant cell lines (Barbie et al. 2009), but KRAS mutations interacting with TBK1 are not the sole driver of the proliferation defects (Pillai et al. 2015). Proliferation stimulated by growth factor signaling is reliant on SINTBAD for the activation of TBK1 rather than NAP1 (Zhu et al. 2019). The subcellular localization of TBK1 and its adaptors in these genetic and environmental contexts as well as TBK1 substrates in these situations have yet to be described, making it uncertain if described differences in proliferation are due to changes in mitosis and/or cytokinesis. Both growth factor signaling and KRAS mutations converge on ERK kinase

signaling pathways (Katz, Amit, and Yarden 2007; Pylayeva-Gupta, Grabocka, and Bar-Sagi 2011), and sustained ERK activation throughout G1 is required for entry into S phase (Yamamoto et al. 2006; Meloche 1995; Jones and Kazlauskas 2001). Thus, it is possible that TBK1 can affect other stages of the cell cycle.

While NAP1 was first identified as an innate immune adaptor (Fujita et al. 2003), our data supports a NAP1-TBK1 activation axis occurring at centrosomes ascribing it a new role as a regulator of mitosis and cytokinesis. We have provided mechanistic insight into its function during cell division by providing evidence of how NAP1 activates TBK1 and provided data on how its own stability may be negatively regulated in a TBK1-dependent manner. Most research studies on TBK1-dependent processes such as mitophagy and innate immunity concentrate on asynchronous cell populations or post-mitotic cells ignoring the interplay between cell division and these other processes. However, the ubiquitous nature of TBK1 signaling across different cell types indicates these considerations are warranted. Future work to understand how innate immunity, selective autophagy, and cell division intersect is highly attractive as all three are implicated in human diseases such as cancer.

Materials and Methods

Cell culture

HeLa and HEK293T cells were maintained in DMEM high glucose medium supplemented with 10% FBS, 2mM L-Glutamine, 10mM HEPES, 0.1 mM non-essential amino acids, and 1mM sodium pyruvate. RPE-1 and DLD-1 cells were a kind gift from Dr. Daniela Cimini's lab. RPE-1 cells were maintained in DMEM/F-12 medium supplemented with 10% FBS. DLD-1 cells were maintained in RPMI-1640 medium with 10% FBS. Penta KO and DKO HeLa cells were a kind gift from Dr. Richard J. Youle's lab. THP1-Lucia™ ISG cells (Invivogen) were maintained in RPMI-1640 medium with 10% FBS, 2 mM L-glutamine, 25 mM HEPES, 100 μg/ml Normocin™, and Pen-Strep (100 U/ml-100 μg/ml). Cells were routinely tested for mycoplasma contamination by PCR (Southern Biotech).

Antibodies

The following antibodies were used for this study: TBK1/NAK (#3504S/#14590S; Cell Signaling Technology (CST)), pTBK1 (Ser172; #5483S; CST), pTBK1 Alexa Fluor 488 or 647 conjugated (Ser172; #14586/#14590; CST), NAP1/AZI2 (#15042-1-AP; Proteintech^{TM}), GAPDH (G9545; Sigma), Vinculin (#700062; Invitrogen), p-Histone H3 (S10; #53348S; CST), SINTBAD (#8605S; CST), TANK (#2141S; CST), FLAG M2 (#F1804; Sigma), p62 (#H00008878-M01; Abnova), NBR1 (#H00004077-M01; Abnova), TAX1BP1 (HPA024432;Sigma), Optineurin (#10837-1-AP; Proteintech), NDP52 (60732; CST), α-Tubulin (#T6074; Sigma)(#2144S; CST)(ab52866;Abcam), GFP (Cat#11814460001; Roche), IKKε (#2905S; CST), pIKKε (S162; #8766S, CST), HA.11 (#901513; BioLegend), IRF3 (#4302; CST), p-IRF3 (S386; ab76493; Abcam), Plk1 (#4513T; CST), p-Plk1 (Thr210; # 5472T; CST),

CREST (#15-234; Antibodies Inc.), CDK1/CDC2 (#77055; CST), pCDK1/CDC2 (Tyr15; #4539; CST), LC3 (NB600-1384; Novus)(#2775S; CST), g-tubulin (#5326; Sigma), Aurora A (#14475; CST), Aurora B (#3094T; CST), Aurora A/B (T288/T232; #2914T; CST), Centrin (#04-1624; EMD Millipore).

Additional chemicals

The following chemicals were used for this study: 10ug/ul cycloheximide (AC357420010; Fisher Scientific), 10μm MG132 (NC9937881; Fisher Scientific), 1 μM TAK243 (30108; Cayman Chemical), 50 μM chloroquine diphosphate (C2301100G; Fisher Scientific), 3μM MRT67307 (inh-mrt; Invivogen), 5mg/mL LPS (eBioscience), 1 mg/mL poly I:C (Fisher Scientific), 5U FastAP Thermosensitive Alkaline Phosphatase (EF0651; ThermoFisher), 1 μM dTAG^{V}-1 (Toris), and10μM BI605906 (50-203-0195; Fisher Scientific).

Plasmids and constructs

To generate NAP1 rescue lines, NAP1 cDNA was cloned into pDONR223 and transferred into the pHAGE-N'-FLAG-HA-IRES-puro, pHAGE-N'-EGFP-Gaw-IRES-Blast, or pHAGE-C'-EGFP-Gaw-IRES-Blast vectors using LR recombinase (Invitrogen). The pHAGE-N'-FLAG-HA-TBK1 cloning has been described previously (Sarraf et al. 2019) and deposited to Addgene #131791. The pHAGE-N'-FLAG-HA-TBK1 K38A construct was a kind gift from Dr. Richard Youle's lab. The following site directed mutagenesis primers were used to generated mutant constructions: NAP1 Δ230-270: TTCATCAAGTGCAGTTTTGTATATGGATCCGTTTGT TTGGCTTTC, GAAAGCCAAACAAACGGATCCATATACAAAACTGCACTTGATGAA; TBK1ΔC' terminus: GGG GACAAG TTT GTACAAAAAAGCAGG CTTCG AGGAGATAGAACCATGATGCAGAGCACTTCTAATCATCTG, GGGGACCACTTTG TACAAGAAAGCTGG GTCCTACTATATCCATTCTTCTGACTTATT. NAP1S318A: AATCCTCCAAGCATGGACAGACA, GCTTTCTCTGATAAAACCTTTACATC. All constructs were confirmed by DNA sequencing and deposited on Addgene.

Retrovirus and lentivirus generation

Dishes were coated with 50μg/mL poly-d-lysine (Sigma); and HEK293T cells were plated at 70-80% confluency before transfection. Lentiviral helpers and constructs were transfected using XtremeGENE 9™ (Roche) according to the manufacturer's instructions at a 1:3 ratio. 24 hrs after transfection, media was changed. Infectious media containing virus was collected 40 hrs later and filtered with a 0.45μm PES membrane filter (Millipore). Viral purification was performed using an Optima MAX-XP ultracentrifuge (Beckman) and spinning media at 100,000 x *g* for 2hr at 4^{o}C. Viral pellet was resuspended in sterile PBS, and tier was quantified using qPCR Lentivirus Titer Kit (abm) according to the manufacturer's directions. Live filtered virus was used to transduce cells with polybrene (10μg/ml, Sigma).

CRISPR knockout cell line generation

In brief, CRISPR design was aided by publicly available software provided by MIT at www.crispr.mit.edu. CRISPR oligos for NAP1: AAA CCA GCT GGA GGA GTT CTA CTT C, CAC CGA AGT AGA ACT CCT CCA GCT G. Primers were annealed with Phusion DNA polymerase (Thermo Fisher Scientific) using the following conditions: 98ºC for 1', 2-3 cycles of (98ºC for 10", 53ºC for 20", 72ºC for 30"), 72ºC for 5.' The annealed primers were cloned into the linearized gRNA vector gRNA, which was a gift from Dr. Feng Zhang (Addgene plasmid #62988) using the Gibson Assembly Cloning Kit (NEB). HeLa cells were cotransfected using XtremeGENE 9™ (Roche) using the above CRISPR plasmid. Cells were selected by puromycin (1mg/ml) and serially diluted into 96 well plates to select for single colony clones. DNA was extracted from individual clones using the Zymo gDNA Isolation Kit and genotyped/sequenced using the following primers: Exon 4 F GAAGCGAATGACATCTGCA, Exon 4 R CCTCTTCTGCTTCATCACAACCT.

shRNA cell line generation

pLKO.1 puro was a gift from Dr. Bob Weinberg (MIT) (Addgene plasmid # 8453) digested with AgeI and EcoRI for 4 hrs at 37ºC. Digested plasmid was excised, and gel purified with GeneJET™ gel extraction kit (Thermo Fisher). Oligos were designed for the following target sequences and annealed (NAP1: CCG GCC ACT GCA TTA CTT GGA TCA ACT CGA GTT GAT CCA AGT AAT GCA GTG GTT TTT G; AAT TCA AAA ACC ACT GCA TTA CTT GGA TCA ACT CGA GTT GAT CCA AGT AAT GCA GTG G, TANK: CCG GCC TCA AAG TCT ACG AGA TCA ACT CGA GTT GAT CTC GTA GAC TTT GAG GTT TTT G; AAT TCA AAA ACC TCA AAG TCT ACG AGA TCA ACT CGA GTT GAT CTC GTA GAC TTT GAG G, SINTBAD: CCG GCC TCT GCC TTT CTG TTC TTA ACT CGA GTT AAG AAC AGA AAG GCA GAG GTT TTT G; AAT TCA AAA ACC TCT GCC TTT CTG TTC TTA ACT CGA GTT AAG AAC AGA AAG GCA GAG G). Annealed oligos were ligated into the digested vector with T4 ligase (NEB); and colonies were screened by sequencing. Scramble shRNA was a gift from Dr. David Sabatini (MIT) (Addgene plasmid # 1864). Cells were selected for using 1mg/mL puromycin.

FKBP12^{F36V} degradation tag-NAP1 cell line generation

The cell line was generated as previously described (Damhofer, Radzisheuskaya, and Helin 2021). For donor vector, the BSD-P2A-2xHA-FKBP12^{F36V} and backbone pCRIS-PITCH cassettes were generated using PCR. The NAP1 homology sequences for N terminal tagging were synthesized as a gBlock gene fragment (IDT) and they were assembled using NEBuilder HiFi DNA Assembly Master Mix (E2621, NEB) according to the manufacturer's instructions. For guide RNA expression targeting NAP1, pX459 was cloned as previously described. Briefly, guides targeting N-terminal of NAP1 were designed using the CHOPCHOP website (https://chopchop.cbu.uib.no/). Oligonucleotides (CAC CGA ACA GTT GTC ATG GAT GCA C, AAA CGT GCA TCC ATG ACA ACT GTT) from IDT were annealed and inserted into the pX459 plasmid after BbsI (NEB) digestion. To develop the FKBP12^{F36V} degradation tag-NAP1

DLD-1 cell, DLD-1 cells were cotransfected using Lipofectamin 3000 (Invitrogen) using above donor vector and pX459 plasmid targeting NAP1. Cells were selected by puromycin (1mg/ml) and diluted into 96 well plates to select for single colony clones. gDNA was extracted from individual clones using lysis buffer (25mM KCl, 5mM Tris HCl pH 8.0, 1.25mM MgCl2, 0.2% NP40, 0.2% Tween-20, 0.4 ug/ml Proteinase K) and heated at 65 ^{o}C for 10 min and 98 ^{o}C for 5 min incubation. PCR for genotyping was conducted using the following primers: AAG AAC TTT TGA AAA TTT ATA AAT TGA G, GAA AAA TAT TTG GAA TAT AAC TCC AAG.

Cell synchronization

Nocodazole treatment: Cells were incubated with 1ug/ml nocodazole (Sigma) containing medium to synchronize at the G2/M border for 16 hours and collected for further experiments.

R0-3306 treatment: To synchronize at G2, cells were reversibly incubated with 9μM RO-3306 (TCI America) containing medium for 20 hrs and collected at the following time points corresponding to their respective cell cycle stages when released in normal growth medium. 0hr – G2; 1hr – M (metaphase); 7hrs – G1. Mitotic shake was employed to obtain maximum number of mitotic cells.

Cell collection and treatment for Phospho-proteomics

WT HeLa and two independent TBK1 CRISPR knockout lines (TBK1 KO clone 2 and clone 4) were treated with 9uM RO-3306 to synchronize at G2. Cells were released in normal growth medium for an hour to collect approximately 20M mitotic cells per sample (using mitotic shake). To account for the off-target gene editing effect, additional groups were added with TBK1 inhibitor treatment. For this, WT HeLa and both TBK1 KO clones were also treated 9μm with R0-3306 for 19.5 hours. 30 mins prior to the G2 wash, the cells were treated with 3μm MRT67307 along with 9μm R03306. After G2 wash the cells were released in normal growth medium with 3μm MRT67307 for 1 hour to collect approximately 20M mitotic cells per sample. 4 biological replicates were collected for each group (Figure 3.1A).

Proteomics - cell lysis and protein digestion

At the indicated times, cells were washed twice with ice cold PBS and snap frozen. Cell pellets were lysed in lysis buffer (25 mM EPPS pH 8.5, 8 M Urea, 150 mM NaCl, phosphatase and protease inhibitor cocktail (in-house)), to produce whole cell extracts. Whole cell extracts were sonicated and clarified by centrifugation (16000×g for 10 min at 4^{o}C) and protein concentrations determined by the Bradford assay. Protein extracts (3 mg) were subjected to disulfide bond reduction with 5 mM TCEP (room temperature, 10 min) and alkylation with 25 mM chloroacetamide (room temperature, 20 min). Methanol–chloroform precipitation was performed prior to protease digestion. In brief, four parts of neat methanol were added to each sample and vortexed, one part chloroform was then added to the sample and vortexed, and finally three parts waters were added to the sample and vortexed. The sample was centrifuged at 6 000 rpm for 5 min at room temperature and subsequently washed twice with 100% methanol. Samples were

resuspended in 100 mM EPPS pH8.5 containing 6 M Urea and digested at 37°C for 2h with Lys-C at a 100:1 protein-to-protease ratio. Samples were then diluted to 0.5 M Urea with 100 mM EPPS pH8.5 solution, trypsin was then added at a 100:1 protein-to-protease ratio and the reaction was incubated for 6 h at 37 °C. Digestion efficiency of a small aliquot was tested, Samples were acidified with 0.1% Trifluoroacetic acid (TFA) final and subjected to C18 solid-phase extraction (SPE) (Sep-Pak, Waters).

Proteomics - Fe2+-NTA phosphopeptide enrichment

Phosphopeptides were enriched using Pierce High-Select Fe2+-NTA phosphopeptide enrichment kit (Thermo Fisher Scientific, A32992) following the provided protocol. In brief, dried peptides were enriched with phosphopeptides and eluted into a tube containing 25 µL 10% formic acid (FA) to neutralize the pH of the elution buffer and dried down. The unbound peptides (flow through) and washes were combined and saved for total proteome analysis.

Proteomics - tandem mass tag labeling

Proline-based reporter isobaric Tandem Mass Tag (TMTpro) labeling of dried peptide samples resuspended in 100 mM EPPS pH 8.5, was carried out as follows. For total proteome analysis (50 mg of flow through peptide) and for phosphopeptide proteomics, (desalted, eluted peptides from phospho-enrichment step), 10 µL of a 12.5 µg/µL stock of TMTpro reagent was added to samples, along with acetonitrile to achieve a final acetonitrile concentration of approximately 30% (v/v). Following incubation at room temperature for 1 h, labeling efficiency of a small aliquot was tested for each set (total proteome and phospho-proteome), and the reaction was then quenched with hydroxylamine to a final concentration of 0.5% (v/v) for 15 min. The TMTpro-labeled samples were pooled together at a 1:1 ratio. The total proteome sample and phospho-proteome sample were vacuum centrifuged to near dryness and subjected to C18 solid-phase extraction (SPE) (50 mg, Sep-Pak, Waters).

Proteomics - off-line basic pH reversed-phase (BPRP) fractionation.

Dried TMTpro-labeled sample was resuspended in 100 µl of 10 mM NH4HCO3 pH 8.0 and fractionated using basic pH reverse phase HPLC (Wang et al. 2011). Briefly, samples were offline fractionated over a 90 min run, into 96 fractions by high pH reverse-phase HPLC (Agilent LC1260) through an 1) aeris peptide xb-c18 column (Phenomenex; 250 mm x 3.6 mm) for total proteome, 2) kinetex EVO-c18 column (Phenomenex; 150 mm x 2.1 mm) for phosphor-proteome, with mobile phase A containing 5% acetonitrile and 10 mM NH4HCO3 in LC-MS grade H2O, and mobile phase B containing 90% acetonitrile and 10 mM NH4HCO3 in LC-MS grade H2O (both pH 8.0). The 96 resulting fractions were then pooled in a non-continuous manner into 24 fractions (as outlined in Supplemental Figure 3.5 of (Paulo et al. 2016)) used for subsequent mass spectrometry analysis. Fractions were vacuum centrifuged to near dryness. Each consolidated fraction was desalted via StageTip, dried again via vacuum centrifugation, and reconstituted in 5% acetonitrile, 1% formic acid for LC-MS/MS processing.

Proteomics – total proteomics analysis using TMTpro.

Mass spectrometry data were collected using an Orbitrap Eclipse Tribrid mass spectrometer (Thermo Fisher Scientific, San Jose, CA) coupled to an UltiMate 3000 RSLCnano system liquid chromatography (LC) pump (Thermo Fisher Scientific). Peptides were separated on a 100 μm inner diameter microcapillary column packed in house with ~40 cm of HALO Peptide ES-C18 resin (2.7 μm, 160 Å, Advanced Materials Technology, Wilmington, DE) with a gradient consisting of 5%–21% (0-85 min), 21-28% (85-110min) (ACN, 0.1% FA) over a total 120 min run at ~500 nL/min. For analysis, we loaded 1/10 of each fraction onto the column. Each analysis used the Multi-Notch MS^3-based TMT method (McAlister et al. 2014), to reduce ion interference compared to MS^2 quantification (Paulo, O'Connell, and Gygi 2016), combined with the FAIMS Pro Interface (using previously optimized 3 CV parameters for TMT multiplexed samples (Schweppe et al. 2019) and combined with newly implemented Real Time Search analysis software (Erickson et al. 2019; Schweppe, Eng, et al. 2020). The scan sequence began with an MS^1 spectrum (Orbitrap analysis; resolution 120,000 at 200 Th; mass range 400−1500 m/z; automatic gain control (AGC) target 4×10^5; maximum injection time 50 ms). Precursors for MS^2 analysis were selected using a cycle type of 1.25 sec/CV method (FAIMS CV=-40/-60/-80). MS^2 analysis consisted of collision-induced dissociation (quadrupole ion trap analysis; Rapid scan rate; AGC 1.0×10^4; isolation window 0.5 Th; normalized collision energy (NCE) 35; maximum injection time 35 ms). Monoisotopic peak assignment was used, and previously interrogated precursors were excluded using a dynamic window (180 s ±10 ppm). Following acquisition of each MS^2 spectrum, a synchronous-precursor-selection (SPS) API-MS^3 scan was collected on the top 10 most intense ions b or y-ions matched by the online search algorithm in the associated MS^2 spectrum (Erickson et al. 2019; Schweppe, Eng, et al. 2020). MS^3 precursors were fragmented by high energy collision-induced dissociation (HCD) and analyzed using the Orbitrap (NCE 45; AGC 2.5×10^5; maximum injection time 200 ms, resolution was 50,000 at 200 Th). The closeout was set at two peptides per protein per fraction, so that MS^3s were no longer collected for proteins having two peptide-spectrum matches (PSMs) that passed quality filters (Schweppe, Eng, et al. 2020).

Proteomics – phosphoproteomics analysis using TMTpro

Mass spectrometry data were collected using an Orbitrap Eclipse Tribrid mass spectrometer (Thermo Fisher Scientific, San Jose, CA) coupled to an UltiMate 3000 RSLCnano system liquid chromatography (LC) pump (Thermo Fisher Scientific). Peptides were separated on a 50 cm μPAC column (PharmaFluidics, Ghent, Belgium) with a gradient consisting of 3%–18% (0-85 min), 18-25% (85-110min) (ACN, 0.1% FA) over a total 125 min run at ~250 nL/min. For analysis, we loaded half of each fraction onto the column. Each analysis used the FAIMS Pro Interface (using previously optimized 3 CV parameters for TMTpro-labeled phosphopeptides (Schweppe, Rusin, et al. 2020)) to reduce ion interference. The scan sequence began with an MS^1 spectrum (Orbitrap analysis; resolution 120,000 at 200 Th; mass range 400−1500 m/z;

automatic gain control (AGC) target 4×10^5; maximum injection time 50 ms). Precursors for MS^2 analysis were selected using a cycle type of 1.25 sec/CV method (FAIMS CV=-40/-60/-80). MS^2 analysis consisted of high energy collision-induced dissociation (HCD) (Orbitrap analysis; resolution 50,000 at 200 Th; isolation window 0.5 Th; normalized collision energy (NCE) 38; AGC 2×10^5; maximum injection time 86 ms). Monoisotopic peak assignment was used, and previously interrogated precursors were excluded using a dynamic window (120 s ±10 ppm).

Proteomics – data analysis

Mass spectra were processed using a Comet-based (2020.01 rev. 4) software pipeline (Eng et al., 2013). Spectra were converted to mzXML and monoisotopic peaks were re-assigned using Monocle (Rad et al. 2021). MS/MS spectra were matched with peptide sequences using the Comet algorithm (Eng, Jahan, and Hoopmann 2013) along with a composite sequence database including the Human Reference Proteome (2020-01 - SwissProt entries only) UniProt database, as well as sequences of common contaminants. This database was concatenated with one composed of all protein sequences in the reversed order. Searches were performed using a 50-ppm precursor ion tolerance for analysis. For total proteomic analysis, the recommended product ion parameters for ion trap ms/ms were used (1.0005 tolerance, 0.4 offset (mono masses), theoretical fragment ions = 1). For phospho proteomics analysis, the recommended product ion parameters for high resolution ms/ms were used (0.02 tolerance, 0.0 offset (mono masses), theoretical fragment ions = 1). TMTpro tags on lysine residues and peptide N termini (+304.207 Da) and carbamidomethylation of cysteine residues (+57.021 Da) were set as static modifications, while oxidation of methionine residues (+15.995 Da) was set as a variable modification. For phosphorylation dataset search, phosphorylation (+79.966 Da) on Serine or Threonine were set as additional variable modifications. Peptide-spectrum matches (PSMs) were adjusted to a 1% false discovery rate (FDR) (Elias and Gygi 2007). PSM filtering was performed using a linear discriminant analysis, (Huttlin et al. 2010), while considering the following parameters: Comet Log Expect, Diff Seq. Delta Log Expect, missed cleavages, peptide length, charge state, and precursor mass accuracy. For protein-level comparisons, PSMs were identified, quantified, and collapsed to a 1% peptide false discovery rate (FDR) and then collapsed further to a final protein-level FDR of 1%(Savitski et al. 2015). Moreover, protein assembly was guided by principles of parsimony to produce the smallest set of proteins necessary to account for all observed peptides. For TMTpro-based reporter ion quantitation, we extracted the summed signal-to-noise (S:N) ratio for each TMTpro channel and found the closest matching centroid to the expected mass of the TMT reporter ion (integration tolerance of 0.003 Da). Reporter ion intensities were adjusted to correct for the isotopic impurities of the different TMTpro reagents according to manufacturer specifications. Proteins were quantified by summing reporter ion signal-to-noise measurements across all matching PSMs, yielding a ‘‘summed signal-to-noise’ measurement. For total proteome, PSMs with poor quality, MS^3 spectra with 8 or more TMTpro reporter ion channels missing, or isolation specificity less than 0.7, or with TMT reporter summed signal-to-noise ratio that were less than 160 or had no MS^3 spectra were excluded from

quantification. For phospho proteome, PSMs with poor quality, MS^3 spectra with 12 or more TMT reporter ion channels missing, or isolation specificity less than 0.8, or with TMT reporter summed signal-to-noise ratio that were less than 160 or had no MS^3 spectra were excluded from quantification. Phosphorylation site localization was determined using the AScorePro algorithm (Beausoleil et al. 2006; Gassaway et al. 2022). AScore is a probability-based approach for high-throughput protein phosphorylation site localization. Specifically, a threshold of 13 corresponded to 95% confidence in site localization.

Protein or peptide quantification values were exported for further analysis in Microsoft Excel, GraphPad Prism, R package and Perseus (Tyanova et al. 2016). Each reporter ion channel was summed across all quantified proteins and normalized assuming equal protein loading of all samples. Phospho peptides were normalized to the protein abundance value (when available) and then normalization of dataset was performed using PhosR package (Kim et al. 2021). Gene Ontology enrichment analyses were performed with R package ClusterProfiler (4.0) (Wu et al. 2021).

Serine/threonine kinase predictions:

Kinase predictions were based on experimental biochemical data of their substrate motifs. We had utilized synthetic peptide libraries, containing 198 peptide mixtures, that explored amino acid preference up to 5 residues N-terminal and C-terminal to the phosphorylated Ser/Thr to determine the optimal substrate sequence specificity for recombinant Ser/Thr kinases. In total, 303 kinases were profiled. Their motifs were quantified into position specific scoring matrices (PSSMs) and then applied computationally to score phosphorylation sites based on their surrounding amino acid sequences. These PSSMs were ranked against each site to identify the most favorable kinds of kinases. This work is in preparation (Johnson et al. 2022).

The Kinase Library enrichment analysis:

The phosphorylation sites detected in this study were scored by all the characterized kinase PSSMs (303 S/T kinases), and their ranks were determined (Johnson et al. 2022). For every non-duplicate, singly phosphorylated site, kinases that ranked within the top-15 out of the 303 S/T total kinases were considered as biochemically predicted kinases for their respective phosphorylation site. For assessing kinase motif enrichment, we compared the percentage of phosphorylation sites for which each kinase was predicted among the downregulated/upregulated phosphorylation sites (sites with $|\log_2$ fold change$|$ greater than or equal 1 and with FDR less than or equal to 0.1), versus the percentage of biochemically favored phosphorylation sites for that kinase within the set of unregulated sites in this study (sites with $|\log_2$ fold change$|$ less than 1 and with FDR greater than 0.1). Statistical significance was determined using one-sided Fisher's exact test, and the corresponding p-values were adjusted using the Benjamini-Hochberg procedure. Kinases that were significant (adjusted *p*-value 0.1) for both upregulated and downregulated analysis were excluded from downstream analysis. Then, for every kinase, the

most significant enrichment side (upregulated or downregulated) was selected based on the adjusted *p*-value and presented in the scatterplot.

Western blots

For immunoblotting, cells were lysed using 1X RIPA buffer (Thermo scientific Pierce ™ RIPA Buffer) containing 1X protease/phosphatase inhibitor cocktails (Thermo Scientific Halt™). Protein concentration was quantified using DC™ Protein Assay Kit (Bio-Rad). Human tissue samples were obtained using the INSTA-Blot Human Tissues pre-run western blot (Novus Biologicals). Cell lysates were boiled for 15 mins with 2X LDS buffer containing 50 mM DTT, and 20ug of protein lysates were resolved by 4%-12% Bis-Tris gels and transferred to PVDF membranes. Blots were blocked using 5% non-fat powdered milk in 1X TBST (150mM NaCl, 20mM Tris, pH 8.0, 0.1% Tween 20). Primary and secondary antibody incubations were carried out in 2.5% non-fat powdered milk in 1X TBST for overnight at 4°C and 1hr at room temperature, respectively. Blots were exposed using Clarity™ Western ECL Substrates (Bio-Rad), ECL™ Select Western Blotting Detection Reagent (GE Healthcare), or SuperSignal™ West Femto Maximum Sensitivity Substrate (Thermo Scientific) and detected by the ChemiDoc Imaging System (BioRad).

PhosTag gels

For protein phosphorylation analysis, 6% Supersep Phos-tag™ gels (Wako Chemicals 192-17401) were used. These gels were run in 1% Tris Glycine and SDS buffer for approximately 2 hours. To increase the transfer efficiency, the phostag gels were soaked for 10 mins (3 times each) in the general transfer buffer containing 5mM EDTA. After washing off the EDTA from the gels using normal transfer buffer, conventional western blot transfer, blocking and antibody incubation steps were followed. For lysates that underwent phosphatase treatment, cells were lysed using 1X RIPA buffer (Thermo scientific Pierce ™ RIPA Buffer) containing 1X protease inhibitor cocktail-EDTA free (Sigma). Approximately 200-250mg of protein lysate was treated with 5U of FastAP alkaline phosphatase (ThermoFisher) for 1 hr at 37ºC.

Immunocytochemistry

Cells for immuno-fluorescence imaging were plated in 6 well cell culture plates (Corning Incorporated) on glass coverslips. Cells were fixed with 4% PFA for 10 mins and permeabilized with 0.1% Triton-X-100 for 10 mins followed by blocking with 10% BSA 5% NGS for 45 mins at RT. Cells were incubated with primary antibodies (diluted in 5% BSA and 2.5% NGS) overnight at 4ºC followed by washing with 1X PBS and incubated with AlexaFluor (Thermo Fisher) conjugated secondary antibodies in the dark for 1 hour. Following the washing step, the cells were stained with .1ug/mL DAPI for 5 mins (Thermo Fisher) and mounted on the slides using Fluoromount (Southern-Biotech). Imaging was carried out using a Nikon C2 confocal microscope.

For p-TBK1 centrosomal intensity analysis, a different permeabilization method was performed. Cells were permeabilized with 100% ice cold methanol in the refrigerator for 10 mins. For mitotic index, multinucleated cell count, and cytokinetic cell count random fields of view were captured for each genotype to sample approximately 1000 cells for each biological replicate (n=3). Mitotic cells were identified by chromosome condensation, kinetochore staining by CREST and verified by α-tubulin morphology. For mitotic defects analysis random fields of view were captured for each genotype to sample approximately 50 mitotic cells per biological replicate, and for cytokinetic defects analysis, random fields of view were captured for each genotype to sample approximately 30 cytokinetic cells per biological replicate.

Cell viability assay for growth curve

Approximately, 200 to 400 cells were plated (4 wells/genotype) in white-coated 96-well plates (Brand Tech Scientific) in growth media. Cell growth curve was obtained by CellTiter-Glo® Luminescent Cell Viability Assay (Promgea) using a luminescence reader every 24 hours. Mean cell number corresponding to the luminescence on each day was normalized to the first day in the graph.

Immunoprecipitation

Cells were lysed with the following lysis buffer: 50 mM Tris/HCl pH 7.5, 150 mM NaCl, 1 mM EGTA, 1 mM EDTA, 0.5(v/v) NP-40, 1 mM sodium orthovanadate, 50 mM NaF, 5 mM sodium pyrophosphate, 0.27 M sucrose, 10 mM Na 2-glycerophosphate, 0.2 mM phenylmethylsulphonyl fluoride, 1x protease/phosphatase inhibitor cocktail (Pierce), and 50 mM iodoacetamide. Cells were incubated for 20 minutes end over end at 4^{o}C then spun at 16,000 x *g* for 15 minutes at 4^{o}C. Supernatant was measured using the Dc^{TM} protein assay (Bio-Rad). 500 ug of protein was incubated on magnetic beads (FLAG M2 beads (Sigma), GFP beads (Chromotek)) end over end at 4^{o}C for 2 hrs. For endogenous IPs, supernatant was precleared on TrueBlot Protein G magnetic beads (Rockland) for 30 min at 4^{o}C. 1.2 mg of protein was incubated with 2uL of TBK1 antibody for 1hr at 4^{o}C (#3013S, Cell Signaling). Magnetic beads were added for 1hr at 4^{o}C. 2X LDS with 50mM DTT was used to elute protein off the beads, and pH was restored with NaOH.

Transfection

HEK293T cells were plated on poly-d-lysine coated dishes and reverse transfected with 1:1 jetOPTIMUS transfection reagent (Polyplus). Cells were treated the next day with 100ng/ml nocodazole (Sigma) and collected 16hrs later. HeLa cells were reverse transfected with 1:3 or 1:6 XtremeGENE 9™ (Roche) transfection reagent according to the manufacturer's instructions.

qPCR

RNA was isolated using Trizol Reagent (Ambion Life Technologies) and converted to cDNA using iScript™ (Bio-Rad) per the manufacturer's directions. SYBR Green Supermix (Bio-Rad),

20 ng of cDNA and 0.4 μM of each primer set was mixed in a 10 μl RT-PCR reaction that was ran on the CFX96 System (Bio-Rad). The primers that were used span exons: Actin F: 5' CCCGCCGCCAGCTCACCAT 3', R: 5' CGATGGAGGGGAAGACGGCCC 3'. TANK F: 5' AGCAAGGAGTCTTGGCAGTC 3', R: 5' GCACTGTGTTTCAGTTGCAGT 3'. SINTBAD F: 5' ACCAGTTCCAGCATGAGTTACA 3', R: 5' TCTCCCTCAGCTCTGTCTCC 3'. AZI2 F: 5' AGGTGGAAACTCAGCAGGTG 3', R: 5' ATGGATCCGTTTGTTTGGCT 3'. IL6 F: 5' AGCCACTCACCTCCTCAGAACGAA 3', R: 5' AGTGCCTCTTTGCTGCTTTCACAC 3'. TNF-α F: 5'TCAATCGGCCCGACTATCTC 3', R: 5' CAGGGCAATGATCCCAAAGT 3'. IL-10 F: 5'AAGACCCAGACATCAAGGCG 3', R: 5' CAGGGAAGAAATCGATGACAGC 3'. RT-PCR was performed in triplicate wells from three independent biological experiments. Expression levels were normalized to β-actin and fold change was determined by comparative C_T method.

Statistical analysis

For comparisons between two groups, a student's t-test was used to determine statistical significance. Ordinary one-way ANOVA followed by Tukey's multiple comparisons were used for three or more groups using GraphPad Prism software. Additional details are available in the figure legends. Differences in means were considered significant if $p < 0.05$ and designated as the following $p<0.05$ - *; $p< 0.01$ - **; $p< 0.001$ - ***. $p<.0001$ - ****; ns – not significant.

Acknowledgments:

We thank Dr. Daniela Cimini and Mathew Bloomfield for advice, reagents, and their expertise. The authors declare no competing financial interests.

Funding:

National Institutes of Health Grants GM142368 (AMP)
Departmental startup funds (AMP)

Author contributions:

Conceptualization: AMP; Planning and methodology: SP, SAS, AO, AMP; Experimentation: SP, SAS, KN, LZ, SRB, LEF, ND, AO, AMP; Data Analysis: SP, SAS, KN, TMY, JMJ, EMH, AO, AMP; Reagents: SAS; Computational Software for Analysis: LCC; Writing – original draft: SP, AMP; Writing – review & editing: SP, SAS, AO, AMP; All authors have read and approved the manuscript.

Competing interests:

The authors declare that the research was conducted in the absence of any commercial or financial relationships that could be construed as a potential conflict of interest.

Data and materials availability:

MS data will be submitted to MassIVE Repository. Constructs used for this study will be available through Addegene.org. Raw western blotting images will be deposited on Mendeley Data. All other reagents, data, and material requests will be fulfilled by the corresponding author, Alicia M. Pickrell, Ph.D. All data are available in the main text or the supplementary materials.

Figures

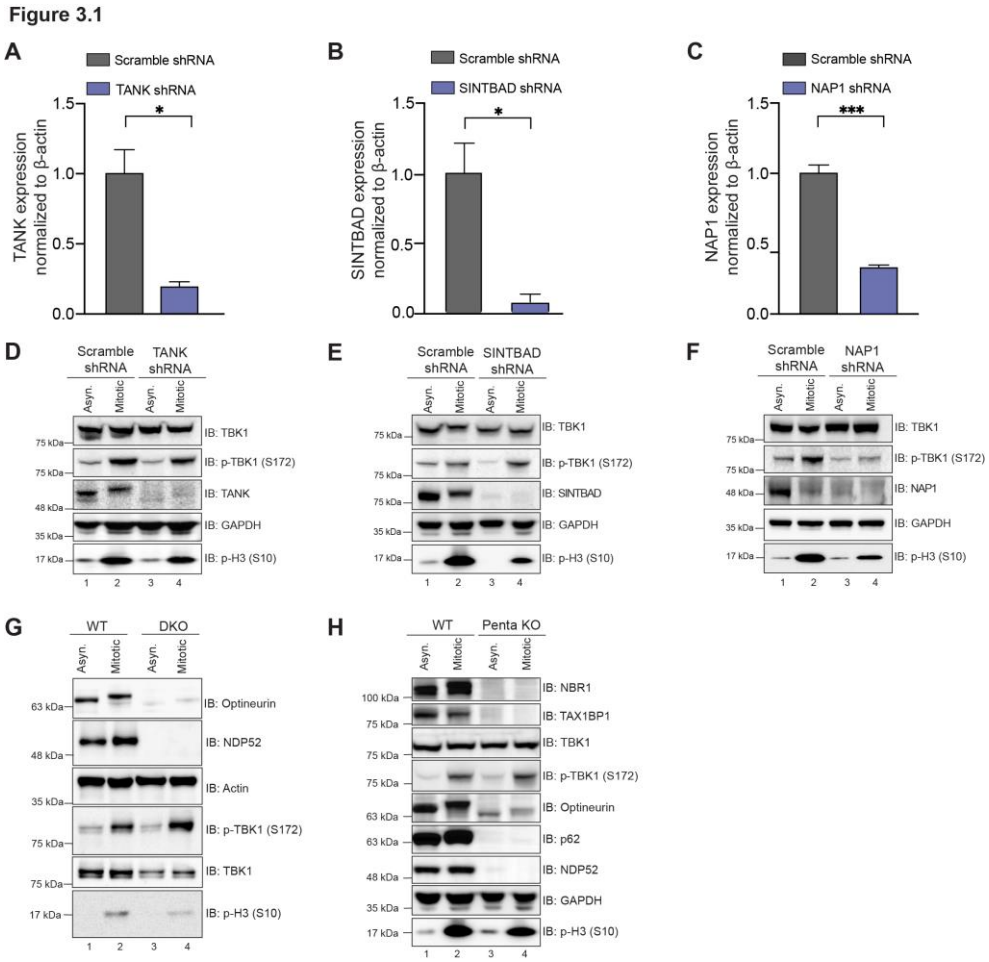

Fig. 3.1. Other known TBK1 adaptors except NAP1 are not required for TBK1 activation during mitosis.

(**A-C)** qRT-PCR showing relative expression of TANK1 **(A)**, SINTBAD **(B)** and NAP1 **(C)** mRNA levels normalized to β-actin in HeLa cells stably expressing shRNAs. N=3 independent experiments. Error bars ±SEM. **(D-F)** Western blot analysis of p-TBK1 in asynchronous and synchronized mitotic cells from scramble control, and cell lines stably expressing TANK **(D)**, SINTBAD **(E)**, and NAP1 **(F)** shRNAs, respectively. Nocodazole was used for cell synchronization. **(G)** Western blot analysis of p-TBK1 levels during mitosis in NDP52/optineurin DKO and parental HeLa cells in asynchronous and mitotic conditions. Nocodazole was used for cell synchronization. **(H)** Western blot analysis of p-TBK1 levels during mitosis in HeLa and Penta KO HeLa cells lacking NBR1, TAX1BP1, optineurin, NDP52, p62 in asynchronous and mitotic cells. Nocodazole was used for cell synchronization.

Unpaired Student's t-test was performed for all statistical analysis. * p < .05, *** p <.001.

Figure 3.2

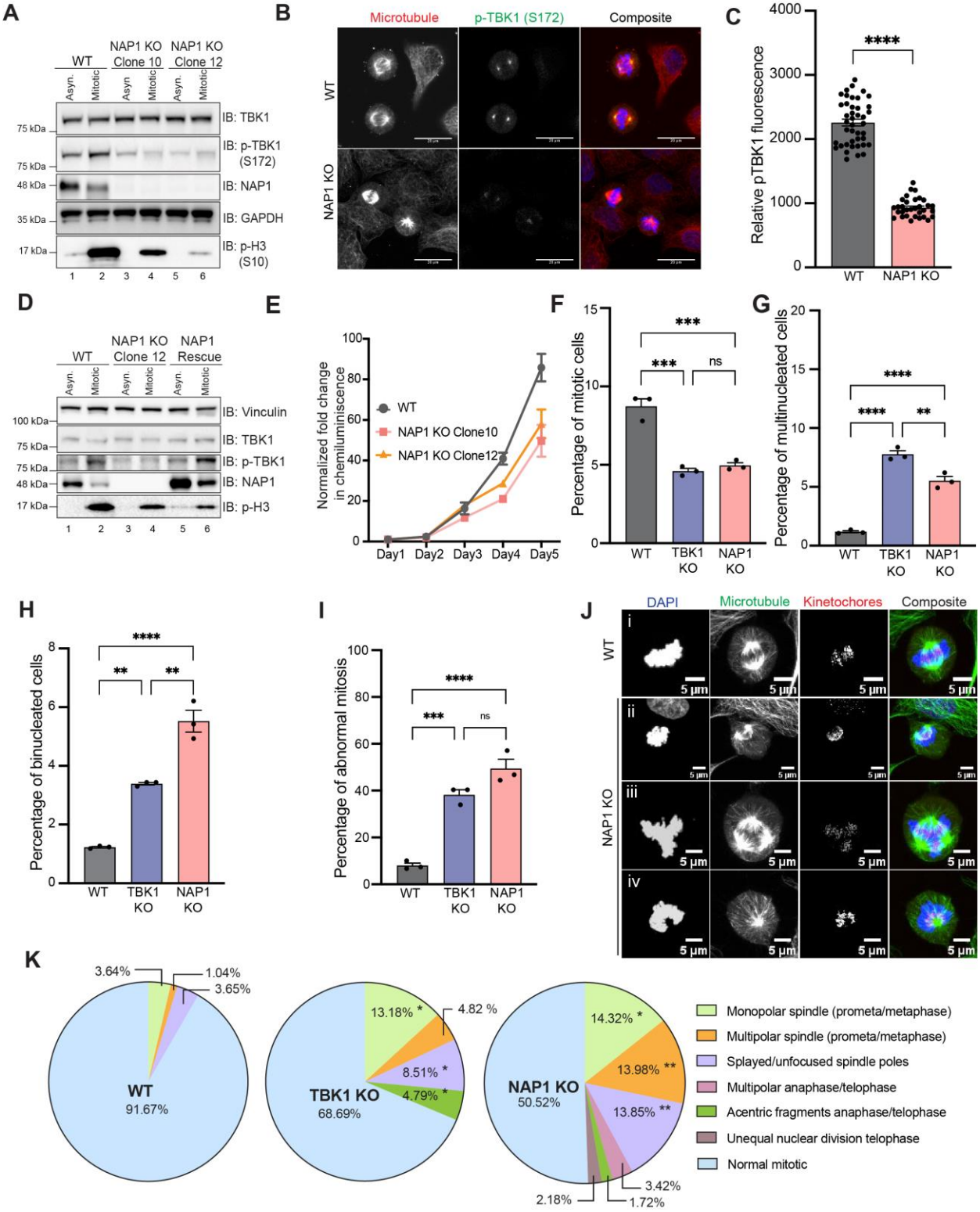

Fig. 3.2. NAP1 KO cells have mitotic defects similar to those lacking TBK1.

(A) Western blot analysis of p-TBK1 in asynchronous and mitotic cells from WT HeLa, NAP1 KO clone 10, and NAP1 KO clone 12. Nocodazole was used for cell synchronization at mitosis.

(B) Representative confocal images of p-TBK1 expression on mitotic centrosomes from WT HeLa and NAP1 KO cells. DAPI (blue) was used as a nuclear counterstain (on composite image), α-tubulin for cytoskeleton staining (red), and p-TBK1 S172 conjugated 488 (green). Scale bar - 20 μm.

(C) Relative intensity of p-TBK1 on centrosomes of mitotic cells from WT HeLa and NAP1 KO cells. 40-50 mitotic cells per group were quantified from 2 biological replicates. Error bars indicate ±SEM.

(**D)** Western blot analysis of p-TBK1 in asynchronous and synchronized mitotic cells from HeLa, NAP1 KO clone 12, and the stable NAP1 rescue line. RO-3306 was used for cell synchronization prior to mitotic release.

(**E**) Growth curve with normalized luminescence for WT HeLa cells, NAP1 KO clone 10 and NAP1 KO clone 12. Error bars indicate ±SD for technical replicates.

(**F-I)** Mitotic (F), multinucleated (G), binucleated (H), and abnormal mitotic (I) percentage cell counts from an asynchronous population of WT HeLa, TBK1 KO, and NAP1 KO cells. Error bars indicate ±SEM; n=3 independent experiments. For mitotic index, multinucleated, and binucleated cell counts, random fields of view were captured sampling approximately 1000 cells per biological replicate from each genotype. For abnormal mitotic cell counts, random fields of view were captured to sample approximately 50 mitotic cells per biological replicate from each genotype.

(**J)** Representative confocal images of (i) normal metaphase, and defective mitotic cells found in NAP1 KO (ii) splayed/unfocused spindle (iii) multipolar prometaphase, and (iv) monopolar prometaphase/metaphase cells. DAPI (blue) was used as a nuclear counterstain, α-tubulin for cytoskeleton staining (green), and CREST for kinetochore staining (red). Scale bar, 5 μm.

(**K**) Pie charts representing the percentage of different types of mitotic defects found in WT HeLa, TBK1 KO, and NAP1 KO cells. At least 50 mitotic cells per biological replicate from each genotype were analyzed. n=3 independent experiments.

One way ANOVA was performed for all statistical analysis. * $p < .05$, ** $p < .01$, *** $p < .001$, **** $p < .0001$, ns = not significant.

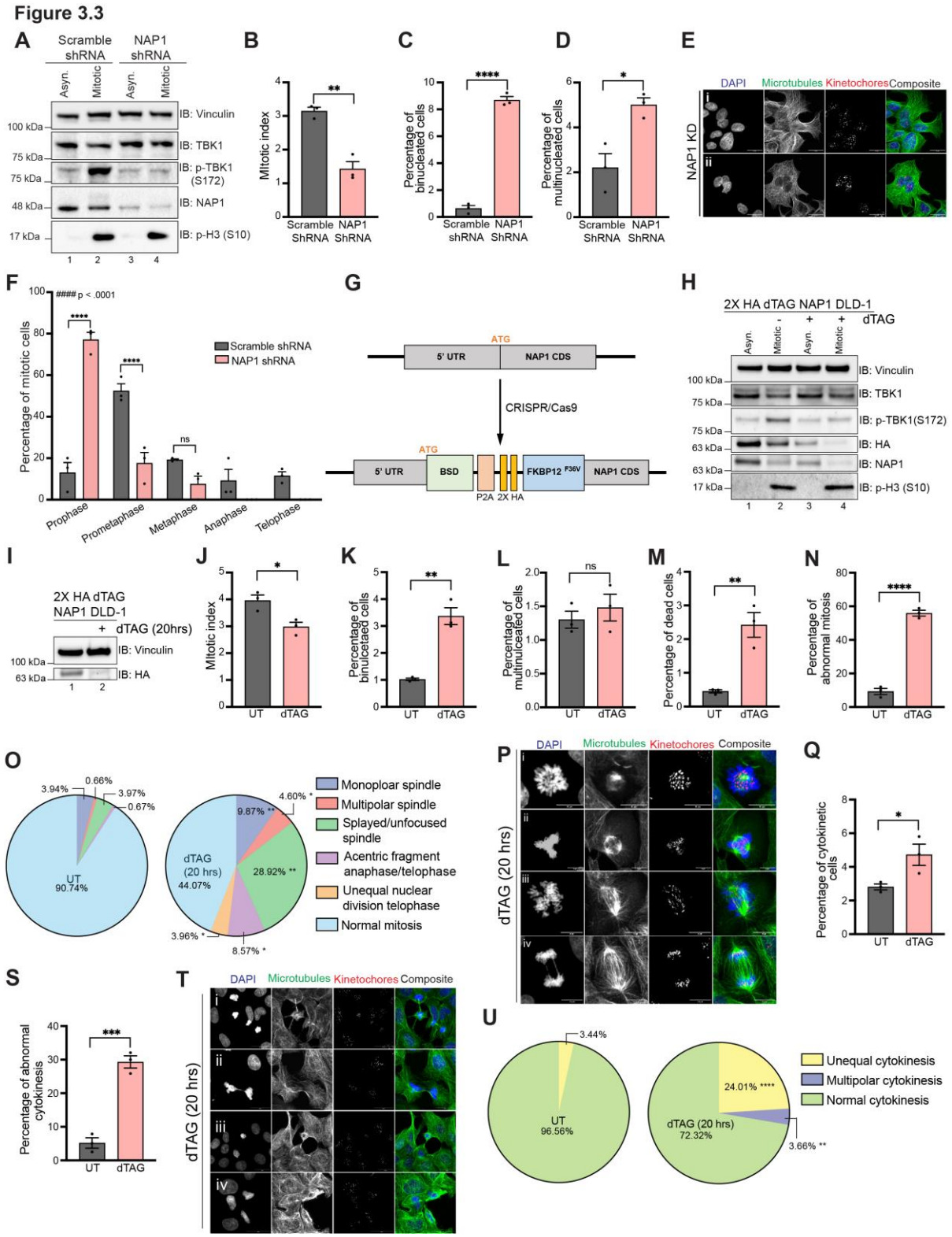

Fig. 3.3. NAP1 loss in a near diploid cell line causes mitotic and cytokinetic defects. (A) Western blot analysis of p-TBK1 in asynchronous and mitotic cells from scramble control and transient NAP1 shRNA KD in DLD-1 cells over 36 hours. RO-3306 was used for cell

synchronization prior to mitotic release. (**B-D)** Mitotic (B), multinucleated (C), and binucleated (D) cell count percentages from an asynchronous population of scramble control and transient NAP1 KD DLD-1 cells. Error bars indicate ±SEM; n=3 independent experiments. Random fields of view were captured sampling approximately 800 cells per biological replicate from each category. (**E**) Representative confocal images of NAP1 KD cells: (i) binucleated, (ii) multinucleated examples. DAPI (blue) was used as a nuclear counterstain, α-tubulin for cytoskeleton staining (green), and CREST for kinetochore staining (red). Scale bar, 20 μm. (**F**) Mitotic stage frequency distribution of scramble control and NAP1 KD DLD-1 cells. Error bars indicate ±SEM; n=3 independent experiments. Random fields of view were captured sampling approximately 800 cells per biological replicate from each category. Unpaired Student's t-test was performed for all statistical analysis (B-D, F). For (F), Student's t-test compared the difference between groups in split in each phase of mitosis. * $p < .05$, ** $p < .01$, **** $p < .0001$, ns = not significant. Kolmogorov-Smirnov nonparametric test was used to analyze the differences between the distribution between groups #### $p < .0001$. **(G)** Cartoon diagram of dTAG knock-in construct designed to add $FKBP12^{F36V}$ to the N-terminus of NAP1. **(H)** Western blot analysis of p-TBK1 and NAP1 levels in asynchronous and mitotic cells from $FKBP12^{F36V}$-NAP1 DLD-1 cells. RO-3306 was used for cell synchronization prior to mitotic release**.** Cells were treated with $dTAG^{V}$-1 for 3 hrs in asynchronous conditions and 3 hrs prior and during release in mitotic conditions. **(I)** Western blot analysis of NAP1 levels in asynchronous cells with or without $dTAG^{V}$-1 treatment for 20 hours. (**J-N)** Mitotic (D), multinucleated (E), binucleated (F), dead (G) and abnormal mitotic (H) cell count percentages from an asynchronous population of $FKBP12^{F36V}$-NAP1 DLD-1 cells untreated or treated with 20 hrs of $dTAG^{V}$-1. Error bars indicate ±SEM; n=3 independent experiments. For mitotic index, multinucleated, and binucleated cell counts, random fields of view were captured sampling approximately 800-900 cells per biological replicate from each genotype. For abnormal mitotic cell counts, random fields of view were captured to sample approximately 50 mitotic cells per biological replicate from each genotype. (**O**) Pie charts representing the percentage of different types of mitotic defects found in untreated and $dTAG^{V}$-1 treated (20 hrs) $FKBP12^{F36V}$-NAP1 DLD-1 cells. At least 50 mitotic cells per biological replicate from each genotype were analyzed. n=3 independent experiments. **(P)** Representative confocal images of mitotic defects seen in DLD-1 cells after 20hrs of $dTAG^{V}$-1 treatment: (i) monopolar spindle, (ii) multipolar spindle, (iii) unfocused spindle poles (iv) acentric fragment during anaphase. DAPI (blue) was used as a nuclear counterstain, α-tubulin for cytoskeleton staining (green), and CREST for kinetochore staining (red). Scale bar, 20 μm.**(Q-S)** Cytokinetic (K) and abnormal cytokinetic (L) cell count percentages from untreated and treated (20 hrs) $FKBP12^{F36V}$-NAP1 cells. Error bars indicate ±SEM; n=3 independent experiments. Random fields of view were captured sampling approximately 800-900 cells per biological replicate from each genotype. **(T)** Representative confocal images of cytokinetic defects seen in $FKBP12^{F36V}$-NAP1 DLD-1 cells after 20hrs of $dTAG^{V}$-1 treatment: (i-ii) unfinished and incomplete cytokinesis, (iii) unequal cytokinesis, (iv)

multipolar cytokinesis. DAPI (blue) was used as a nuclear counterstain, α-tubulin for cytoskeleton staining (green), and CREST for kinetochore staining (red). Scale bar, 20 μm. Student's t-test was performed for all statistical analysis. * p < .05, ** p < .01, *** p <.001, **** p <.0001, ns = not significant **(U)** Pie chart representing the percentage of different types of cytokinetic defects found in untreated and dTAG^{V}-1 treated (20 hrs) FKBP12^{F36V}-NAP1 DLD-1 cells. Random fields of view were captured sampling approximately 30-40 cytokinetic cells per biological replicate from each genotype.

Figure 3.4

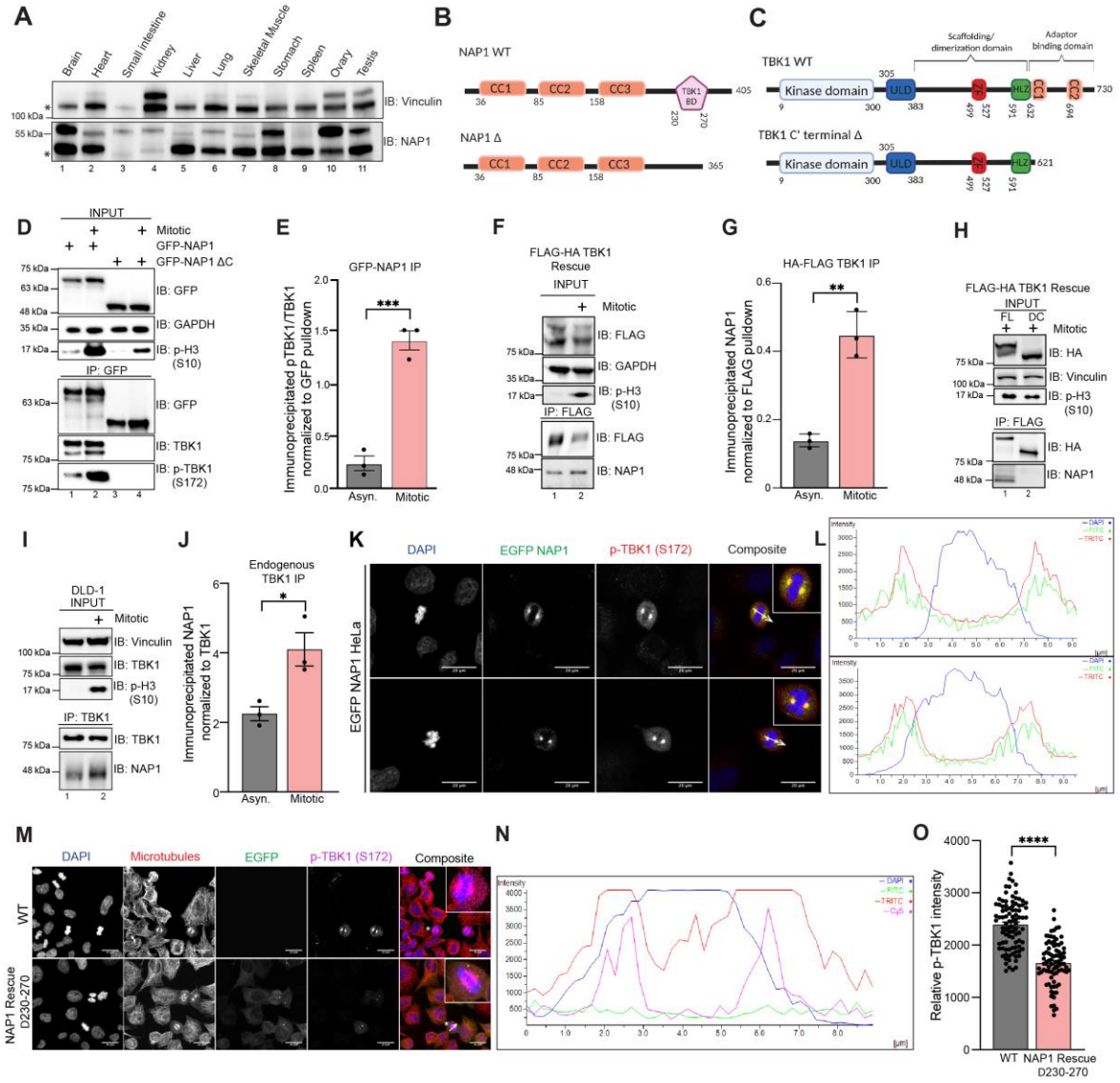

Fig. 3.4. NAP1 binds to TBK1 during mitosis and is localized to centrosomes.

(A) Western blot analysis of multiple different human tissue samples probed for NAP1. Vinculin was used as a loading control. * Indicates non-specific bands.

(B) Cartoon representing protein domains of full length (FL) NAP1, and NAP1 lacking the TBK1 binding domain (Δ230-270).

(C) Cartoon representing protein domains of full length (FL) TBK1, TBK1 lacking adaptor binding domain (Δ C' terminal).
(**D)** Representative immunoblots of the pulldown of transiently expressed GFP-NAP1 or GFP-NAP1 Δ230-270 (lacking TBK1 binding domain) in asynchronous and synchronized mitotic HEK293T cells. Nocodazole was used for cell synchronization.
(E) Quantification of the ratio of pTBK1/TBK1 signal after normalization to the pulldown efficiency. Error bars indicate ±SEM; n = 3 independent experiments.
(**F)** Representative immunoblots of the pulldown of HA-FLAG TBK1 in asynchronous and synchronized mitotic TBK1 rescue HeLa cells. Nocodazole was used for cell synchronization.
(G) Quantification of the ratio of NAP1 signal after normalization to the pulldown efficiency of TBK1. Error bars indicate ± SEM; n = 3 independent experiments.
(**H)** Representative immunoblots of the pulldown of HA-FLAG TBK1 and HA-FLAG TBK1 Δ C' (lacking adaptor binding domain) in synchronized mitotic TBK1 rescue HeLa cells. Nocodazole was used for cell synchronization.
(I) Representative immunoblots of the pulldown of endogenous TBK1 in asynchronous and synchronized mitotic DLD-1 cells. Nocodazole was used for cell synchronization.
(J) Quantification of the ratio of endogenous NAP1 signal after normalization to the pulldown efficiency of TBK1. Nocodazole was used for cell synchronization. Error bars indicate ± SEM; n = 3 independent experiments.
(**K)** Representative confocal images of HeLa cells transiently expressing EGFP-NAP1 with immunocytochemical detection of p-TBK1 (red). DAPI (blue) was used as a nuclear counterstain. White arrow depicts area used for line scan analysis in (H). Scale bar = 20μm.
(L) Line scan analysis of images in (K) generated from Nikon Elements software.
(M) Representative confocal images of WT HeLa and stable EGFP NAP1 Δ230-270 rescue cells with immunocytochemical detection of p-TBK1 (magenta). DAPI (blue) was used as a nuclear counterstain, and α-tubulin for cytoskeleton staining (red). Scale bar = 20 μm.
(N) Line scan analysis of images in (M) generated from Nikon Elements software.
(O) Relative intensity of pTBK1 on centrosomes of mitotic cells from WT HeLa and stable EGFP NAP1 Δ230-270 rescue cells. 40-50 mitotic cells per group were quantified from 2 biological replicates. Error bars indicate ±SEM.
Unpaired Student's t-test was performed for all statistical analysis. * $p < .05$, ** $p < .01$, *** $p < .001$, **** $p < .0001$

Figure 3.5

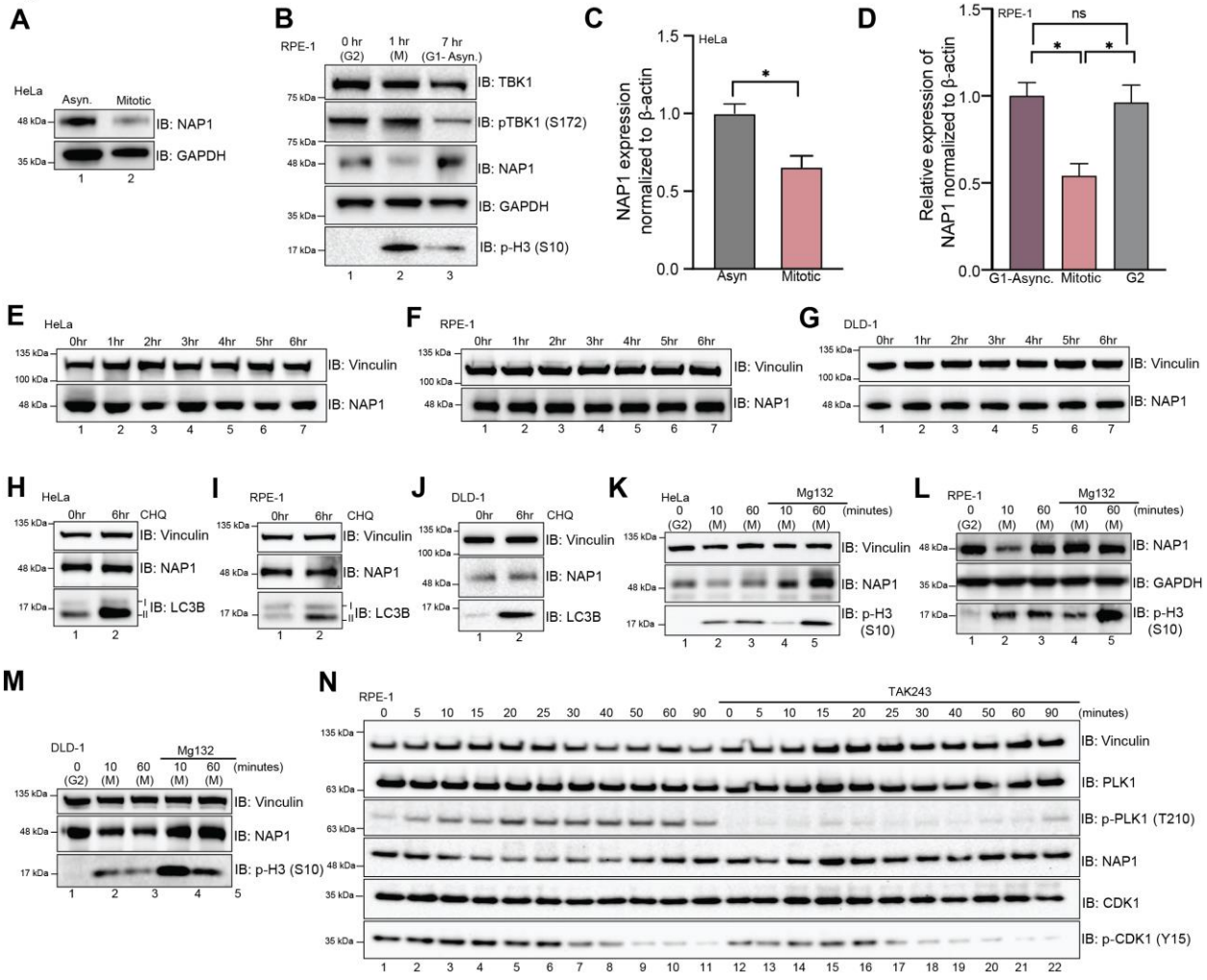

Fig. 3.5. NAP1 protein expression is cell cycle regulated.

(A) Western blot analysis of NAP1 in asynchronous and synchronized mitotic cells from WT HeLa cells. Nocodazole was used for cell synchronization at mitosis.

(**B**) Western blot analysis of NAP1 in G2, mitotic, and G1-asynchrnous RPE-1 cells. RO-3306 was used for cell synchronization prior to mitotic release**.**

(C) NAP1 mRNA expression normalized relative to Actin in asynchronous and synchronized mitotic HeLa cells. Nocodazole was used for cell synchronization at mitosis.

(D) NAP1 mRNA expression normalized relative to Actin in G2, mitotic, and G1-asyn RPE-1 cells. Error bars indicate ±SD; n = 3 independent experiments. Cells were synchronized at G2 using RO-3306. G2 cells were released for approximately 45-60 minutes to collect mitotic, and for approximately 7 hours to collect G1 samples.

(**E-G)** Western blot analysis of NAP1 protein levels after cycloheximide treatment up to 6 hours in HeLa (D), RPE-1 (E), and DLD-1 (F) cells.

(H-J) Western blot analysis of NAP1 protein levels after 6 hrs of chloroquine treatment in HeLa (G), RPE-1 (H), and (I) cells.

(**K-M)** Western blot analysis of NAP1 protein level after MG132 treatment followed by G2 release in HeLa (B), RPE-1 (C), and DLD-1 (D) cells. RO-3306 was used for cell synchronization prior to mitotic release.

(E) Western blot analysis of NAP1 after TAK243 treatment after G2 release in RPE-1 cells. RO-3306 was used for cell synchronization prior to mitotic release.

Student's t-test or one way ANOVA was performed for all statistical analysis. * $p < .05$, ns = not significant.

Figure 3.6

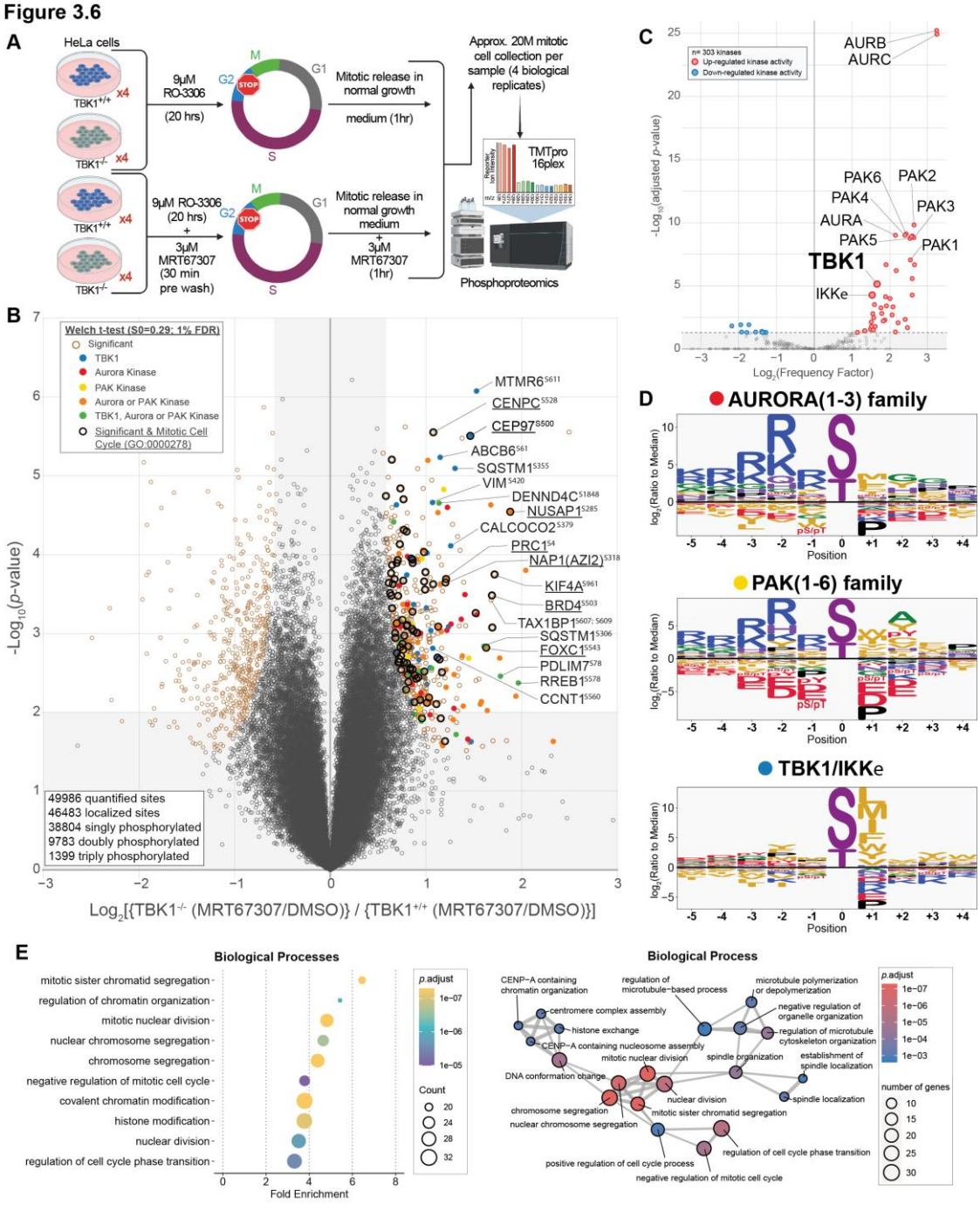

Fig. 3.6. ***Quantitative phospho-proteomics pipeline identifies the mitotic downstream substrates of TBK1.***

(A) Workflow for TMTpro-based phosphoproteomics of approximately 20M (million) mitotic cells. 16plex proteomics was performed in quadruplicate on samples harvested 1-hour post-mitotic release.
(B) Volcano plots [Log_{10} (*p*-value) versus Log_2 ratio] for representing phosphorylation sites that are affected by MRT67307 and loss of TBK1. Proteins are shown in black circles (non-significant) and red circle (Tier 1 significant). Circles were color coded for the motif that most likely fit TBK1 (blue), Aurora kinases (red), PAK kinases (yellow), Aurora or PAK kinases (orange), or all three (green). Bolded black circles categorize known mitotic proteins (GO:0000278). The inset indicated additional color coding for the statistical analysis.
(C) Volcano plot scoring each identified substrate against the 303 kinase motifs panel from (Johnson et al., 2022) to determine statistically significant enriched activated kinases.
(D) Motif analysis using the pLogo tool (plogo.uconn.edu) identifies the motif for the substrate candidates based on synthetic peptide analysis. The y-axis is the log odds of the binomial probability.
(E) Gene Ontology terms enrichment analysis among the Biological Processes for enriched phosphosites Tier 2. Mitotic and cell cycle related classes were significantly enriched (left panel). Enrichment map networks, each node represents a gene set (i.e., a GO term) and each edge represents the overlap between two gene sets (right panel).

Figure 3.7

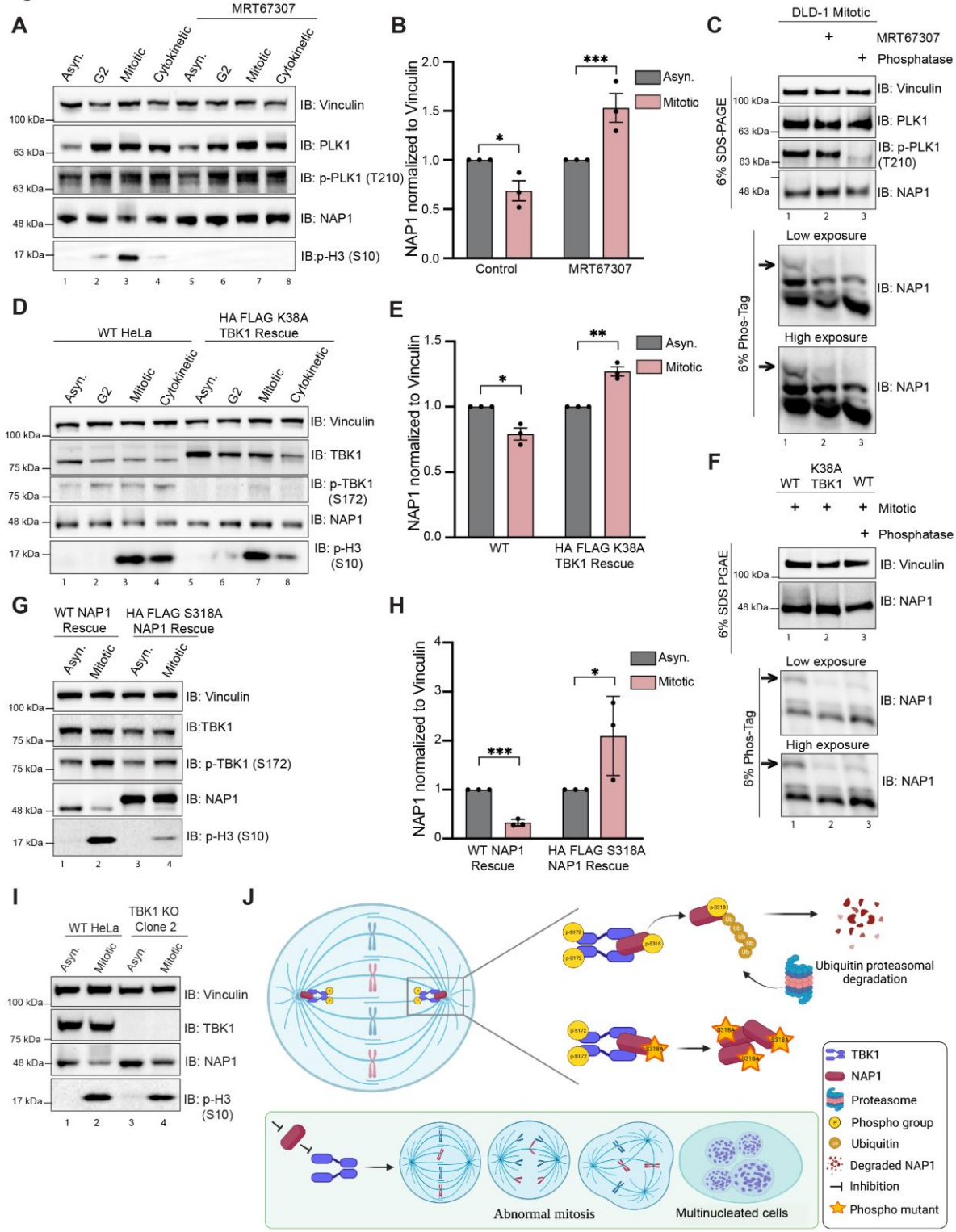

Fig. 3.7. TBK1 phosphorylation of NAP1 at S318 impacts its stability during mitosis.
(A) Representative immunoblots of asynchronous, G2, mitotic, and cytokinetic DLD-1 cells with or without TBK1 inhibitor treatment (MRT67307) for 1 hr prior to G2 and throughout release

timepoints. Asynchronous cells were treated for 2 hrs. Cells were synchronized at G2 using RO-3306. G2 cells were released for approximately 30-45 minutes to collect mitotic samples and for approximately 80-90 minutes to collect cytokinetic cells.
(B) Quantification of normalized NAP1 protein levels during asynchronous and mitotic conditions with or without MRT67307. Error bars indicate ±SEM; n=3 independent experiments.
(C) Phos-Tag gel analysis of NAP1 mitotic protein from DLD-1 cells either with MRT67307 for 1 hr prior to G2 and throughout release or with 1 hr phosphatase treatment. 6% SDS-PAGE gel was run in tandem to ensure equal protein loading.
(D) Representative immunoblots of asynchronous, G2, mitotic, and cytokinetic cells from WT HeLa and stable TBK1 K38A rescue lines. Cells were synchronized at G2 using RO-3306. G2 cells were released for approximately 30-45 minutes to collect mitotic samples and for approximately 80-90 minutes to collect cytokinetic cells.
(E) Quantification of normalized NAP1 protein levels during asynchronous and mitotic conditions in WT HeLa and stable TBK1 K38A rescue lines. Error bars indicate ±SEM; n=3 independent experiments.
(F) Phos-Tag gel analysis of NAP1 mitotic protein from HeLa, K38A TBK1 rescue, and HeLa cells treated 1 hr with phosphatase. 6% SDS-PAGE gel was run in tandem to ensure equal protein loading.
(G) Representatives immunoblot analysis of NAP1 in asynchronous and mitotic cells from stable NAP1 and NAP1 S318A rescue lines. Cells were synchronized using RO-3306 prior to mitotic release.
(H) Quantification of normalized NAP1 protein levels during asynchronous and mitotic conditions in stable NAP1 rescue, and stable NAP1 S318A rescue lines. Error bars indicate ±SEM; n=3 independent experiments.
(I) Western blot analysis of NAP1 levels in HeLa and TBK1 KO cells in asynchronous and mitotic cells. Nocodazole was used for cell synchronization at mitosis.
(**J**) Cartoon representing mechanistic regulation of NAP1 and TBK1 during mitosis. NAP1 activates TBK1 on centrosomes by binding to its adaptor binding C' domain. Activated TBK1 phosphorylates NAP1 on S318 which acts as a signal for ubiquitin proteasomal degradation of NAP1. Loss of either of these centrosomal proteins, NAP1 or TBK1, impairs mitosis and cytokinesis leading to retention of multinucleated cells.
Unpaired Student's t-test was performed for all statistical analysis. * $p < .05$, ** $p < .01$, *** $p < .001$.

Supplementary Figures:

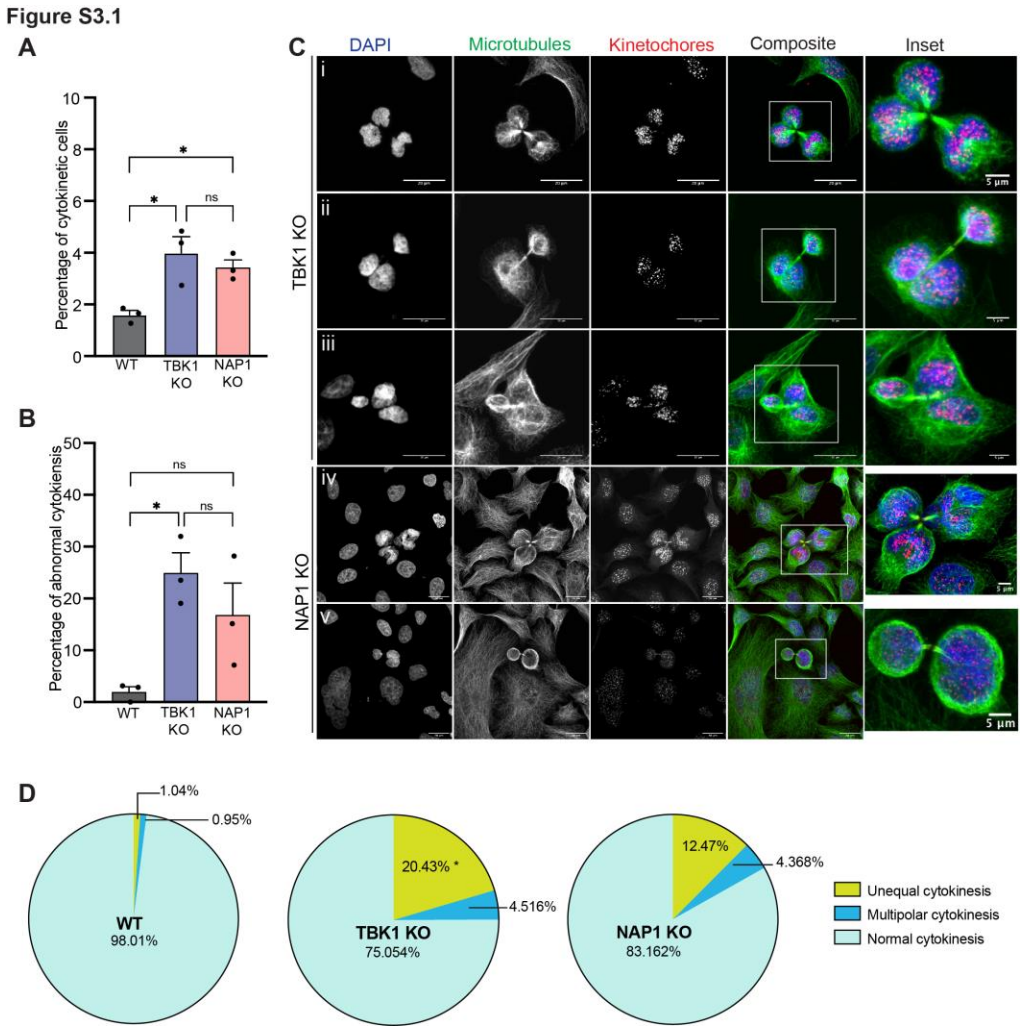

Fig. S3.1: Loss of NAP1 and TBK1 causes similar cytokinetic defects.

(A-B) Cytokinetic (A) and abnormal cytokinetic (B) cell count percentages from an asynchronous population of WT HeLa, TBK1 KO and NAP1 KO. Error bars indicate ±SD; n=3 independent experiments. Random fields of view were captured sampling approximately 1000 cells per biological replicate from each genotype.

(C) Representative confocal images of cytokinetic defects seen in TBK1 KO (i-iii) and NAP1 KO (iv-v): (i) multipolar cytokinesis, (ii) unequal cytokinesis, (iii) combination of unequal multipolar cytokinesis, (iv) multipolar cytokinesis, (v) unequal cytokinesis. DAPI (blue) was used as a nuclear counterstain, α-tubulin for cytoskeleton staining (green), and CREST for kinetochore staining (red). Scale bar, 20 µm, insets, 5µm.

(**D**) Pie chart representing the percentage of different types of cytokinetic defects found in HeLa, TBK1, and NAP1 KO cells. Random fields of view were captured sampling approximately 30-40 cytokinetic cells per biological replicate from each genotype. * $p < .05$ compared to HeLa. One way ANOVA was performed for all statistical analysis. * $p < .05$, ns = not significant.

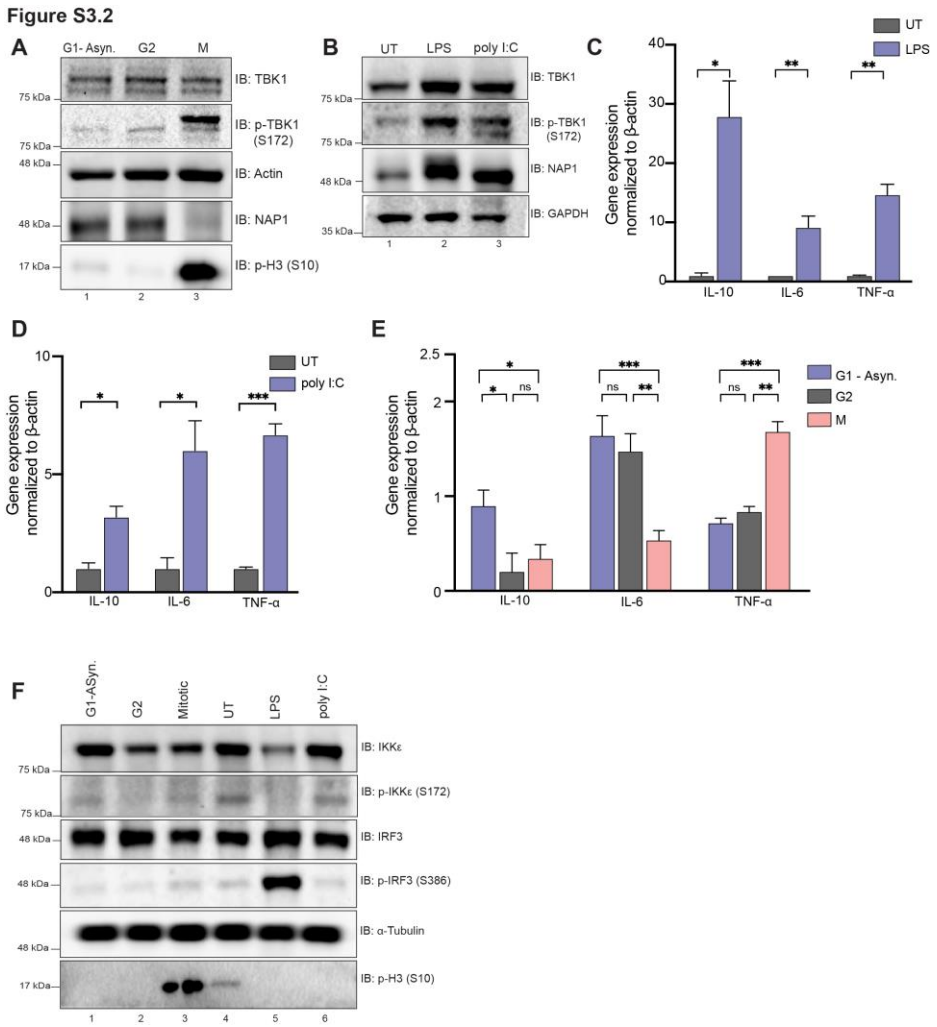

Fig. S3.2: Mitosis does not elicit an innate immune response.

(A) Western blot analysis of THP-1 cells synchronized at G2, M, or G1-Async to determine p-TBK1 levels. Cells were synchronized at G2 using RO-3306. G2 cells were released for approximately 45-60 minutes to collect mitotic cells and for approximately 7 hours to collect G1 samples. (**B)** Western blot analysis of THP-1 cells stimulated with LPS or poly I:C for 1 hrs and 8 hrs, respectively. Blots were probed for p-TBK1 and NAP1. Cells were synchronized using RO-3306. (**C-D)** Relative mRNA expression of cytokines upregulated during innate immunity normalized to β-actin when stimulated with LPS (C) for 1 hrs or poly I:C (D) for 8 hrs. Error bars indicate ±SD; n = 3 independent experiments. (**E)** Relative mRNA expression of cytokines during different cell cycle stages normalized to β-actin. Error bars indicate ±SD; n = 3 independent experiments. Cells were synchronized at G2 using RO-3306. G2 cells were released for approximately 45-60 minutes to collect mitotic and for approximately 7 hours to collect G1 samples. (**F)** Western blot analysis of p-IRF3 and p-IKKε of THP-1 cells synchronized at G2, M, or G1-Async or stimulated with LPS or poly I:C for 1 hrs and 8 hrs, respectively. Cells were synchronized at G2 using RO-3306. G2 cells were released for approximately 45-60 minutes to collect mitotic, and for approximately 7 hours to collect G1 samples. Student's t-test or one way

ANOVA was performed for all statistical analysis. * p < .05, ** p < .01, *** p <.001, ns = not significant.

Figure S3.3

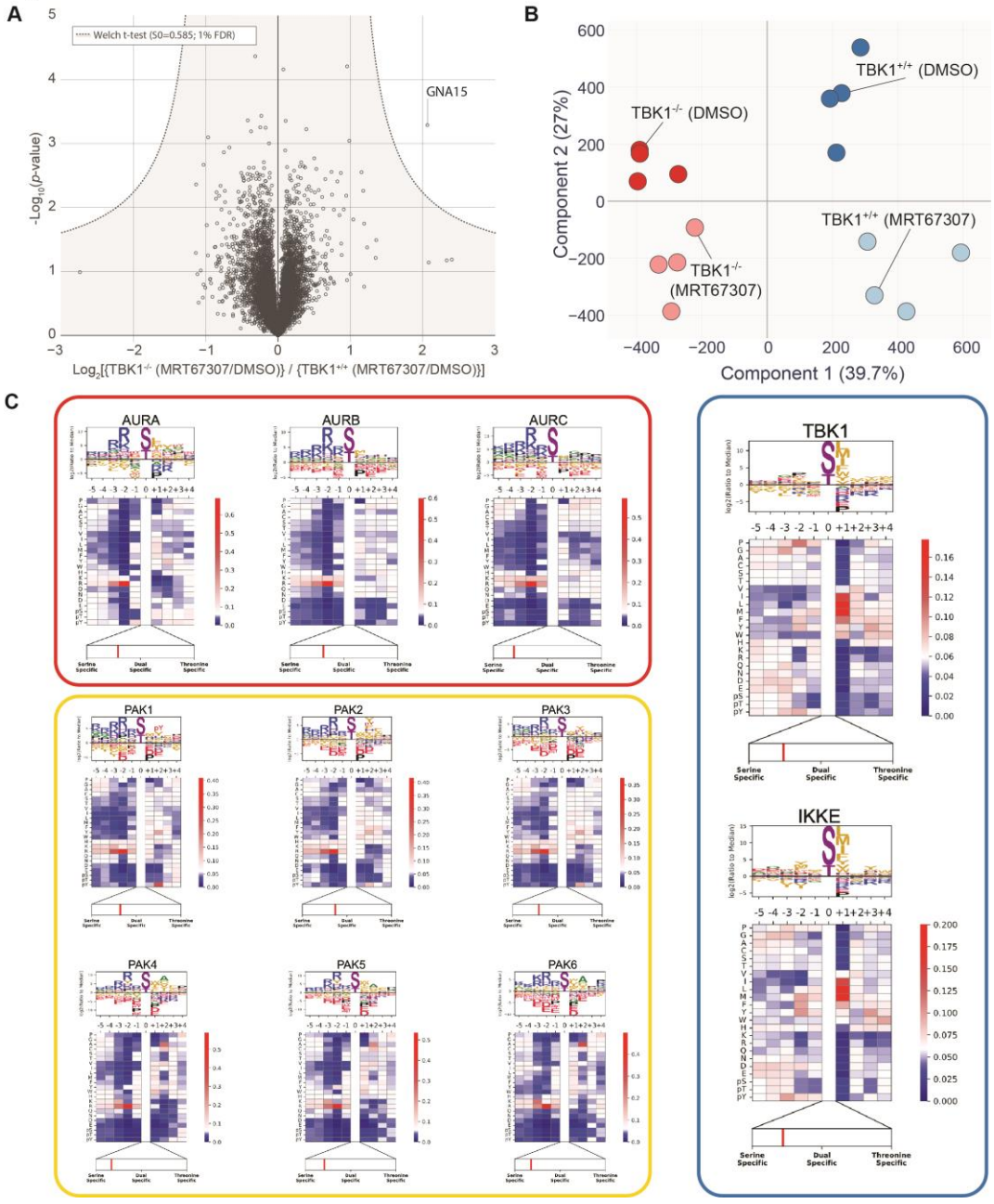

Fig. S3.3: Quantitative proteomics pipeline identifies downstream substrates regulated upon mitosis. (A) Volcano plots [Log10 (p-value) versus Log2 ratio] representing protein abundance that are affected by MRT67307 and loss of TBK1. Proteins are shown in black circles. The inset indicated additional color coding for the statistical analysis. **(B)** Principal component analysis (PCA) of the phosphoproteome data. Replicate samples are shown separately. 39.7% of the changes in phospho abundance are provided by Component 1, which represents the genetic background component, while 27% of the change are provided by

component 2, which represents the small molecule inhibitor treatment. **(C)** Individual motifs for experimentally derived substrate sequence specificity for Aurora family, PAK famliy, TBK1 and ε kinases. Data derived from (Johnson et al., 2022).

Figure S3.4

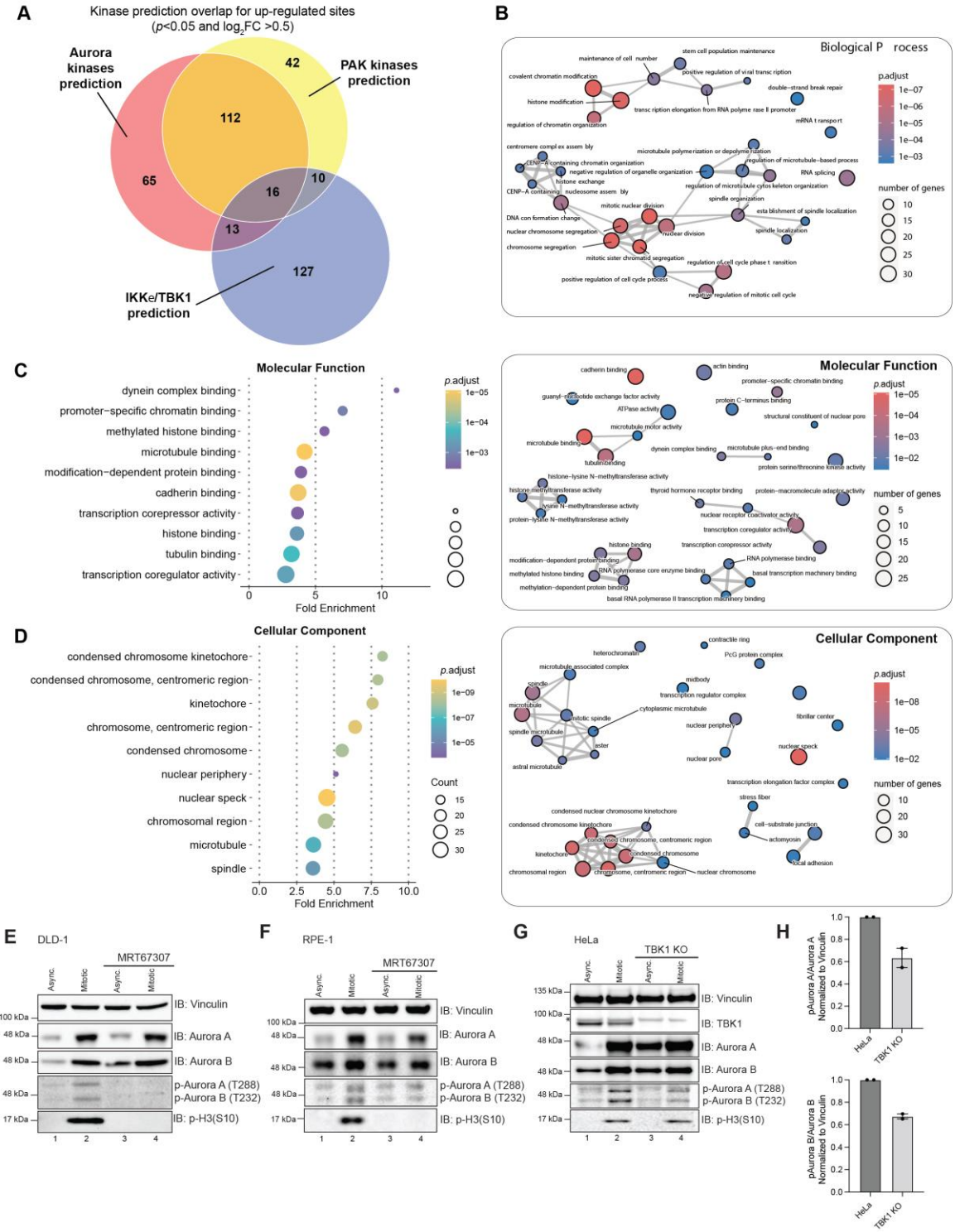

Figure S3.4: Identification of TBK1 downstream substrates upon mitosis.
(A) Venn diagram illustrating the kinase prediction overlap for up-regulated sites passing the *p*-value cutoff of $p<0.05$ and $\log_2$ ratio cutoff of +0.5. Related to Table S2.
(B-D) Gene Ontology terms enrichment analysis and associated enrichment map networks for enriched phosphor-sites (Tier 2). For enrichment map networks, each node represents a gene set (i.e., a GO term) and each edge represents the overlap between two gene sets.
(E-G) Western blot analysis of p-Aurora A (T288) and p-Aurora B (T232) in asynchronous and synchronized mitotic cells from DLD-1 (A) and RPE-1 (B) treated with MRT67307 or HeLa WT compared to TBK1 KO cells (C). Cells were synchronized at G2 using RO-3306 prior to mitotic release. MRT67307 treatment occurred 1 hr prior to G2 and throughout release. Asynchronous cells were treated for 2 hrs.
(H) Densitometry quantification of HeLa WT and TBK1 KO cells synchronized in mitosis (G) for p-Aurora A (T288) and p-Aurora B (T232) normalized to Aurora A and B and vinculin levels for 2 experimental replicates. One dot equals one replicate.

Figure S3.5

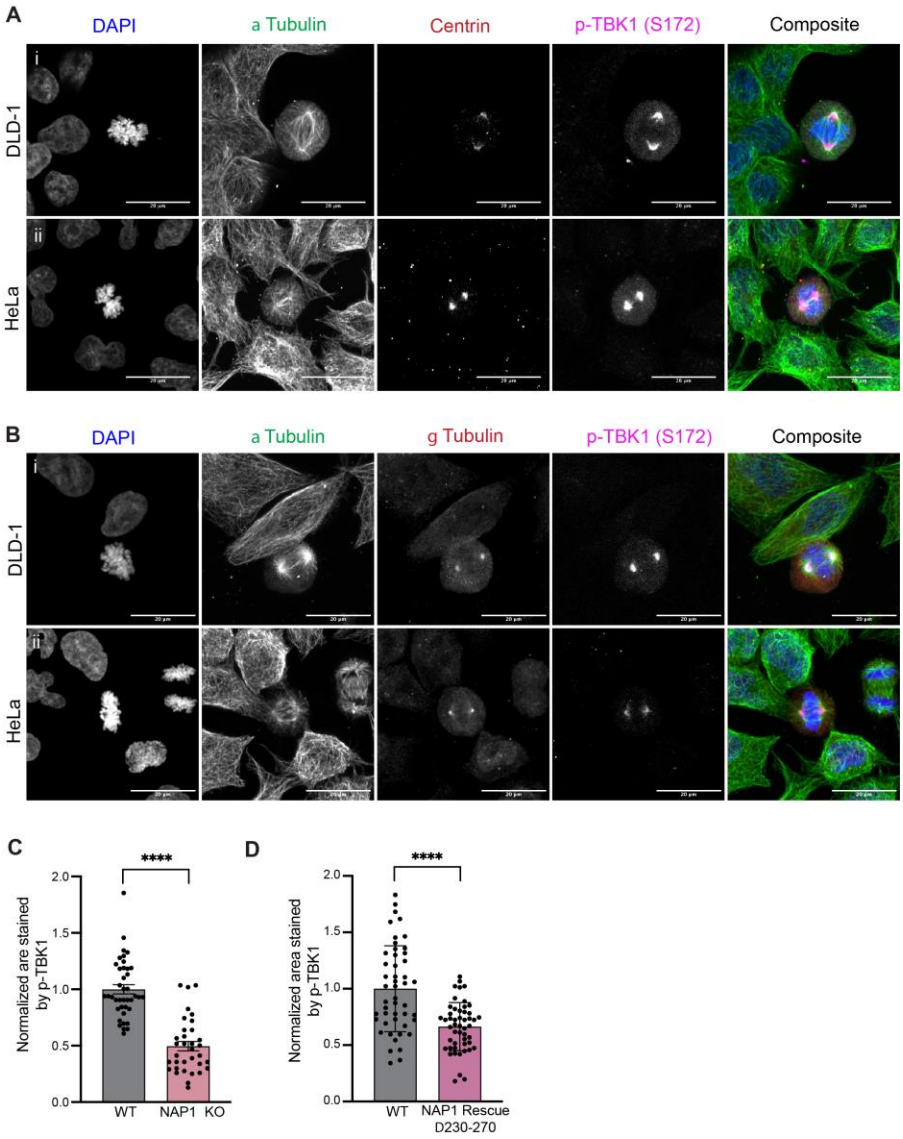

Figure S3.5: Activated TBK1 is not confined to only centrosomes.

(**A**) Representative confocal images of Centrin (red) and p-TBK1 (magenta) staining in (i) DLD-1, (ii) HeLa cells. DAPI (blue) was used as a nuclear counterstain, and α-tubulin for cytoskeleton staining (green). Scale bar, 20 μm. (**B**) Representative confocal images of g-tubulin (red) and p-TBK1 (magenta) staining in (i) DLD-1, (ii) HeLa cells. DAPI (blue) was used as a nuclear counterstain, and α-tubulin for cytoskeleton staining (green). Scale bar, 20 μm. **(C)** Relative area of p-TBK1 staining around centrosomes of mitotic cells from WT HeLa and NAP1 KO. 40-50 mitotic cells per group were quantified from 2 biological replicates. Error bars indicate ±SEM. **(D)** Relative area of p-TBK1 staining around centrosomes of mitotic cells from WT HeLa and stable EGFP NAP1 Δ230-270 rescue cells. 40-50 mitotic cells per group were quantified from 2 biological replicates. Error bars indicate ±SEM. Students' t-test was performed for all statistical analysis. **** $p < .0001$.

Chapter 4

Impaired autophagy results in the formation of micronuclei driven by mitotic errors due to the abnormal activation of TBK1

This manuscript is in preparation for journal submission.

Impaired autophagy results in the formation of micronuclei driven by mitotic errors due to the abnormal activation of TBK1

Short title: Impaired autophagy results in chromosomal instability

Swagatika Paul[1], Nicole DeFoor[2,3], Leila Zavar[2], Sahitya Ranjan Biswas[3], Yairis Soto[2], and Alicia M. Pickrell[2*]

Affiliations

[1]Graduate Program in Biomedical and Veterinary Sciences, Virginia-Maryland College of Veterinary Medicine, Blacksburg, VA 24061 USA.

[2]School of Neuroscience, Virginia Polytechnic Institute and State University, Blacksburg, VA 24061 USA.

[3]Translational Biology, Medicine, and Health Graduate Program, Virginia Polytechnic Institute and State University, Roanoke, VA 24016 USA.

[*]Correspondence should be addressed to:
Alicia M. Pickrell, Life Science I Room 217, 970 Washington Street SW, Blacksburg, VA 24061
Tel: 540-232-8465; Email: alicia.pickrell@vt.edu

Abstract
Micronuclei, a hallmark of tumorigenesis, are formed during cell division when acentric fragments or lagging chromosomes cannot be incorporated into the primary nucleus before the nuclear envelope forms. Previous studies indicated that autophagy may reduce chromosomal instability (CIN) by clearing these isolated, atypical micronuclei and degrading them in the lysosome. In this study, we evaluated whether impaired autophagy contributes to chromosomal instability and surprisingly found that the loss of autophagy proteins facilitates the formation of micronuclei. Our results demonstrate that cells lacking FIP200 or ATG9A contain a significantly higher number of micronuclei. Furthermore, blocking autophagy initiation with PI4K inhibitors also results in significantly higher number of micronuclei. The fact that micronuclei appeared after one division period in our pharmacological experiments suggested that loss of ATG9A could promote mitotic errors leading to the accumulation of micronuclei. Interestingly, genetic, and pharmacological inhibition of autophagy led to overactivation and mislocalization of Tank binding kinase 1 (TBK1) which is a multifunctional signaling kinase that localizes on the centrosomes and is required for proper mitotic progression. Overexpression and overactivation of TBK1 alone also resulted in similar mitotic defects and increased micronucleus formation as observed in autophagy deficient cells. We have found clinical evidence of increased TBK1 activation and altered autophagy processes in patient liver tumors. These results indicate that aberrant autophagy may contribute to the formation of micronuclei and tumorigenesis indirectly by altering TBK1 activity.

Introduction
Macroautophagy, hereafter referred to as autophagy, removes cytosolic components, proteins, and organelles by sequestering them into double membrane vesicles called autophagosomes for delivery to the lysosome, where autophagosomes are enzymatically degraded (Mizushima and Komatsu 2011). Thus, autophagy is an important non-selective mechanism for the physiological turnover and recycling of cytosolic components to maintain cellular health. Specifically ablating autophagy genes *ATG5* and *ATG7* in mouse neurons has demonstrated the importance of basal autophagy as these mice eventually accumulate dysfunctional organelles and ubiquitinated, aggregated proteins causing neurodegenerative phenotypes with age (Komatsu et al. 2006; Hara et al. 2006). Considering the positive effects of replacing worn out or damaged proteins and organelles, autophagy is an attractive pharmacological target for several diseases and disorders, especially for post-mitotic cells (Menzies et al. 2017; Aman et al. 2021). However, the contribution of autophagy to the functioning of dividing cells is less well understood.

Autophagy has the potential to maintain proper cell division by safeguarding genomic integrity by degrading micronuclei. Micronuclei are partial or whole chromosomes in the cytosol formed during anaphase when acentric fragments or lagging chromosomes cannot be incorporated in the primary nucleus (Krupina, Goginashvili, and Cleveland 2021). This type of chromosomal instability (CIN) is a hallmark of tumorigenesis. Not only are micronuclei a consequence or marker of genomic instability, but also act as a contributor to facilitate genomic

aberrations and stimulate DNA sensing innate immune inflammatory pathways (Kwon, Leibowitz, and Lee 2020). Previous studies indicate that lysosomal mediated autophagy may reduce CIN by clearing up isolated, atypical micronuclei (Rello-Varona et al. 2012). However, another study challenged the view that micronuclei can be substantially degraded by autophagy. Following cells over multiple division periods, micronuclei in HeLa cells, which have intact autophagy pathways, were rarely degraded, and often persisted in daughter cells through each subsequent generation (Reimann, Stopper, and Hintzsche 2020).

To investigate the influence of autophagy on CIN and micronucleation, we tested the hypothesis micronucleation may increase when autophagy is perturbed in dividing cells. Using both genetic and pharmacological approaches we show that autophagy contributes to genomic stability by inhibiting the formation of micronuclei across many different cells. Loss of autophagic proteins caused numerous types of mitotic defects that directly contribute to micronucleation. These lines deficient in autophagy all display the overactivation and mislocalization of Tank Binding Kinase 1 (TBK1), a kinase necessary for mitosis. The aberrant expression of TBK1 causes the type of mitotic defects that can contribute to the formation of micronuclei. We also found that this overactivation of TBK1 is a common feature in liver tumors from patients, which coincide with altered autophagy markers.

Results

Inhibition of autophagy results in the appearance of cells with micronucleation.

Previous data indicated that autophagy could degrade micronuclei and that the loss of autophagy could result in the accumulation of micronuclei (Rello-Varona et al. 2012). ATG9A is the only integral membrane protein required for autophagy, which is important for the expansion of the autophagosome membrane around cargo (Guardia et al. 2020; Noda et al. 2000; Kim et al. 2002; Yamamoto et al. 2012; Mari et al. 2010). FIP200 is another essential autophagy protein in the ULK1 complex important for autophagy initiation (Hara et al. 2008; Ganley et al. 2009). Using HeLa cells where both proteins are knocked out (KO) (**Figure 4.1A-B**), we examined if these cell lines had abnormal nuclear phenotypes and signs of CIN such as micronucleation, binucleation, or multinucleation.

First, we confirmed that our CRISPR generated ATG9A KO cell line displayed defective starvation induced autophagy using the Halo-Tag assay. In brief, we generated the parental and ATG9A KO cell line to stably express the Halo-GFP fusion protein. Upon a 20 min pulse of HaloTMR ligand, Halo tag is stabilized and resistant to proteolysis in the lysosome, while GFP is still sensitive to degradation (Yim, Yamamoto, and Mizushima 2022)(**Supplementary Figure 4.1A**). Upon starvation, proteolytic cleavage of the Halo-GFP protein was apparent in autophagy competent WT cells but abolished in ATG9A KO cells (**Supplementary Figure 4.1B-C**).

Cells lacking ATG9A and FIP200 accumulated abnormal nuclear phenotypes (**Figure 4.1C, G**) with significant increases in the number of micronuclei in both genotypes (**Figure 4.1D, G, H**). Although ATG9A KO cells displayed a significantly higher number of bi- and

multinucleated cells, this was not significant in FIP200 KO cells (**Figure 4.1E-G**). These results indicated that autophagy has an influence on micronucleation. However, considering that these cell lines have been passaged over multiple cell divisions since their generation, and HeLa cells are known to contain extra chromosomes (Macville et al. 1999), we decided to confirm these results in a near diploid cell line.

PI4KIIIb inhibitors block ATG9A trafficking and inhibit autophagy by preventing PI4KIIIβ from interacting with ATG9A and ATG13, a prerequisite for PI4P production at the growing autophagophore (Judith et al. 2019). We treated DLD-1 cells with the PI4KIIIβ inhibitor PIK93 for 24 hours and analyzed whether cells displayed a significant increase in micronucleation. We found that both the number of cells displaying abnormal nuclear phenotypes and micronucleation were significantly increased following treatment (**Figure 4.1I-K**). These data indicated that CIN was increased upon the loss of autophagy.

Mitotic defects occur after the loss of ATG9A.

It was unclear whether the observed increase in the number of micronuclei was due to a lack of degradation by autophagy or to increased formation of micronuclei during cell division because of mitotic defects. We first performed a cell viability assay and found that cell growth was impaired in ATG9A KO cells (**Figure 4.2A**). Next, we characterized cell division defects in asynchronous conditions to understand whether defects in cell division could contribute to the appearance of micronuclei. Fewer number of mitotic cells were apparent in ATG9A KO cells (**Figure 4.2B**) and upon further characterization there were numerous types of mitotic defects in this line (**Figure 4.2C-E**). There was a significant prevalence of mitotic defects that occurred across all stages of mitosis that could cause the formation of acentric fragments or cause whole chromosomes to lag, leading to micronucleation. ATG9A KO cells also had a higher cytokinetic index with significantly higher number of cells exhibiting abnormal cytokinesis (**Figure 4.2F-G**), which could account for the increased number of binucleated and multinucleated cells (**Figure 4.1E-F**).

Inhibition of autophagy causes the overactivation and mislocalization of TBK1.

It was unclear why the perturbations in autophagy proteins led to mitotic defects. However, ATG9A may have alternative functions apart from its requirement during autophagy sue to the fact that loss of ATG9A results in overactivation of TBK1-STING mediated innate immune response post dsDNA stimulus (Saitoh et al. 2009). TBK1 is also necessary for mitosis and loss of this protein causes a plethora of mitotic defects (Pillai et al. 2015; Sarraf et al. 2019). Thus, we examined whether TBK1 activation was altered in ATG9A KO cells.

Activation of TBK1 depends on its trans-autophosphorylation on serine 172 of its kinase domain (Ma et al. 2012; Shu et al. 2013; Larabi et al. 2013). ATG9A KO cells displayed increased p-TBK1 (S172) signal in immunoblot indicating that it is overactive during both asynchronous condition and synchronized mitosis (**Figure 4.3A-B**). Using immunofluorescence to verify our western blot data, we found that mitotic cells displayed p-TBK1 at centrosomes as

expected (Pillai et al. 2015; Sarraf et al. 2019), but ATG9A KO cells had p-TBK1 punctate staining throughout interphase (**Figure 4.3C**). We attribute this phenotype to the loss of ATG9A as the GFP-ATG9A rescue lines restored p-TBK1 levels to levels seen in the parental line (**Figure 4.3D**).

To test whether this phenotype was solely attributed to the loss of ATG9A or whether inhibition of autophagy also reproduced this phenotype, we used pharmacological inhibition and the knockdown of other autophagy genes. We used the PI4K inhibitor in both DLD-1 and HeLa cell lines to see if overactivation of TBK1 occurred with pharmacological inhibition of autophagosome formation. After 24 hours of treatment, both cell lines displayed elevated p-TBK1 signal when compared to untreated, vehicle samples (**Figure 4.3E-I**). A similar but not as pronounced p-TBK1 punctate staining pattern also occurred upon PI4K inhibition in DLD-1 cells (**Figure 4.3G**).

This was also the case for FIP200 KO cells, which displayed the same upregulation of p-TBK1 levels and localization patterns (**Supplementary Figure S4.2A-B**). We also used siRNAs targeting ATG101, another essential autophagy protein that interacts with ATG13 and the ULK1 kinase (Mercer, Kaliappan, and Dennis 2009). ATG101 knockdown (KD) recapitulated the same mislocalized, upregulated p-TBK1 expression patterns in DLD-1 and HeLa cell lines as compared to scramble control treated cells (**Supplementary Figure S4.2C-E**). These data indicate that inhibition of autophagy abnormally activates TBK1.

To determine where p-TBK1 punctate are localized, we performed IF staining for various organelle markers. We did not see colocalization with staining for antibodies to detect the following organelles: endoplasmic reticulum, early and late endosomes, or Golgi (data not shown). However, we observed partial colocalization between mitochondria (stained with the outer mitochondrial membrane protein TOM20) and p-TBK1 punctate (**Figure 4.3J**). We also performed endogenous IF staining with various TBK1 adaptors and found the autophagy adaptor protein p62 also colocalized with p-TBK1 punctate (**Figure 4.3J**).

Overexpression of TBK1 causes overactivation and leads to mitotic defects.

We previously showed that overexpression of exogenous N' tagged HA-FLAG TBK1 also causes mislocalization and overactivation of TBK1 (Sarraf et al. 2019). However, the localization of TBK1 in those experiments appeared different than the punctate pattern we observed in the autophagy deficient cell lines. Thus, we generated a HeLa cell line that stably overexpressed untagged TBK1 to determine if the tag may have influenced the localization patterns that we visualized previously. The untagged cell line overexpressed TBK1 and displayed increased levels of p-TBK1 in asynchronous conditions (**Figure 4.4A**). Additionally, the pTBK1 positive punctate were also present and appeared like those found in the autophagy deficient cell lines (**Figure 4.4B**). Cells that overexpressed TBK1 displayed increases in CIN with multinucleated and binucleated phenotypes (**Figure 4.4C-E, G**), but most of all micronuclei (**Figure 4.4F-G**). These changes resembled those seen in the ATG9A KO cell line (**Figure 4.1C-G**).

Liver tumors display altered autophagy proteins and overactive TBK1.

High expression of TBK1 is associated with poor outcomes for pancreatic and liver cancers (Cruz and Brekken 2018; Jiang et al. 2021), and proto-oncogenic KRAS tumors are driven by high TBK1 expression (Barbie et al. 2009). In liver samples from two different patients, tumor tissue displayed elevated p-TBK1 levels and high levels of autophagy adaptor protein p62, an autophagy adaptor protein, as compared to adjacent healthy tissue from the same patient (**Figure 4.5**). One patient also had elevated TBK1 levels (**Figure 4.5A**), but the other patient did not display an apparent alteration in TBK1 levels between tumor and healthy liver (**Figure 4.5B**). This data indicate that altered TBK1 levels and activation is possible in some tumors.

Discussion

This study sought out to better understand how autophagy contributes to CIN, finding that the loss of autophagy increases the appearance of micronucleation. Although this could be due to the lack of degradation of micronuclei by autophagic processes, our results indicate that autophagy deficient cell lines also display the types of mitotic errors and defects that are known to give rise to micronuclei (Krupina, Goginashvili, and Cleveland 2021; Rello-Varona et al. 2012). We attribute these mitotic defects to the abnormal activation of TBK1. Our evidence that both TBK1 and autophagy marks are dysregulated in human liver cancer samples indicates that these mechanisms could enhance tumorigenesis.

There is limited evidence that micronuclei are substantially degraded by autophagy. Micronucleus engulfment by the autophagosome, visualized by electron microscopy, has been previously reported (Rello-Varona et al. 2012). Also, pharmacological upregulation of autophagy processesby mTOR inhibitors leads to reduced levels of micronucleation (Bartsch et al. 2017). However, most micronuclei appear to persist or be reincorporated into the primary nucleus upon successive cell divisions (Reimann, Stopper, and Hintzsche 2020, 2023).

Nucleophagy, the specific autophagic removal of pieces of the nucleus for recycling by the lysosome, originally described in yeast, but is less well defined in mammalian cells (Pan et al. 2000; Roberts et al. 2003). Under nitrogen starvation conditions (Mochida et al. 2015) and activation of mTOR signaling (Rahman, Mostofa, and Ushimaru 2018), nucleophagy requires most of the same proteins necessary for autophagy (Krick et al. 2008). Nucleophagy degrades outer nuclear membrane proteins, nucleolar proteins, and parts of the nucleoplasm (Mostofa et al. 2018; Mochida et al. 2015; Dawaliby and Mayer 2010). There is someevidence that nucleophagy occurs in mammalian cells, albeit mostly under pathological conditions. Dentatorubral-pallidoluysian atrophy (DRPLA) is a rare autosomal dominant neurodegenerative disease that can cause neurodevelopmental abnormalities (Licht and Lynch 2002; Nagafuchi et al. 1994; Maruyama, Saito, et al. 2012). Rodent models of the disease and patient fibroblasts display signs of nucleophagy with abnormally shaped nuclei and autophagosome formation colocalizing with lamins, and structural nuclear proteinsduring the upregulation of autophagy (Baron et al. 2017). Activating Ras mutations in mammalian cell lines promote the interaction of lamin B1 with the

autophagosome protein LC3 indicating nucelophagy may play a role in tumorigenesis (Dou et al. 2015). Mouse embryonic fibroblasts containing *LMNA* (encodes for lamin A) mutations also display LC3 accumulation on micronuclear buds that colocalize with lysosomes (Park et al. 2009). Micronuclei have varying degrees of nuclear envelope ensheathment (Hatch et al. 2013), so revisiting whether markers of autophagy truly result in the clearance of micronuclei is warranted.

Our data demonstrate that perturbing autophagy upstream of autophagosome formation. results in TBK1 overactivation and mislocalization. It is unclear how mechanistically these are connected. ATG9A is an integral membrane protein normally found on Golgi and endosomes and is most well-studied for its role in autophagy as it is involved in nucleation, biogenesis, and maturation of autophagosomes during nutrient stress (Yamamoto et al. 2012; Young et al. 2006; Reggiori et al. 2004). TBK1 does colocalize with ATG9A punctae during innate immunity signaling to phosphorylate interferon regulator factor proteins (Saitoh et al. 2009). ATG9A is also found at damaged mitochondria during mitophagy and is essential for autophagophore formation (Yamano et al. 2018; Saitoh et al. 2009; Kishi-Itakura et al. 2014). During mitophagy, the translocation and activation of TBK1 also occurs at damaged mitochondria, where TBK1 phosphorylates autophagy receptors, enhancing the association between the developing autophagosome and damaged mitochondria (Heo et al. 2015; Lazarou et al. 2015; Moore and Holzbaur 2016; Richter et al. 2016; Sarraf et al. 2019). However, pTBK1 punctate appear in the absence of ATG9A present in the KO cells (**Figure 4.3**), and it is unclear why loss of autophagy is causing TBK1 overactivation. Considering that TBK1 needs an adaptor protein to dimerize to allow for the trans-autophosphorylation of its kinase domain for activation (Larabi et al. 2013; Ma et al. 2012), mass spectrometry experiments are warranted to uncover what is binding to TBK1 in these autophagy deficient cells.

Our data demonstrate that micronuclei accumulate when autophagy is inhibited. Although it is possible that this accumulation is due to decreased clearance of micronuclei, our data suggest that the loss of autophagy results in the dysregulation of TBK1, resulting in the increase of CIN, inducing mitotic errors. Cells that ectopically overexpress TBK1, mimic ATG9A KO and to an extent FIP200 KO cells. Future studies into the mechanism causing aberrant TBK1 activity upon the loss or disruption of proteins that control autophagosome initiation and formation are warranted.

Material and Methods

Cell Culture

HeLa and HEK293T cells were maintained in DMEM high glucose medium supplemented with 10% FBS, 2mM L-Glutamine, 10mM HEPES, 0.1 mM non-essential amino acids, and 1mM sodium pyruvate. DLD-1 cells were a kind gift from Dr. Daniela Cimini's lab. DLD-1 cells were maintained in RPMI-1640 medium with 10% FBS. FIP200 KO HeLa cells were a kind gift from Dr. Richard J. Youle's lab. Cells were routinely tested for mycoplasma contamination by PCR (Southern Biotech).

Chemicals

The following chemicals were used for this study: PIK-93 (MedChem), RO-3306 (VWR), Halo TMR ligand (**Promega)**.

Antibodies

The following antibodies were used for this study: TBK1/NAK (#3504S/#14590S; Cell Signaling Technology (CST)), pTBK1 (Ser172; #5483S; CST), pTBK1 Alexa Fluor 488 or 647 conjugated (Ser172; #14586/#14590; CST), GAPDH (G9545; Sigma), Vinculin (#700062; Invitrogen), p62 (#H00008878-M01; Abnova), α-Tubulin (#T6074; Sigma)(#2144S; CST)(ab52866;Abcam), ATG9A (#ab108338, Abcam), b-actin (#A2228; Sigma), FIP200 (#17250-1-AP, Proteintech), ATG101 (#26562-1-AP, Proteintech), TOM20 (#sc-17764; SCBT), Histone H3 (#4499S, CST), Anti-Centromere (#15-234-0001; Antibodies Incorp.), anti-HaloTag (#G9211, Promega), and p-H3 S10 (#53348S, Cell Signaling).

siRNAs

The siRNA used in this study are as follows: ON-TARGETplus Human ATG101 siRNA, SMARTpool L-017816-01-0005 and ON-TARGETplus Non-targeting Pool (Horizon Discovery). Transfections were performed with 30nM of siRNAs and 1:1 DharmaFECT Transfection Reagent (Horizon Discovery) in Opti-Mem (Gibco) for 20 minutes RT.

Lentivirus and Retrovirus generation

Dishes were coated with 50μg/mL poly-d-lysine (Sigma), and HEK293T cells were plated at 70-80% confluency before transfection. Lentiviral helpers and constructs were transfected using XtremeGENE 9™ (Roche) according to the manufacturer's instructions at a 1:3 ratio. 24 hrs after transfection, media was changed. Infectious media containing virus was collected 40 hrs later and filtered with a 0.45μm PES membrane filter (Millipore). Live filtered virus was used to transduce cells with polybrene (10μg/ml, Sigma).

Cell synchronization

RO-3306 treatment: To synchronize at G2, cells were reversibly incubated with 9uM RO-3306 containing medium for 20 hrs and collected at the following time points corresponding to their respective cell cycle stages when released in normal growth medium: 1hr – M (metaphase). Mitotic shake was employed to obtain maximum number of mitotic cells.

Starvation protocol

Cells were incubated with 200nM of HaloTag TMR ligand for 20 minutes and subsequently washed with HBSS twice. Cells were then starved for 1 hour in HBSS prior to collection to induce autophagy.

CRISPR knockout cell line generation

CRISPR oligos for ATG9A exon 8: CACCGGACCCCCAGGAGTGTGACGG, AAACCCGTCACACTCCTGGGGGTCC. Primers were annealed with Phusion DNA polymerase (Thermo Fisher Scientific) using the following conditions: 98ºC for 1', 2-3 cycles of (98ºC for 10", 53ºC for 20", 72ºC for 30"), 72ºC for 5.' The annealed primers were cloned into the linearized gRNA vector gRNA, which was a gift from Dr. Feng Zhang (Addgene plasmid #62988) using the Gibson Assembly Cloning Kit (NEB). HeLa cells were cotransfected using XtremeGENE 9™ (Roche) using the above CRISPR plasmid. Cells were selected by puromycin (1mg/ml) and serially diluted into 96 well plates to select for single colony clones.

Cloning

To generate ATG9A rescue lines, ATG9A cDNA was cloned into pDONR223 and transferred into the pHAGE-N'-EGFP-Gaw-IRES-Blast vector using LR recombinase (Invitrogen). pMRX-IB-HaloTag7-mGFP was a gift from Noboru Mizushima (Addgene plasmid #184903; http://n2t.net/addgene:184903; RRID: Addgene_184903). The untagged TBK1 construct was generated in our laboratory previously (Addgene plasmid # 131792). All constructs generated for this manuscript were confirmed by DNA sequencing and deposited on Addgene.

Western blots

For immunoblotting, cells were lysed using 1X RIPA buffer (Thermo scientific Pierce ™ RIPA Buffer) containing 1X protease/phosphatase inhibitor cocktails (Thermo Scientific Halt™). Protein concentration was quantified using DC™ Protein Assay Kit (Bio-Rad). Cell lysates were boiled for 15 mins with 2X LDS buffer containing 50 mM DTT, and 20ug of protein lysates were resolved by 4%-12% Bis-Tris gels and transferred to PVDF membranes. Blots were blocked using 5% non-fat powdered milk in 1X TBST (150mM NaCl, 20mM Tris, pH 8.0, 0.1% Tween 20). Primary and secondary antibody incubations were carried out in 2.5% non-fat powdered milk in 1X TBST for overnight at 4°C and 1hr at room temperature, respectively. Blots were exposed using Clarity™ Western ECL Substrates (Bio-Rad), ECL™ Select Western Blotting Detection Reagent (GE Healthcare), or SuperSignal™ West Femto Maximum Sensitivity Substrate (Thermo Scientific) and detected by the ChemiDoc Imaging System (BioRad).

Immunocytochemistry

Cells for immunofluorescence imaging were plated in 6 well cell culture plates (Corning Incorporated) on glass coverslips. Cells were fixed with 4% PFA for 10 mins and permeabilized with 0.1% Triton-X-100 for 10 mins followed by blocking with 10% BSA 5% NGS for 45 mins at RT. Cells were incubated with primary antibodies (diluted in 5% BSA and 2.5% NGS) overnight at 4ºC followed by washing with 1X PBS and incubated with AlexaFluor (Thermo Fisher) conjugated secondary antibodies in the dark for 1 hour. Following the washing step, the cells were stained with .1ug/mL DAPI for 5 mins (Thermo Fisher) and mounted on the slides

using Fluoromount (Southern-Biotech). Imaging was carried out using a Nikon C2 confocal microscope.

Cell viability assay for growth curve

Approximately, 200 to 400 cells were plated (4 wells/genotype) in white-coated 96-well plates (Brand Tech Scientific) in growth media. Cell growth curve was obtained by CellTiter-Glo® Luminescent Cell Viability Assay (Promgea) using a luminescence reader every 24 hours. Mean cell number corresponding to the luminescence on each day was normalized to the first day in the graph.

Statistical Analysis

For comparisons between two groups, a student's t-test was used to determine statistical significance. Ordinary one-way ANOVA followed by Tukey's multiple comparisons were used for three or more groups using GraphPad Prism software. Additional details are available in the figure legends. Differences in means were considered significant if $p < 0.05$ and designated as the following $p<0.05$ - *; $p< 0.01$ - **; $p< 0.001$ - ***. $p<.0001$ - ****; ns – not significant.

Acknowledgments:

We thank Dr. Daniela Cimini and Mathew Bloomfield for advice, reagents, and their expertise. The authors declare no competing financial interests.

Funding:

National Institutes of Health Grants GM142368 (AMP)
Departmental startup funds (AMP)

Author Contributions:

Conceptualization: AMP; Planning and methodology: SP, AMP; Experimentation: SP, ND, LZ, SRB, AMP; Data Analysis: SP, ND, AMP; Writing – original draft: SP and AMP; Writing – review & editing: SP and AMP. All authors have read and approved the manuscript.

Competing Interests

The authors declare that the research was conducted in the absence of any commercial or financial relationships that could be construed as a potential conflict of interest.

Data and Materials Availability:

Constructs used for this study will be available through Addegene.org. Raw western blotting images will be deposited on Mendeley Data. All other reagents, data, and material requests will be fulfilled by the corresponding author, Alicia M. Pickrell, Ph.D. All data are available in the main text or the supplementary materials.

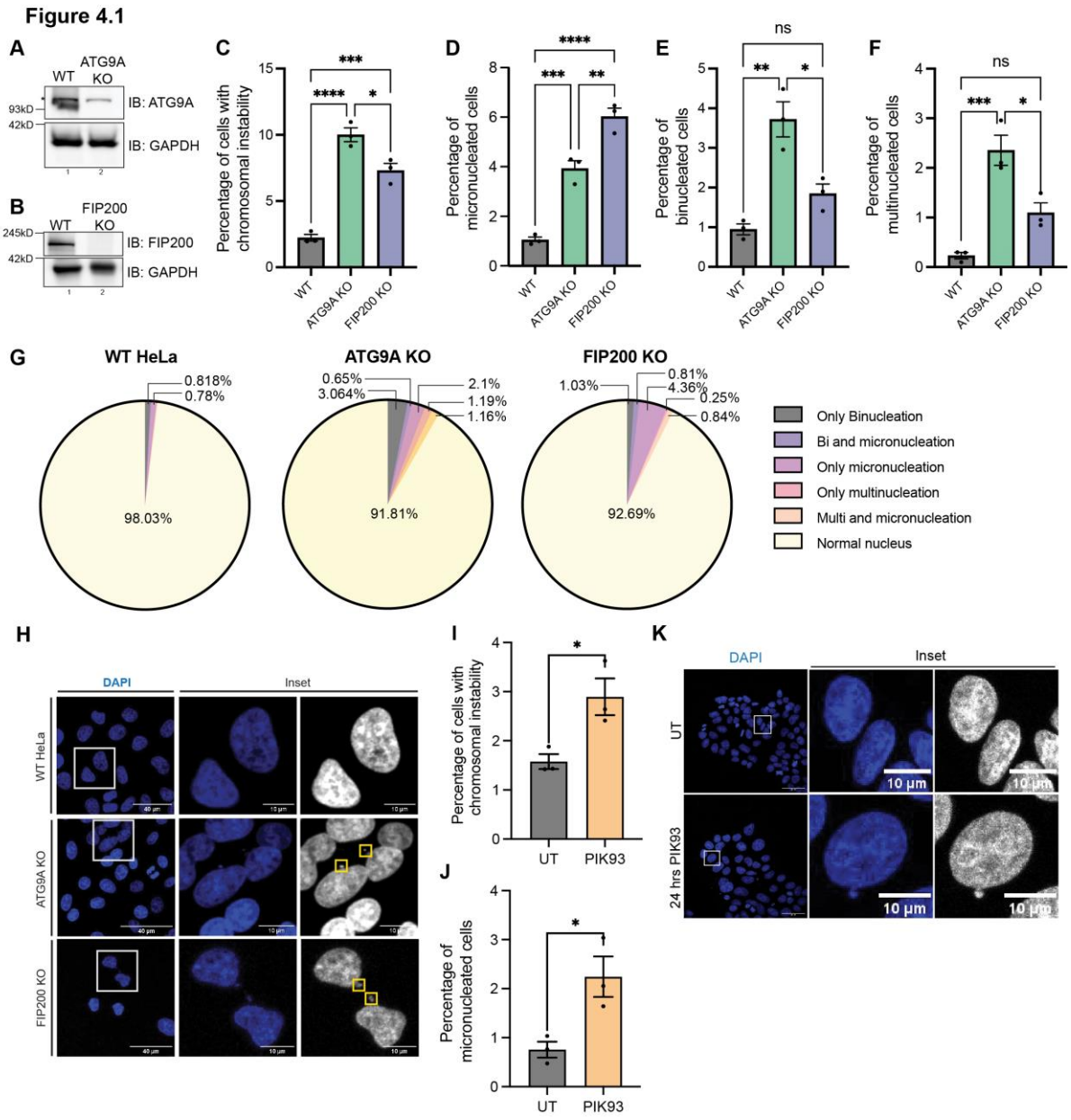

Fig. 4.1. Inhibition of autophagy results in the appearance of cells with micronucleation. (A-B) Western blots showing the loss of core autophagy proteins ATG9A (A) and FIP200 (B) in HeLa cells. C-F) Bar graphs showing the percentage of cells with CIN (C), micronuleated cells (D), binucleated cells (E), and multinucleated cells (F) quantified from HeLa, ATG9A KO, and FIP200 KO cells. At least 1000 cells were counted per genotype, n=3/experiments. G) Pie chart with the distribution of different types of CINs found across WT, ATG9A KO and FIP200 KO cells. H) Representative confocal images of micronuclei found in autophagy deficient ATG9A KO and FIP200 KO cells. I-J) Bar graphs showing the percentage of cells with CIN (abnormal nuclear phenotypes) DAPI was used for nuclear staining. (I) and cells with micronuclei (J) quantified from untreated DLD-1 and cells after 24 hours of 4mM PIK93 treatment. At least 1000 cells were counted per genotype, n=3/experiments. Scale bar = 40mM and 10mM for

insets. One dot equals an experimental replicate. One-way ANOVA was performed for statistical analysis. Error bars ± SEM. * p < .05, ** p < .01, *** p <.001, **** p <.0001, and ns= not significant. K) Representative confocal images of micronuclei found in the DLD-1 cells after 24 hours of 4mM PIK93 treatment. DAPI was used for nuclear staining. Scale bar = 10uM.

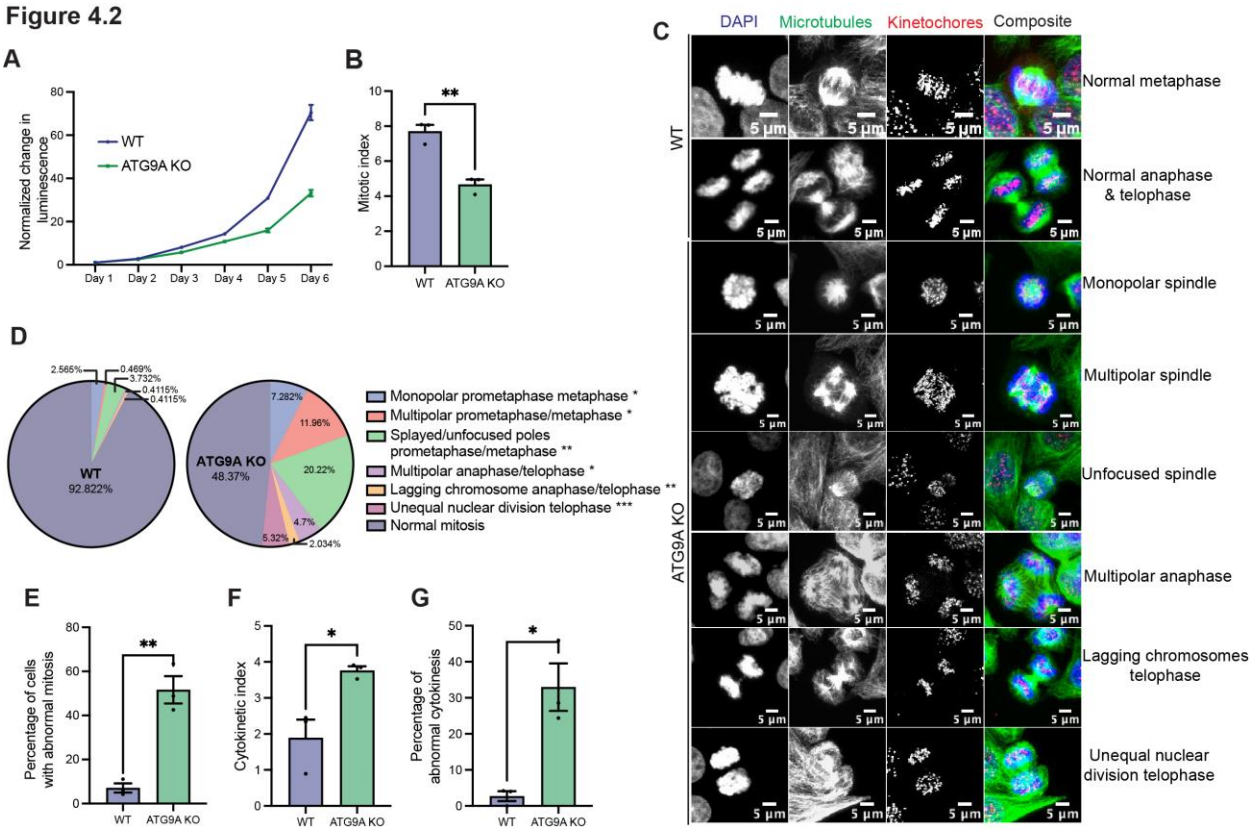

Fig. 4.2. Mitotic defects occur after the loss of ATG9A.

(A) Growth curve with normalized luminescence for WT HeLa and ATG9A KO cells. Error bars indicate ±SD for technical replicates. n=2 experiments B) Percentage of mitotic cells from an asynchronous population of WT and ATG9A KO HeLa cells. C) Representative confocal images of different mitotic defects observed in ATG9A KO cells. DAPI (blue) was used as a nuclear counterstain, α-tubulin for cytoskeleton staining (green), and CREST for kinetochore staining (red). Scale bar = 5mM. D) Pie chart demonstrating the distribution of different types of mitotic defects found in WT and ATG9A KO cells. At least 1000 cells were counted per genotype, n= 3/experiments E-G) Percentage of mitotic cells from an asynchronous population with (E) mitotic defects, the number of cytokinetic cells (F), and the number of cells with cytokinetic defects (G) between HeLa and ATG9A KO cells. One dot equals an experimental replicate. Error bars ± SEM. Student's t-test was performed for statistical analysis. * p < .05, ** p < .01, and *** p <.001.

Figure 4.3

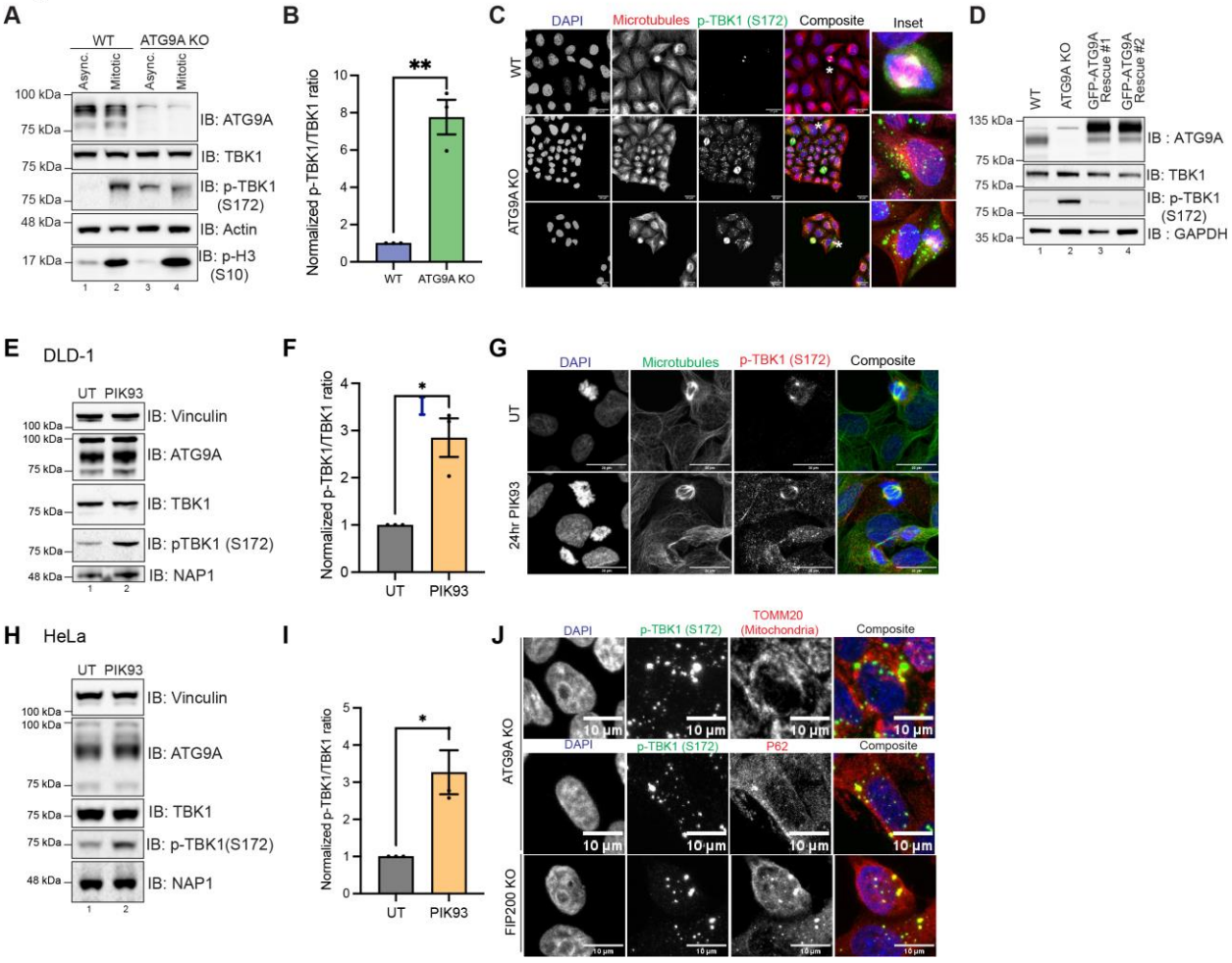

Fig. 4.3. Inhibition of autophagy causes the overactivation and mislocalization of TBK1.

A) Representative western blot for p-TBK1 in HeLa and ATG9A KO cells. B-actin is used as a loading control. B) Quantification of p-TBK1 normalized to TBK1 levels and the loading control between HeLa and ATG9A KO cells in asynchronous conditions. C) Representative confocal images showing abnormal activation of TBK1 in ATG9A KO. α-tubulin (red) was used for cytoskeleton staining, p-TBK1 (green), and DAPI (blue) was used as nuclear counterstain. Scale bar =20mM, and 5mM for insets. D) Western blot analysis for p-TBK1 in ATG9A rescue cell lines. GAPDH was used as a loading control. E) Representative western blotting for p-TBK1 in DLD-1 cells treated with 4mM PIK93 for 24 hours. F) Bar graph quantification of I between p-TBK1 normalized to TBK1 levels and the loading control. G) Representative confocal images showing abnormal activation of p-TBK1 in DLD-1 cells treated with 4mM PIK93 for 24 hours. a-tubulin (red) was used for cytoskeleton staining, p-TBK1 (green), and DAPI (blue) was used as nuclear counterstain. Scale bar =10uM. H) Representative western blotting for p-TBK1 in HeLa cells treated with 4mM PIK93 for 24 hours. I) Bar graph quantification of (H) between p-TBK1 normalized to TBK1 levels and the loading control. J) Representative confocal images showing abnormal activation of p-

TBK1 in ATG9A and FIP200 KO colocalizing with TOM20 and p62. p62 or TOM20 (red), p-TBK1 (green), and DAPI (blue) were used as nuclear counterstain. Scale bar = 10uM. One dot equals an experimental replicate. Error bars ± SEM. Student's t-test was performed for statistical analysis. * p < .05 and ** p < .01.

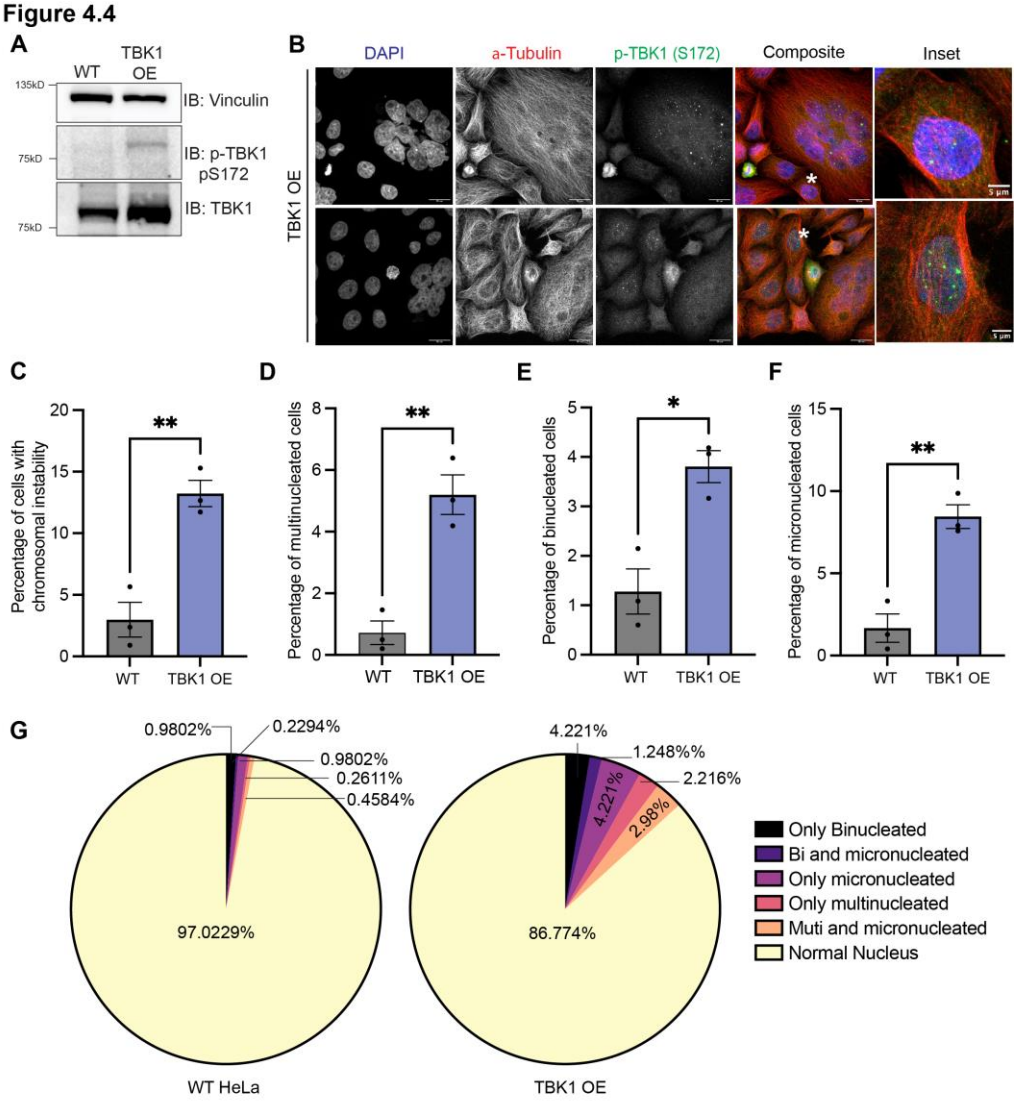

Fig. 4.4. Overexpression of TBK1 causes overactivation and leads to mitotic defects.
(A) Western blotting for TBK1 and p-TBK1 in the HeLa and untagged TBK1 OE cell line. Vinculin was used as a loading control. B) Representative confocal images of p-TBK1 (pseudo colored green) expression and localization patterns when overexpressed. a-tubulin (red) was used for cytoskeleton staining, and DAPI (blue) was used as nuclear counterstain. Scale bar = 20mM, and 5mM for insets. C-F) Bar graphs showing the percentage of cells with CIN (C), multinucleated cells (D), binucleated cells (E), and micronucleated cells (F) quantified from HeLa and TBK1 OE cells. K) Pie chart demonstrating the distribution of different types of CIN

defects found in WT and TBK1 OE cells. At least 1000 cells were counted per genotype, n= 3/experiments.

One dot equals an experimental replicate. Error bars ± SEM. Student's t-test was performed for statistical analysis. * $p < .05$ and ** $p < .01$.

Figure 4.5

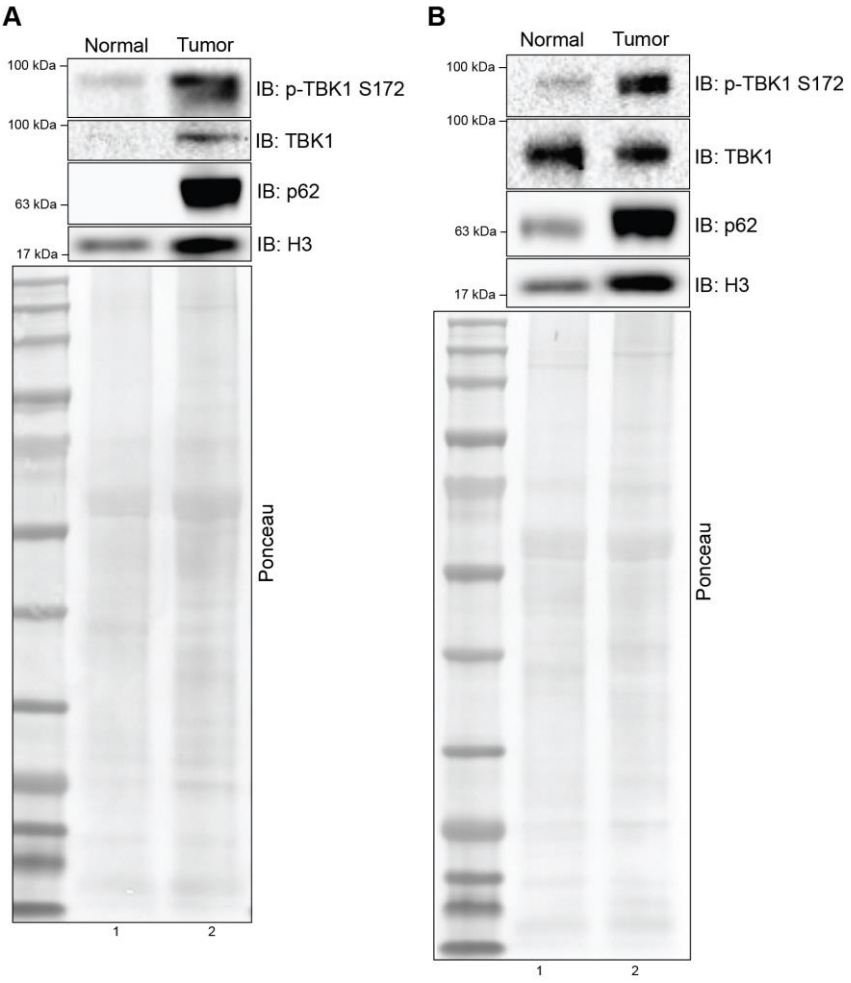

Fig 4.5. Liver tumors display altered autophagy proteins and overactive TBK1.

(A) Western blotting for p-TBK1 and p62 in liver samples from a 39-year-old male with trabecular adenocarcinoma. A) Western blotting for p-TBK1 and p62 in liver samples from a 55-year-old male with hepatocellular carcinoma. Ponceau staining was used as a loading control.

Supplementary Figures:

Fig S4.1

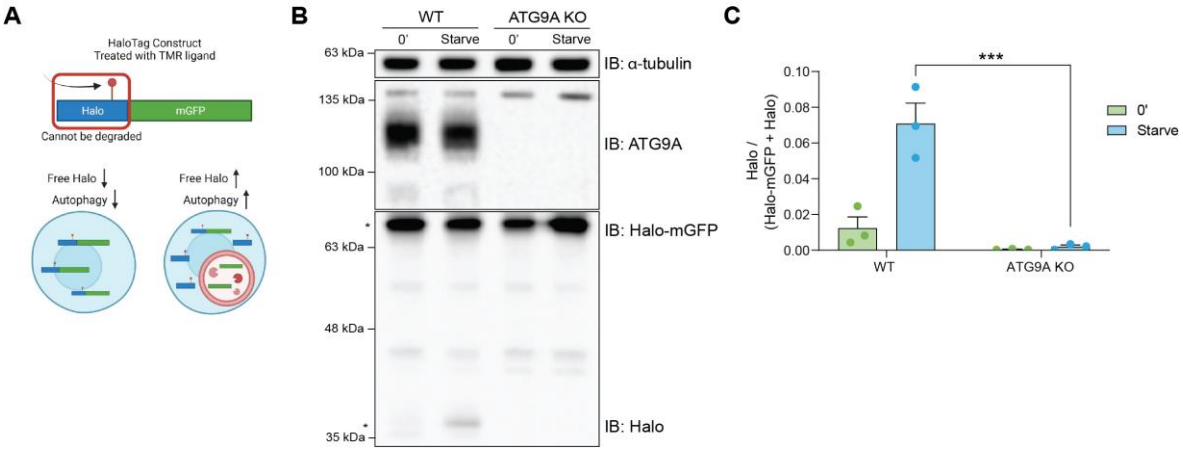

Supplementary Fig. 4.1. ATG9A abolishes basal and starvation induced autophagy.
A) Cartoon depiction of HaloTag mGFP autophagy reporter stabilized and cleaved upon lysosomal digestion. B) Representative western blotting for free Halo protein after starvation between WT and ATG9A KO HeLa cell lines. C) Quantification of free Halo protein normalized to total tagged full-length Halo-mGFP fusion protein. Error bars ± SEM. One-way ANOVA was performed for statistical analysis. *** = $p < 0.001$. One dot equals an experimental replicate.

Figure S4.2

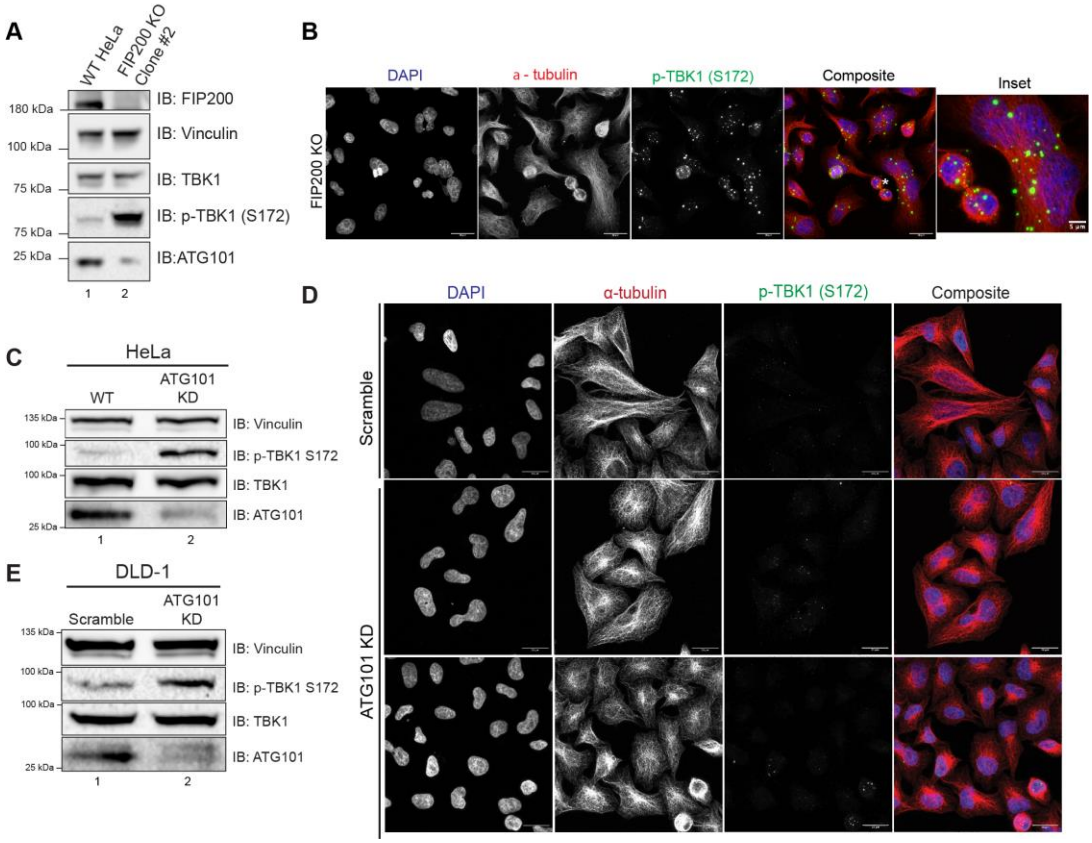

Supplementary Fig. 4.2. Alteration of other autophagy genes also causes the overactivation and mislocalization of TBK1.

A) Western blotting for p-TBK1 levels between WT HeLa and FIP200 KO cell lines. B) Representative confocal images of FIP200 KO cells for immunocytochemical detection of p-TBK1 (green). DAPI (blue) was used as a nuclear counterstain, and α-tubulin for cytoskeleton staining (red). Scale bar = 20 μm. Inset = 5 μm. Asterisks denote the inset area. C) Western blotting for p-TBK1 levels in HeLa cell lines treated with scramble or ATG101 siRNAs for 48 hours. D) Representative confocal images of siRNA treated HeLa cells for immunocytochemical detection of p-TBK1 (green). KD occurred over a 48-hour period. DAPI (blue) was used as a nuclear counterstain, and α-tubulin for cytoskeleton staining (red). Scale bar = 20 μm. Inset = 5 μm. Asterisks denote the inset area. E) Western blotting for p-TBK1 levels in DLD-1 cell lines treated with scramble or ATG101 siRNAs for 48 hours. Vinculin was used as a loading control for panels A, C, and E.

Chapter 5

Summary and Future Directions

Summary of findings

This study investigated the non-canonical roles of TBK1 during cell division. TBK1 has been shown to play key roles during innate immune signaling, selective autophagy, and mitosis. Due to its multifunctionality, aberrant expression or aberrant activation of TBK1 can impact these three distinct cellular processes. Therefore, TBK1 activation is tightly regulated under physiological conditions. While both the upstream regulation and downstream targets of TBK1 have been extensively investigated in innate immunity and selective autophagy, its regulation of mitosis is relatively undefined. This study identifies the novel adaptor of TBK1 during mitosis along with its potential substrates and indirect targets which ensure proper progression through cell division. Additionally, we have identified an underlying connection between autophagy and TBK1 activation. The following are the key findings presented in this dissertation:

1) We identified that the established innate immune response protein NAP1 plays a significant role in regulating multiple aspects of cell division by binding and activating TBK1 at the centrosomes. Loss of NAP1 results in several mitotic and cytokinetic defects phenocopying the loss of TBK1.

2) We provide evidence that NAP1 levels are tightly regulated during mitosis in a feedback mechanism where TBK1 phosphorylates serine 318 on NAP1 for ubiquitin-mediated proteasomal degradation.

3) With an unbiased quantitative phosphoproteomics approach, we identified novel mitotic TBK1 substrates other than the few currently reported. We show that the activity of major cell cycle regulatory kinases, Aurora A and Aurora B, are downregulated due to the loss of TBK1.

4) We evaluated how autophagy regulates cell cycle by modulating TBK1 activation and localization.

5) This work further showed that loss of autophagy results in a significantly higher number of micronuclei and other abnormal nuclear phenotypes. Impaired autophagy correlates with defects in mitosis and cytokinesis possibly due to abnormal activation of TBK1 during interphase.

Taken together, we establish a non-canonical role of the NAP1-TBK1 complex during mitosis and conclude that NAP1 localization and binding with TBK1 is essential for mitosis. TBK1 functions upstream of major cell cycle kinases like Aurora A and Aurora B, thereby regulating different aspects of mitosis. However, abnormal overactivation of TBK1 due to impaired autophagy also results in defective cell division resulting in chromosomal instability,

suggesting an underlying connection between autophagy and cell cycle regulation via TBK1 activity.

Future Directions

This work provides an overall understanding of the non-canonical function and the upstream regulation of TBK1. However, there are several follow up questions that remain to be answered to improve our understanding of the role this multifunctional kinase plays in regulating the cell cycle.

The work presented in Chapter 3 demonstrates that TBK1 activation is significantly reduced but not completely abolished during mitosis. Since TBK1 has multiple, redundant adaptors for binding-mediated activation during innate immune signaling and selective autophagy (Fu et al. 2018; Matsumoto et al. 2015; Heo et al. 2015; Matsumoto et al. 2011; Goncalves et al. 2011; Ryzhakov and Randow 2007; Fujita et al. 2003), it is possible that other adaptor(s) could compensate or maintain a minimum TBK1 activation level for cells to survive in the absence of NAP1. Identifying the redundant TBK1 adaptors during mitosis will provide greater insight into the upstream mitotic regulation of TBK1. Although quantitative phosphoproteomics identified multiple TBK1 substrates that are phosphorylated by TBK1 during mitosis, the validation of those substrates and their physiological relevance remains to be elucidated. We show that activities of Aurora A and Aurora B are significantly downregulated due to the loss of TBK1, and this establishes that TBK1 acts upstream of these major cell cycle regulating kinases. However, both these Aurora kinases do not appear to be directly phosphorylated by TBK1 in this dataset. Therefore, identifying the intermediate signaling cascade between TBK1 and Aurora kinases is necessary to gain increased mechanistic insight into the function of TBK1 during mitosis. We show that NAP1 is phosphorylated on serine 318 as soon as TBK1 gets activated during mitosis. We hypothesize that this regulation of NAP1 protein level probably maintains the level of TBK1 activation as TBK1 overactivation is correlated with heightened cell proliferation and chromosomal instability (see Chapter 4). However, the physiological relevance of NAP1 regulation remains to be studied. Although previous work has reported TBK1 as a centrosomal kinase (Maan et al. 2021; Sarraf et al. 2019; Pillai et al. 2015), we provide evidence that the localization of activated TBK1 spreads beyond centrosomes toward the plus end of the microtubules towards chromosomes. This explains why the majority of TBK1 mitotic substrates identified in the phosphoproteomics screening are spindle assembly proteins. Further investigation is required to segregate the role of TBK1 at the centrosomes and microtubules.

The work from Chapter 4 evaluates how autophagy impacts cell cycle by modulating the activation and localization of TBK1. We show that impaired autophagy contributes to chromosomal instability and various types of mitotic and cytokinetic defects. However, the mechanism by which TBK1 is overactivated when core autophagy proteins are either knocked out or inhibited is not known. Since TBK1 requires adaptor proteins (Shu et al. 2013; Goncalves et al. 2011), it is imperative to identify the adaptor(s) for TBK1 overactivation in cells lacking functional autophagy machinery to gain insight into the connection between autophagy and cell

cycle regulation. Investigating the cause for the aberrant localization of activated TBK1 due to impaired autophagy will help us understand how TBK1 translocates from one place to another during distinct cellular processes. Furthermore, it is unclear how loss of autophagy contributes to a significant increase in micronucleation in the cells. Our data suggests that micronucleation is caused by abnormal chromosome segregation due to overactivation of the mitotic kinase TBK1, which could result in lagging chromosomes or acentric fragments during mitosis. However, further investigation and proper analysis of mitotic progression in cells lacking autophagy is required.

Overall, the scientific findings from this work could be utilized to evaluate the therapeutic potential of NAP1 during abnormal cell proliferation in cancer. With the discovery of NAP1 as an upstream regulator of TBK1 has provided us with an opportunity to develop NAP1 inhibitors and study their specificity for modulating TBK1 activation levels in cancer and other developmental pathologies. It is imperative to study the role of NAP1 during embryonic development in the mouse model as the data from this work suggests NAP1 could be an essential developmental protein. However, the fact that we could not generate NAP1 KO cell lines in non-cancerous RPE-1 cells, there is a strong possibility that NAP1 KO mice would also have a similar phenotype as TBK1 KO mice which die at embryonic day 14.5 due to excessive cell death and liver failure (Bonnard et al. 2000). Therefore, to study these essential indispensable genes in normal context, especially during embryonic development which is reliant on the proper functioning of the mitotic genes, it is essential to adopt methods like rapid and transient degradation of endogenous proteins in animal model. Targeted protein degradation using a degron system like dTAG degron offers a way to temporally degrade an endogenous protein in different stages of embryonic development and study the effect of the reduced protein level in vivo (Abuhashem et al. 2022; Abuhashem and Hadjantonakis 2022). The reversible nature of this method can also be useful for tracking any postnatal developmental changes that may occur due to the transient reduction of NAP1 or TBK1 during embryonic stage.

References

Abdu, U., D. Bar, and T. Schupbach. 2006. 'spn-F encodes a novel protein that affects oocyte patterning and bristle morphology in Drosophila', *Development*, 133: 1477-84.

Abuhashem, A., and A. K. Hadjantonakis. 2022. 'Generation of knock-in degron tags for endogenous proteins in mice using the dTAG system', *STAR Protoc*, 3: 101660.

Abuhashem, A., A. S. Lee, A. L. Joyner, and A. K. Hadjantonakis. 2022. 'Rapid and efficient degradation of endogenous proteins in vivo identifies stage-specific roles of RNA Pol II pausing in mammalian development', *Dev Cell*, 57: 1068-80 e6.

Aman, Y., T. Schmauck-Medina, M. Hansen, R. I. Morimoto, A. K. Simon, I. Bjedov, K. Palikaras, A. Simonsen, T. Johansen, N. Tavernarakis, D. C. Rubinsztein, L. Partridge, G. Kroemer, J. Labbadia, and E. F. Fang. 2021. 'Autophagy in healthy aging and disease', *Nat Aging*, 1: 634-50.

Bakshi, S., J. Taylor, S. Strickson, T. McCartney, and P. Cohen. 2017. 'Identification of TBK1 complexes required for the phosphorylation of IRF3 and the production of interferon beta', *Biochem J*, 474: 1163-74.

Barbie, D. A., P. Tamayo, J. S. Boehm, S. Y. Kim, S. E. Moody, I. F. Dunn, A. C. Schinzel, P. Sandy, E. Meylan, C. Scholl, S. Frohling, E. M. Chan, M. L. Sos, K. Michel, C. Mermel, S. J. Silver, B. A. Weir, J. H. Reiling, Q. Sheng, P. B. Gupta, R. C. Wadlow, H. Le, S. Hoersch, B. S. Wittner, S. Ramaswamy, D. M. Livingston, D. M. Sabatini, M. Meyerson, R. K. Thomas, E. S. Lander, J. P. Mesirov, D. E. Root, D. G. Gilliland, T. Jacks, and W. C. Hahn. 2009. 'Systematic RNA interference reveals that oncogenic KRAS-driven cancers require TBK1', *Nature*, 462: 108-12.

Baron, O., A. Boudi, C. Dias, M. Schilling, A. Nolle, G. Vizcay-Barrena, I. Rattray, H. Jungbluth, W. Scheper, R. A. Fleck, G. P. Bates, and M. Fanto. 2017. 'Stall in Canonical Autophagy-Lysosome Pathways Prompts Nucleophagy-Based Nuclear Breakdown in Neurodegeneration', *Curr Biol*, 27: 3626-42 e6.

Barros, C. S., and T. Bossing. 2021. 'Microtubule disruption upon CNS damage triggers mitotic entry via TNF signaling activation', *Cell Rep*, 36: 109325.

Bartsch, K., K. Knittler, C. Borowski, S. Rudnik, M. Damme, K. Aden, M. E. Spehlmann, N. Frey, P. Saftig, A. Chalaris, and B. Rabe. 2017. 'Absence of RNase H2 triggers generation of immunogenic micronuclei removed by autophagy', *Hum Mol Genet*, 26: 3960-72.

Beausoleil, S. A., J. Villen, S. A. Gerber, J. Rush, and S. P. Gygi. 2006. 'A probability-based approach for high-throughput protein phosphorylation analysis and site localization', *Nat Biotechnol*, 24: 1285-92.

Bell, S. L., K. L. Lopez, J. S. Cox, K. L. Patrick, and R. O. Watson. 2021. 'Galectin-8 Senses Phagosomal Damage and Recruits Selective Autophagy Adapter TAX1BP1 To Control Mycobacterium tuberculosis Infection in Macrophages', *mBio*, 12: e0187120.

Bitan, A., G. M. Guild, D. Bar-Dubin, and U. Abdu. 2010. 'Asymmetric microtubule function is an essential requirement for polarized organization of the Drosophila bristle', *Mol Cell Biol*, 30: 496-507.

Bonnard, M., C. Mirtsos, S. Suzuki, K. Graham, J. Huang, M. Ng, A. Itie, A. Wakeham, A. Shahinian, W. J. Henzel, A. J. Elia, W. Shillinglaw, T. W. Mak, Z. Cao, and W. C. Yeh. 2000. 'Deficiency of T2K leads to apoptotic liver degeneration and impaired NF-kappaB-dependent gene transcription', *EMBO J*, 19: 4976-85.

Bouwmeester, T., A. Bauch, H. Ruffner, P. O. Angrand, G. Bergamini, K. Croughton, C. Cruciat, D. Eberhard, J. Gagneur, S. Ghidelli, C. Hopf, B. Huhse, R. Mangano, A. M. Michon, M. Schirle, J. Schlegl, M. Schwab, M. A. Stein, A. Bauer, G. Casari, G. Drewes, A. C. Gavin, D. B. Jackson, G. Joberty, G. Neubauer, J. Rick, B. Kuster, and G. Superti-Furga. 2004. 'A physical and functional map of the human TNF-alpha/NF-kappa B signal transduction pathway', *Nat Cell Biol*, 6: 97-105.

Boyle, K. B., B. J. Ravenhill, and F. Randow. 2019. 'CALCOCO2/NDP52 initiates selective autophagy through recruitment of ULK and TBK1 kinase complexes', *Autophagy*, 15: 1655-56.

Budzik, J. M., D. L. Swaney, D. Jimenez-Morales, J. R. Johnson, N. E. Garelis, T. Repasy, A. W. Roberts, L. M. Popov, T. J. Parry, D. Pratt, T. Ideker, N. J. Krogan, and J. S. Cox. 2020. 'Dynamic post-translational modification profiling of Mycobacterium tuberculosis-infected primary macrophages', *Elife*, 9.

Carmena, M., S. Ruchaud, and W. C. Earnshaw. 2009. 'Making the Auroras glow: regulation of Aurora A and B kinase function by interacting proteins', *Curr Opin Cell Biol*, 21: 796-805.

Chen, W., K. Luo, Z. Ke, B. Kuai, S. He, W. Jiang, W. Huang, and Z. Cai. 2017. 'TBK1 Promote Bladder Cancer Cell Proliferation and Migration via Akt Signaling', *J Cancer*, 8: 1892-99.

Cheng, G., and D. Baltimore. 1996. 'TANK, a co-inducer with TRAF2 of TNF- and CD 40L-mediated NF-kappaB activation', *Genes Dev*, 10: 963-73.

Clark, K., K. F. MacKenzie, K. Petkevicius, Y. Kristariyanto, J. Zhang, H. G. Choi, M. Peggie, L. Plater, P. G. Pedrioli, E. McIver, N. S. Gray, J. S. Arthur, and P. Cohen. 2012. 'Phosphorylation of CRTC3 by the salt-inducible kinases controls the interconversion of classically activated and regulatory macrophages', *Proc Natl Acad Sci U S A*, 109: 16986-91.

Clark, K., M. Peggie, L. Plater, R. J. Sorcek, E. R. Young, J. B. Madwed, J. Hough, E. G. McIver, and P. Cohen. 2011. 'Novel cross-talk within the IKK family controls innate immunity', *Biochem J*, 434: 93-104.

Clark, K., O. Takeuchi, S. Akira, and P. Cohen. 2011. 'The TRAF-associated protein TANK facilitates cross-talk within the IkappaB kinase family during Toll-like receptor signaling', *Proc Natl Acad Sci U S A*, 108: 17093-8.

Colas, P. 2020. 'Cyclin-dependent kinases and rare developmental disorders', *Orphanet J Rare Dis*, 15: 203.

Cruz, V. H., and R. A. Brekken. 2018. 'Assessment of TANK-binding kinase 1 as a therapeutic target in cancer', *J Cell Commun Signal*, 12: 83-90.

Damhofer, H., A. Radzisheuskaya, and K. Helin. 2021. 'Generation of locus-specific degradable tag knock-ins in mouse and human cell lines', *STAR Protoc*, 2: 100575.

Dawaliby, R., and A. Mayer. 2010. 'Microautophagy of the nucleus coincides with a vacuolar diffusion barrier at nuclear-vacuolar junctions', *Mol Biol Cell*, 21: 4173-83.

Dephoure, N., C. Zhou, J. Villen, S. A. Beausoleil, C. E. Bakalarski, S. J. Elledge, and S. P. Gygi. 2008. 'A quantitative atlas of mitotic phosphorylation', *Proc Natl Acad Sci U S A*, 105: 10762-7.

Dos Santos, A., D. E. Rollins, Y. Hari-Gupta, H. McArthur, M. Du, S. Y. Z. Ru, K. Pidlisna, A. Stranger, F. Lorgat, D. Lambert, I. Brown, K. Howland, J. Aaron, L. Wang, P. J. I. Ellis, T. L. Chew, M. Martin-Fernandez, A. L. B. Pyne, and C. P. Toseland. 2023. 'Autophagy receptor NDP52 alters DNA conformation to modulate RNA polymerase II transcription', *Nat Commun*, 14: 2855.

Dou, Z., C. Xu, G. Donahue, T. Shimi, J. A. Pan, J. Zhu, A. Ivanov, B. C. Capell, A. M. Drake, P. P. Shah, J. M. Catanzaro, M. D. Ricketts, T. Lamark, S. A. Adam, R. Marmorstein, W. X. Zong, T. Johansen, R. D. Goldman, P. D. Adams, and S. L. Berger. 2015. 'Autophagy mediates degradation of nuclear lamina', *Nature*, 527: 105-9.

Dubin-Bar, D., A. Bitan, A. Bakhrat, R. Kaiden-Hasson, S. Etzion, B. Shaanan, and U. Abdu. 2008. 'The Drosophila IKK-related kinase (Ik2) and Spindle-F proteins are part of a complex that regulates cytoskeleton organization during oogenesis', *BMC Cell Biol*, 9: 51.

Eapen, V. V., S. Swarup, M. J. Hoyer, J. A. Paulo, and J. W. Harper. 2021. 'Quantitative proteomics reveals the selectivity of ubiquitin-binding autophagy receptors in the turnover of damaged lysosomes by lysophagy', *Elife*, 10.

Elias, J. E., and S. P. Gygi. 2007. 'Target-decoy search strategy for increased confidence in large-scale protein identifications by mass spectrometry', *Nat Methods*, 4: 207-14.

Eng, J. K., T. A. Jahan, and M. R. Hoopmann. 2013. 'Comet: an open-source MS/MS sequence database search tool', *Proteomics*, 13: 22-4.

Enserink, J. M., and R. D. Kolodner. 2010. 'An overview of Cdk1-controlled targets and processes', *Cell Div*, 5: 11.

Erickson, B. K., J. Mintseris, D. K. Schweppe, J. Navarrete-Perea, A. R. Erickson, D. P. Nusinow, J. A. Paulo, and S. P. Gygi. 2019. 'Active Instrument Engagement Combined with a Real-Time Database Search for Improved Performance of Sample Multiplexing Workflows', *J Proteome Res*, 18: 1299-306.

Fagerberg, L., B. M. Hallstrom, P. Oksvold, C. Kampf, D. Djureinovic, J. Odeberg, M. Habuka, S. Tahmasebpoor, A. Danielsson, K. Edlund, A. Asplund, E. Sjostedt, E. Lundberg, C. A. Szigyarto, M. Skogs, J. O. Takanen, H. Berling, H. Tegel, J. Mulder, P. Nilsson, J. M. Schwenk, C. Lindskog, F. Danielsson, A. Mardinoglu, A. Sivertsson, K. von Feilitzen, M. Forsberg, M. Zwahlen, I. Olsson, S. Navani, M. Huss, J. Nielsen, F. Ponten, and M. Uhlen. 2014. 'Analysis of the human tissue-specific expression by genome-wide integration of transcriptomics and antibody-based proteomics', *Mol Cell Proteomics*, 13: 397-406.

Fitzgerald, K. A., S. M. McWhirter, K. L. Faia, D. C. Rowe, E. Latz, D. T. Golenbock, A. J. Coyle, S. M. Liao, and T. Maniatis. 2003. 'IKKepsilon and TBK1 are essential components of the IRF3 signaling pathway', *Nat Immunol*, 4: 491-6.

Fu, T., J. Liu, Y. Wang, X. Xie, S. Hu, and L. Pan. 2018. 'Mechanistic insights into the interactions of NAP1 with the SKICH domains of NDP52 and TAX1BP1', *Proc Natl Acad Sci U S A*, 115: E11651-E60.

Fu, T., M. Zhang, Z. Zhou, P. Wu, C. Peng, Y. Wang, X. Gong, Y. Li, Y. Wang, X. Xu, M. Li, L. Shen, and L. Pan. 2021. 'Structural and biochemical advances on the recruitment of the autophagy-initiating ULK and TBK1 complexes by autophagy receptor NDP52', *Sci Adv*, 7.

Fujita, F., Y. Taniguchi, T. Kato, Y. Narita, A. Furuya, T. Ogawa, H. Sakurai, T. Joh, M. Itoh, M. Delhase, M. Karin, and M. Nakanishi. 2003. 'Identification of NAP1, a regulatory subunit of IkappaB kinase-related kinases that potentiates NF-kappaB signaling', *Mol Cell Biol*, 23: 7780-93.

Fukasaka, M., D. Ori, T. Kawagoe, S. Uematsu, K. Maruyama, T. Okazaki, T. Kozaki, T. Imamura, S. Tartey, T. Mino, T. Satoh, S. Akira, and O. Takeuchi. 2013. 'Critical role of AZI2 in GM-CSF-induced dendritic cell differentiation', *J Immunol*, 190: 5702-11.

Furuya, N., S. Kakuta, K. Sumiyoshi, M. Ando, R. Nonaka, A. Suzuki, S. Kazuno, S. Saiki, and N. Hattori. 2018. 'NDP52 interacts with mitochondrial RNA poly(A) polymerase to promote mitophagy', *EMBO Rep*, 19.

Gachon, F., A. Peleraux, S. Thebault, J. Dick, I. Lemasson, C. Devaux, and J. M. Mesnard. 1998. 'CREB-2, a cellular CRE-dependent transcription repressor, functions in association with Tax as an activator of the human T-cell leukemia virus type 1 promoter', *J Virol*, 72: 8332-7.

Ganley, I. G., H. Lam du, J. Wang, X. Ding, S. Chen, and X. Jiang. 2009. 'ULK1.ATG13.FIP200 complex mediates mTOR signaling and is essential for autophagy', *J Biol Chem*, 284: 12297-305.

Gassaway, B. M., J. Li, R. Rad, J. Mintseris, K. Mohler, T. Levy, M. Aguiar, S. A. Beausoleil, J. A. Paulo, J. Rinehart, E. L. Huttlin, and S. P. Gygi. 2022. 'A multi-purpose, regenerable, proteome-scale, human phosphoserine resource for phosphoproteomics', *Nat Methods*.

Gatot, J. S., R. Gioia, T. L. Chau, F. Patrascu, M. Warnier, P. Close, J. P. Chapelle, E. Muraille, K. Brown, U. Siebenlist, J. Piette, E. Dejardin, and A. Chariot. 2007. 'Lipopolysaccharide-mediated interferon regulatory factor activation involves TBK1-IKKepsilon-dependent Lys(63)-linked polyubiquitination and phosphorylation of TANK/I-TRAF', *J Biol Chem*, 282: 31131-46.

Gleason, C. E., A. Ordureau, R. Gourlay, J. S. C. Arthur, and P. Cohen. 2011. 'Polyubiquitin binding to optineurin is required for optimal activation of TANK-binding kinase 1 and production of interferon beta', *J Biol Chem*, 286: 35663-74.

Goncalves, A., T. Burckstummer, E. Dixit, R. Scheicher, M. W. Gorna, E. Karayel, C. Sugar, A. Stukalov, T. Berg, R. Kralovics, M. Planyavsky, K. L. Bennett, J. Colinge, and G. Superti-Furga. 2011. 'Functional dissection of the TBK1 molecular network', *PLoS One*, 6: e23971.

Gu, M., Z. Liu, R. Lai, S. Liu, W. Lin, C. Ouyang, S. Ye, H. Huang, and X. Wang. 2016. 'RKIP and TBK1 form a positive feedback loop to promote type I interferon production in innate immunity', *EMBO J*, 35: 2553-65.

Guardia, C. M., X. F. Tan, T. Lian, M. S. Rana, W. Zhou, E. T. Christenson, A. J. Lowry, J. D. Faraldo-Gomez, J. S. Bonifacino, J. Jiang, and A. Banerjee. 2020. 'Structure of Human ATG9A, the Only Transmembrane Protein of the Core Autophagy Machinery', *Cell Rep*, 31: 107837.

Hara, T., K. Nakamura, M. Matsui, A. Yamamoto, Y. Nakahara, R. Suzuki-Migishima, M. Yokoyama, K. Mishima, I. Saito, H. Okano, and N. Mizushima. 2006. 'Suppression of basal autophagy in neural cells causes neurodegenerative disease in mice', *Nature*, 441: 885-9.

Hara, T., A. Takamura, C. Kishi, S. Iemura, T. Natsume, J. L. Guan, and N. Mizushima. 2008. 'FIP200, a ULK-interacting protein, is required for autophagosome formation in mammalian cells', *J Cell Biol*, 181: 497-510.

Hatch, E. M., A. H. Fischer, T. J. Deerinck, and M. W. Hetzer. 2013. 'Catastrophic nuclear envelope collapse in cancer cell micronuclei', *Cell*, 154: 47-60.

Helgason, E., Q. T. Phung, and E. C. Dueber. 2013. 'Recent insights into the complexity of Tank-binding kinase 1 signaling networks: the emerging role of cellular localization in the activation and substrate specificity of TBK1', *FEBS Lett*, 587: 1230-7.

Hemmi, H., O. Takeuchi, S. Sato, M. Yamamoto, T. Kaisho, H. Sanjo, T. Kawai, K. Hoshino, K. Takeda, and S. Akira. 2004. 'The roles of two IkappaB kinase-related kinases in lipopolysaccharide and double stranded RNA signaling and viral infection', *J Exp Med*, 199: 1641-50.

Heo, J. M., A. Ordureau, J. A. Paulo, J. Rinehart, and J. W. Harper. 2015. 'The PINK1-PARKIN Mitochondrial Ubiquitylation Pathway Drives a Program of OPTN/NDP52 Recruitment and TBK1 Activation to Promote Mitophagy', *Mol Cell*, 60: 7-20.

Hirota, T., J. J. Lipp, B. H. Toh, and J. M. Peters. 2005. 'Histone H3 serine 10 phosphorylation by Aurora B causes HP1 dissociation from heterochromatin', *Nature*, 438: 1176-80.

Huang, K. L., A. D. Scott, D. C. Zhou, L. B. Wang, A. Weerasinghe, A. Elmas, R. Liu, Y. Wu, M. C. Wendl, M. A. Wyczalkowski, J. Baral, S. Sengupta, C. W. Lai, K. Ruggles, S. H. Payne, B. Raphael, D. Fenyo, K. Chen, G. Mills, and L. Ding. 2021. 'Spatially interacting phosphorylation sites and mutations in cancer', *Nat Commun*, 12: 2313.

Huang, S., P. Wan, S. Huang, S. Liu, Q. Xiang, G. Yang, M. A. Shereen, P. Pan, J. Wang, W. Liu, K. Wu, and J. Wu. 2021. 'The APC10 subunit of the anaphase-promoting

complex/cyclosome orchestrates NLRP3 inflammasome activation during the cell cycle', *FEBS Lett*, 595: 2463-78.

Huttlin, E. L., M. P. Jedrychowski, J. E. Elias, T. Goswami, R. Rad, S. A. Beausoleil, J. Villen, W. Haas, M. E. Sowa, and S. P. Gygi. 2010. 'A tissue-specific atlas of mouse protein phosphorylation and expression', *Cell*, 143: 1174-89.

Hyer, M. L., M. A. Milhollen, J. Ciavarri, P. Fleming, T. Traore, D. Sappal, J. Huck, J. Shi, J. Gavin, J. Brownell, Y. Yang, B. Stringer, R. Griffin, F. Bruzzese, T. Soucy, J. Duffy, C. Rabino, J. Riceberg, K. Hoar, A. Lublinsky, S. Menon, M. Sintchak, N. Bump, S. M. Pulukuri, S. Langston, S. Tirrell, M. Kuranda, P. Veiby, J. Newcomb, P. Li, J. T. Wu, J. Powe, L. R. Dick, P. Greenspan, K. Galvin, M. Manfredi, C. Claiborne, B. S. Amidon, and N. F. Bence. 2018. 'A small-molecule inhibitor of the ubiquitin activating enzyme for cancer treatment', *Nat Med*, 24: 186-93.

Ikeda, F., C. M. Hecker, A. Rozenknop, R. D. Nordmeier, V. Rogov, K. Hofmann, S. Akira, V. Dotsch, and I. Dikic. 2007. 'Involvement of the ubiquitin-like domain of TBK1/IKK-i kinases in regulation of IFN-inducible genes', *EMBO J*, 26: 3451-62.

Ishii, K. J., T. Kawagoe, S. Koyama, K. Matsui, H. Kumar, T. Kawai, S. Uematsu, O. Takeuchi, F. Takeshita, C. Coban, and S. Akira. 2008. 'TANK-binding kinase-1 delineates innate and adaptive immune responses to DNA vaccines', *Nature*, 451: 725-9.

Iwamura, T., M. Yoneyama, K. Yamaguchi, W. Suhara, W. Mori, K. Shiota, Y. Okabe, H. Namiki, and T. Fujita. 2001. 'Induction of IRF-3/-7 kinase and NF-kappaB in response to double-stranded RNA and virus infection: common and unique pathways', *Genes Cells*, 6: 375-88.

Jiang, Y., S. Chen, Q. Li, J. Liang, W. Lin, J. Li, Z. Liu, M. Wen, M. Cao, and J. Hong. 2021. 'TANK-Binding Kinase 1 (TBK1) Serves as a Potential Target for Hepatocellular Carcinoma by Enhancing Tumor Immune Infiltration', *Front Immunol*, 12: 612139.

Johansen, T., and T. Lamark. 2011. 'Selective autophagy mediated by autophagic adapter proteins', *Autophagy*, 7: 279-96.

Johnson, Jared L., Tomer M. Yaron, Emily M. Huntsman, Alexander Kerelsky, Junho Song, Amit Regev, Ting-Yu Lin, Katarina Liberatore, Daniel M. Cizin, Benjamin M. Cohen, Neil Vasan, Yilun Ma, Konstantin Krismer, Jaylissa Torres Robles, Bert van de Kooij, Anne E. van Vlimmeren, Nicole Andrée-Busch, Norbert Käufer, Maxim V. Dorovkov, Alexey G. Ryazanov, Yuichiro Takagi, Edward R. Kastenhuber, Marcus D. Goncalves, Olivier Elemento, Dylan J. Taatjes, Alexandre Maucuer, Akio Yamashita, Alexei Degterev, Rune Linding, John Blenis, Peter V. Hornbeck, Benjamin E. Turk, Michael B. Yaffe, and Lewis C. Cantley. 2022. 'A global atlas of substrate specificities for the human serine/threonine kinome', *bioRxiv*: 2022.05.22.492882.

Jones, S. M., and A. Kazlauskas. 2001. 'Growth-factor-dependent mitogenesis requires two distinct phases of signalling', *Nat Cell Biol*, 3: 165-72.

Joung, I., J. L. Strominger, and J. Shin. 1996. 'Molecular cloning of a phosphotyrosine-independent ligand of the p56lck SH2 domain', *Proc Natl Acad Sci U S A*, 93: 5991-5.

Judith, D., H. B. J. Jefferies, S. Boeing, D. Frith, A. P. Snijders, and S. A. Tooze. 2019. 'ATG9A shapes the forming autophagosome through Arfaptin 2 and phosphatidylinositol 4-kinase IIIbeta', *J Cell Biol*, 218: 1634-52.

Katz, M., I. Amit, and Y. Yarden. 2007. 'Regulation of MAPKs by growth factors and receptor tyrosine kinases', *Biochim Biophys Acta*, 1773: 1161-76.

Kawagoe, T., O. Takeuchi, Y. Takabatake, H. Kato, Y. Isaka, T. Tsujimura, and S. Akira. 2009. 'TANK is a negative regulator of Toll-like receptor signaling and is critical for the prevention of autoimmune nephritis', *Nat Immunol*, 10: 965-72.

Kim, H. J., T. Kim, N. J. Hoffman, D. Xiao, D. E. James, S. J. Humphrey, and P. Yang. 2021. 'PhosR enables processing and functional analysis of phosphoproteomic data', *Cell Rep*, 34: 108771.

Kim, J., W. P. Huang, P. E. Stromhaug, and D. J. Klionsky. 2002. 'Convergence of multiple autophagy and cytoplasm to vacuole targeting components to a perivacuolar membrane compartment prior to de novo vesicle formation', *J Biol Chem*, 277: 763-73.

Kim, J. Y., E. A. Welsh, U. Oguz, B. Fang, Y. Bai, F. Kinose, C. Bronk, L. L. Remsing Rix, A. A. Beg, U. Rix, S. A. Eschrich, J. M. Koomen, and E. B. Haura. 2013. 'Dissection of TBK1 signaling via phosphoproteomics in lung cancer cells', *Proc Natl Acad Sci U S A*, 110: 12414-9.

Kirkin, V., and V. V. Rogov. 2019. 'A Diversity of Selective Autophagy Receptors Determines the Specificity of the Autophagy Pathway', *Mol Cell*, 76: 268-85.

Kishi-Itakura, C., I. Koyama-Honda, E. Itakura, and N. Mizushima. 2014. 'Ultrastructural analysis of autophagosome organization using mammalian autophagy-deficient cells', *J Cell Sci*, 127: 4089-102.

Kodani, A., K. A. Knopp, E. Di Lullo, H. Retallack, A. R. Kriegstein, J. L. DeRisi, and J. F. Reiter. 2022. 'Zika virus alters centrosome organization to suppress the innate immune response', *EMBO Rep*, 23: e52211.

Komatsu, M., S. Waguri, T. Chiba, S. Murata, J. Iwata, I. Tanida, T. Ueno, M. Koike, Y. Uchiyama, E. Kominami, and K. Tanaka. 2006. 'Loss of autophagy in the central nervous system causes neurodegeneration in mice', *Nature*, 441: 880-4.

Krick, R., Y. Muehe, T. Prick, S. Bremer, P. Schlotterhose, E. L. Eskelinen, J. Millen, D. S. Goldfarb, and M. Thumm. 2008. 'Piecemeal microautophagy of the nucleus requires the core macroautophagy genes', *Mol Biol Cell*, 19: 4492-505.

Krupina, K., A. Goginashvili, and D. W. Cleveland. 2021. 'Causes and consequences of micronuclei', *Curr Opin Cell Biol*, 70: 91-99.

Kuusisto, E., A. Salminen, and I. Alafuzoff. 2001. 'Ubiquitin-binding protein p62 is present in neuronal and glial inclusions in human tauopathies and synucleinopathies', *Neuroreport*, 12: 2085-90.

Kuusisto, E., A. Salminen, and I. Alafuzoff. 2002. 'Early accumulation of p62 in neurofibrillary tangles in Alzheimer's disease: possible role in tangle formation', *Neuropathol Appl Neurobiol*, 28: 228-37.

Kwon, M., M. L. Leibowitz, and J. H. Lee. 2020. 'Small but mighty: the causes and consequences of micronucleus rupture', *Exp Mol Med*, 52: 1777-86.

Larabi, A., J. M. Devos, S. L. Ng, M. H. Nanao, A. Round, T. Maniatis, and D. Panne. 2013. 'Crystal structure and mechanism of activation of TANK-binding kinase 1', *Cell Rep*, 3: 734-46.

Lazarou, M., D. A. Sliter, L. A. Kane, S. A. Sarraf, C. Wang, J. L. Burman, D. P. Sideris, A. I. Fogel, and R. J. Youle. 2015. 'The ubiquitin kinase PINK1 recruits autophagy receptors to induce mitophagy', *Nature*, 524: 309-14.

Lee, Y., B. Song, C. Park, and K. S. Kwon. 2013. 'TRIM11 negatively regulates IFNbeta production and antiviral activity by targeting TBK1', *PLoS One*, 8: e63255.

Li, F., X. Xie, Y. Wang, J. Liu, X. Cheng, Y. Guo, Y. Gong, S. Hu, and L. Pan. 2016. 'Structural insights into the interaction and disease mechanism of neurodegenerative disease-associated optineurin and TBK1 proteins', *Nat Commun*, 7: 12708.

Li, F., D. Xu, Y. Wang, Z. Zhou, J. Liu, S. Hu, Y. Gong, J. Yuan, and L. Pan. 2018. 'Structural insights into the ubiquitin recognition by OPTN (optineurin) and its regulation by TBK1-mediated phosphorylation', *Autophagy*, 14: 66-79.

Li, J., J. G. Van Vranken, L. Pontano Vaites, D. K. Schweppe, E. L. Huttlin, C. Etienne, P. Nandhikonda, R. Viner, A. M. Robitaille, A. H. Thompson, K. Kuhn, I. Pike, R. D. Bomgarden, J. C. Rogers, S. P. Gygi, and J. A. Paulo. 2020. 'TMTpro reagents: a set of isobaric labeling mass tags enables simultaneous proteome-wide measurements across 16 samples', *Nat Methods*, 17: 399-404.

Licht, D. J., and D. R. Lynch. 2002. 'Juvenile dentatorubral-pallidoluysian atrophy: new clinical features', *Pediatr Neurol*, 26: 51-4.

Lin, T., P. Y. Pan, Y. T. Lai, K. W. Chiang, H. L. Hsieh, Y. P. Wu, J. M. Ke, M. C. Lee, S. S. Liao, H. T. Shih, C. Y. Tang, S. B. Yang, H. C. Cheng, J. T. Wu, Y. N. Jan, and H. H. Lee. 2015. 'Spindle-F Is the Central Mediator of Ik2 Kinase-Dependent Dendrite Pruning in Drosophila Sensory Neurons', *PLoS Genet*, 11: e1005642.

Liu, S., X. Cai, J. Wu, Q. Cong, X. Chen, T. Li, F. Du, J. Ren, Y. T. Wu, N. V. Grishin, and Z. J. Chen. 2015. 'Phosphorylation of innate immune adaptor proteins MAVS, STING, and TRIF induces IRF3 activation', *Science*, 347: aaa2630.

Ma, X., E. Helgason, Q. T. Phung, C. L. Quan, R. S. Iyer, M. W. Lee, K. K. Bowman, M. A. Starovasnik, and E. C. Dueber. 2012. 'Molecular basis of Tank-binding kinase 1 activation by transautophosphorylation', *Proc Natl Acad Sci U S A*, 109: 9378-83.

Maan, M., N. J. Agrawal, J. Padmanabhan, C. C. Leitzinger, Y. Rivera-Rivera, H. I. Saavedra, and S. P. Chellappan. 2021. 'Tank Binding Kinase 1 modulates spindle assembly checkpoint components to regulate mitosis in breast and lung cancer cells', *Biochim Biophys Acta Mol Cell Res*, 1868: 118929.

Macville, M., E. Schrock, H. Padilla-Nash, C. Keck, B. M. Ghadimi, D. Zimonjic, N. Popescu, and T. Ried. 1999. 'Comprehensive and definitive molecular cytogenetic characterization of HeLa cells by spectral karyotyping', *Cancer Res*, 59: 141-50.

Mari, M., J. Griffith, E. Rieter, L. Krishnappa, D. J. Klionsky, and F. Reggiori. 2010. 'An Atg9-containing compartment that functions in the early steps of autophagosome biogenesis', *J Cell Biol*, 190: 1005-22.

Maruyama, K., M. Fukasaka, S. Uematsu, O. Takeuchi, T. Kondo, T. Saitoh, M. M. Martino, and S. Akira. 2015. '5-Azacytidine-induced protein 2 (AZI2) regulates bone mass by fine-tuning osteoclast survival', *J Biol Chem*, 290: 9377-86.

Maruyama, K., T. Kawagoe, T. Kondo, S. Akira, and O. Takeuchi. 2012. 'TRAF family member-associated NF-kappaB activator (TANK) is a negative regulator of osteoclastogenesis and bone formation', *J Biol Chem*, 287: 29114-24.

Maruyama, S., Y. Saito, E. Nakagawa, T. Saito, H. Komaki, K. Sugai, M. Sasaki, S. Kumada, Y. Saito, H. Tanaka, N. Minami, and Y. Goto. 2012. 'Importance of CAG repeat length in childhood-onset dentatorubral-pallidoluysian atrophy', *J Neurol*, 259: 2329-34.

Matsumoto, G., T. Shimogori, N. Hattori, and N. Nukina. 2015. 'TBK1 controls autophagosomal engulfment of polyubiquitinated mitochondria through p62/SQSTM1 phosphorylation', *Hum Mol Genet*, 24: 4429-42.

Matsumoto, G., K. Wada, M. Okuno, M. Kurosawa, and N. Nukina. 2011. 'Serine 403 phosphorylation of p62/SQSTM1 regulates selective autophagic clearance of ubiquitinated proteins', *Mol Cell*, 44: 279-89.
McAlister, G. C., D. P. Nusinow, M. P. Jedrychowski, M. Wuhr, E. L. Huttlin, B. K. Erickson, R. Rad, W. Haas, and S. P. Gygi. 2014. 'MultiNotch MS3 enables accurate, sensitive, and multiplexed detection of differential expression across cancer cell line proteomes', *Anal Chem*, 86: 7150-8.
McWhirter, S. M., K. A. Fitzgerald, J. Rosains, D. C. Rowe, D. T. Golenbock, and T. Maniatis. 2004. 'IFN-regulatory factor 3-dependent gene expression is defective in Tbk1-deficient mouse embryonic fibroblasts', *Proc Natl Acad Sci U S A*, 101: 233-8.
Meloche, S. 1995. 'Cell cycle reentry of mammalian fibroblasts is accompanied by the sustained activation of p44mapk and p42mapk isoforms in the G1 phase and their inactivation at the G1/S transition', *J Cell Physiol*, 163: 577-88.
Menzies, F. M., A. Fleming, A. Caricasole, C. F. Bento, S. P. Andrews, A. Ashkenazi, J. Fullgrabe, A. Jackson, M. Jimenez Sanchez, C. Karabiyik, F. Licitra, A. Lopez Ramirez, M. Pavel, C. Puri, M. Renna, T. Ricketts, L. Schlotawa, M. Vicinanza, H. Won, Y. Zhu, J. Skidmore, and D. C. Rubinsztein. 2017. 'Autophagy and Neurodegeneration: Pathogenic Mechanisms and Therapeutic Opportunities', *Neuron*, 93: 1015-34.
Mercer, C. A., A. Kaliappan, and P. B. Dennis. 2009. 'A novel, human Atg13 binding protein, Atg101, interacts with ULK1 and is essential for macroautophagy', *Autophagy*, 5: 649-62.
Minowa-Nozawa, A., T. Nozawa, K. Okamoto-Furuta, H. Kohda, and I. Nakagawa. 2017. 'Rab35 GTPase recruits NDP52 to autophagy targets', *EMBO J*, 36: 2790-807.
Miyagawa, J., M. Muguruma, H. Aoto, I. Suetake, M. Nakamura, and S. Tajima. 1999. 'Isolation of the novel cDNA of a gene of which expression is induced by a demethylating stimulus', *Gene*, 240: 289-95.
Mizushima, N., and M. Komatsu. 2011. 'Autophagy: renovation of cells and tissues', *Cell*, 147: 728-41.
Mochida, K., Y. Oikawa, Y. Kimura, H. Kirisako, H. Hirano, Y. Ohsumi, and H. Nakatogawa. 2015. 'Receptor-mediated selective autophagy degrades the endoplasmic reticulum and the nucleus', *Nature*, 522: 359-62.
Moore, A. S., and E. L. Holzbaur. 2016. 'Dynamic recruitment and activation of ALS-associated TBK1 with its target optineurin are required for efficient mitophagy', *Proc Natl Acad Sci U S A*, 113: E3349-58.
Morton, S., L. Hesson, M. Peggie, and P. Cohen. 2008. 'Enhanced binding of TBK1 by an optineurin mutant that causes a familial form of primary open angle glaucoma', *FEBS Lett*, 582: 997-1002.
Mostofa, M. G., M. A. Rahman, N. Koike, A. M. Yeasmin, N. Islam, T. M. Waliullah, S. Hosoyamada, M. Shimobayashi, T. Kobayashi, M. N. Hall, and T. Ushimaru. 2018. 'CLIP and cohibin separate rDNA from nucleolar proteins destined for degradation by nucleophagy', *J Cell Biol*, 217: 2675-90.
Munitic, I., M. L. Giardino Torchia, N. P. Meena, G. Zhu, C. C. Li, and J. D. Ashwell. 2013. 'Optineurin insufficiency impairs IRF3 but not NF-kappaB activation in immune cells', *J Immunol*, 191: 6231-40.
Nabet, B., F. M. Ferguson, B. K. A. Seong, M. Kuljanin, A. L. Leggett, M. L. Mohardt, A. Robichaud, A. S. Conway, D. L. Buckley, J. D. Mancias, J. E. Bradner, K. Stegmaier,

and N. S. Gray. 2020. 'Rapid and direct control of target protein levels with VHL-recruiting dTAG molecules', *Nat Commun*, 11: 4687.
Nabet, B., J. M. Roberts, D. L. Buckley, J. Paulk, S. Dastjerdi, A. Yang, A. L. Leggett, M. A. Erb, M. A. Lawlor, A. Souza, T. G. Scott, S. Vittori, J. A. Perry, J. Qi, G. E. Winter, K. K. Wong, N. S. Gray, and J. E. Bradner. 2018. 'The dTAG system for immediate and target-specific protein degradation', *Nat Chem Biol*, 14: 431-41.
Nagafuchi, S., H. Yanagisawa, K. Sato, T. Shirayama, E. Ohsaki, M. Bundo, T. Takeda, K. Tadokoro, I. Kondo, N. Murayama, and et al. 1994. 'Dentatorubral and pallidoluysian atrophy expansion of an unstable CAG trinucleotide on chromosome 12p', *Nat Genet*, 6: 14-8.
Nasa, I., and A. N. Kettenbach. 2018. 'Coordination of Protein Kinase and Phosphoprotein Phosphatase Activities in Mitosis', *Front Cell Dev Biol*, 6: 30.
Newman, A. C., C. L. Scholefield, A. J. Kemp, M. Newman, E. G. McIver, A. Kamal, and S. Wilkinson. 2012. 'TBK1 kinase addiction in lung cancer cells is mediated via autophagy of Tax1bp1/Ndp52 and non-canonical NF-kappaB signalling', *PLoS One*, 7: e50672.
Nguyen, T. N., J. Sawa-Makarska, G. Khuu, W. K. Lam, E. Adriaenssens, D. Fracchiolla, S. Shoebridge, D. Bernklau, B. S. Padman, M. Skulsuppaisarn, R. S. J. Lindblom, S. Martens, and M. Lazarou. 2023. 'Unconventional initiation of PINK1/Parkin mitophagy by Optineurin', *Mol Cell*, 83: 1693-709 e9.
Nigg, E. A. 2001. 'Mitotic kinases as regulators of cell division and its checkpoints', *Nat Rev Mol Cell Biol*, 2: 21-32.
Noda, T., J. Kim, W. P. Huang, M. Baba, C. Tokunaga, Y. Ohsumi, and D. J. Klionsky. 2000. 'Apg9p/Cvt7p is an integral membrane protein required for transport vesicle formation in the Cvt and autophagy pathways', *J Cell Biol*, 148: 465-80.
Okamoto, T., S. K. Yeo, M. Hao, M. R. Copley, M. A. Haas, S. Chen, and J. L. Guan. 2020. 'FIP200 Suppresses Immune Checkpoint Therapy Responses in Breast Cancers by Limiting AZI2/TBK1/IRF Signaling Independent of Its Canonical Autophagy Function', *Cancer Res*, 80: 3580-92.
Olsen, J. V., M. Vermeulen, A. Santamaria, C. Kumar, M. L. Miller, L. J. Jensen, F. Gnad, J. Cox, T. S. Jensen, E. A. Nigg, S. Brunak, and M. Mann. 2010. 'Quantitative phosphoproteomics reveals widespread full phosphorylation site occupancy during mitosis', *Sci Signal*, 3: ra3.
Onorati, M., Z. Li, F. Liu, A. M. M. Sousa, N. Nakagawa, M. Li, M. T. Dell'Anno, F. O. Gulden, S. Pochareddy, A. T. N. Tebbenkamp, W. Han, M. Pletikos, T. Gao, Y. Zhu, C. Bichsel, L. Varela, K. Szigeti-Buck, S. Lisgo, Y. Zhang, A. Testen, X. B. Gao, J. Mlakar, M. Popovic, M. Flamand, S. M. Strittmatter, L. K. Kaczmarek, E. S. Anton, T. L. Horvath, B. D. Lindenbach, and N. Sestan. 2016. 'Zika Virus Disrupts Phospho-TBK1 Localization and Mitosis in Human Neuroepithelial Stem Cells and Radial Glia', *Cell Rep*, 16: 2576-92.
Outlioua, A., M. Pourcelot, and D. Arnoult. 2018. 'The Role of Optineurin in Antiviral Type I Interferon Production', *Front Immunol*, 9: 853.
Ozlu, N., F. Monigatti, B. Y. Renard, C. M. Field, H. Steen, T. J. Mitchison, and J. J. Steen. 2010. 'Binding partner switching on microtubules and aurora-B in the mitosis to cytokinesis transition', *Mol Cell Proteomics*, 9: 336-50.

Pan, X., P. Roberts, Y. Chen, E. Kvam, N. Shulga, K. Huang, S. Lemmon, and D. S. Goldfarb. 2000. 'Nucleus-vacuole junctions in Saccharomyces cerevisiae are formed through the direct interaction of Vac8p with Nvj1p', *Mol Biol Cell*, 11: 2445-57.

Pankiv, S., T. H. Clausen, T. Lamark, A. Brech, J. A. Bruun, H. Outzen, A. Overvatn, G. Bjorkoy, and T. Johansen. 2007. 'p62/SQSTM1 binds directly to Atg8/LC3 to facilitate degradation of ubiquitinated protein aggregates by autophagy', *J Biol Chem*, 282: 24131-45.

Park, Y. E., Y. K. Hayashi, G. Bonne, T. Arimura, S. Noguchi, I. Nonaka, and I. Nishino. 2009. 'Autophagic degradation of nuclear components in mammalian cells', *Autophagy*, 5: 795-804.

Paulo, J. A., J. D. O'Connell, R. A. Everley, J. O'Brien, M. A. Gygi, and S. P. Gygi. 2016. 'Quantitative mass spectrometry-based multiplexing compares the abundance of 5000 S. cerevisiae proteins across 10 carbon sources', *J Proteomics*, 148: 85-93.

Paulo, J. A., J. D. O'Connell, and S. P. Gygi. 2016. 'A Triple Knockout (TKO) Proteomics Standard for Diagnosing Ion Interference in Isobaric Labeling Experiments', *J Am Soc Mass Spectrom*, 27: 1620-5.

Pillai, S., J. Nguyen, J. Johnson, E. Haura, D. Coppola, and S. Chellappan. 2015. 'Tank binding kinase 1 is a centrosome-associated kinase necessary for microtubule dynamics and mitosis', *Nat Commun*, 6: 10072.

Pomerantz, J. L., and D. Baltimore. 1999. 'NF-kappaB activation by a signaling complex containing TRAF2, TANK and TBK1, a novel IKK-related kinase', *EMBO J*, 18: 6694-704.

Pourcelot, M., N. Zemirli, L. Silva Da Costa, R. Loyant, D. Garcin, D. Vitour, I. Munitic, A. Vazquez, and D. Arnoult. 2016. 'The Golgi apparatus acts as a platform for TBK1 activation after viral RNA sensing', *BMC Biol*, 14: 69.

Prescott, D. M., and M. A. Bender. 1962. 'Synthesis of RNA and protein during mitosis in mammalian tissue culture cells', *Exp Cell Res*, 26: 260-8.

Pylayeva-Gupta, Y., E. Grabocka, and D. Bar-Sagi. 2011. 'RAS oncogenes: weaving a tumorigenic web', *Nat Rev Cancer*, 11: 761-74.

Rad, R., J. Li, J. Mintseris, J. O'Connell, S. P. Gygi, and D. K. Schweppe. 2021. 'Improved Monoisotopic Mass Estimation for Deeper Proteome Coverage', *J Proteome Res*, 20: 591-98.

Rahman, M. A., M. G. Mostofa, and T. Ushimaru. 2018. 'The Nem1/Spo7-Pah1/lipin axis is required for autophagy induction after TORC1 inactivation', *FEBS J*, 285: 1840-60.

Ravenhill, B. J., K. B. Boyle, N. von Muhlinen, C. J. Ellison, G. R. Masson, E. G. Otten, A. Foeglein, R. Williams, and F. Randow. 2019. 'The Cargo Receptor NDP52 Initiates Selective Autophagy by Recruiting the ULK Complex to Cytosol-Invading Bacteria', *Mol Cell*, 74: 320-29 e6.

Reggiori, F., K. A. Tucker, P. E. Stromhaug, and D. J. Klionsky. 2004. 'The Atg1-Atg13 complex regulates Atg9 and Atg23 retrieval transport from the pre-autophagosomal structure', *Dev Cell*, 6: 79-90.

Reimann, H., H. Stopper, and H. Hintzsche. 2020. 'Long-term fate of etoposide-induced micronuclei and micronucleated cells in Hela-H2B-GFP cells', *Arch Toxicol*, 94: 3553-61.

Reimann, H., H. Stopper, and H. Hintzsche. 2023. 'Fate of micronuclei and micronucleated cells after treatment of HeLa cells with different genotoxic agents', *Arch Toxicol*, 97: 875-89.

Rello-Varona, S., D. Lissa, S. Shen, M. Niso-Santano, L. Senovilla, G. Marino, I. Vitale, M. Jemaa, F. Harper, G. Pierron, M. Castedo, and G. Kroemer. 2012. 'Autophagic removal of micronuclei', *Cell Cycle*, 11: 170-6.

Revach, O. Y., S. Liu, and R. W. Jenkins. 2020. 'Targeting TANK-binding kinase 1 (TBK1) in cancer', *Expert Opin Ther Targets*, 24: 1065-78.

Richter, B., D. A. Sliter, L. Herhaus, A. Stolz, C. Wang, P. Beli, G. Zaffagnini, P. Wild, S. Martens, S. A. Wagner, R. J. Youle, and I. Dikic. 2016. 'Phosphorylation of OPTN by TBK1 enhances its binding to Ub chains and promotes selective autophagy of damaged mitochondria', *Proc Natl Acad Sci U S A*, 113: 4039-44.

Roberts, P., S. Moshitch-Moshkovitz, E. Kvam, E. O'Toole, M. Winey, and D. S. Goldfarb. 2003. 'Piecemeal microautophagy of nucleus in Saccharomyces cerevisiae', *Mol Biol Cell*, 14: 129-41.

Runde, A. P., R. Mack, J. Pb S, and J. Zhang. 2022. 'The role of TBK1 in cancer pathogenesis and anticancer immunity', *J Exp Clin Cancer Res*, 41: 135.

Ryzhakov, G., and F. Randow. 2007. 'SINTBAD, a novel component of innate antiviral immunity, shares a TBK1-binding domain with NAP1 and TANK', *EMBO J*, 26: 3180-90.

Saitoh, T., N. Fujita, T. Hayashi, K. Takahara, T. Satoh, H. Lee, K. Matsunaga, S. Kageyama, H. Omori, T. Noda, N. Yamamoto, T. Kawai, K. Ishii, O. Takeuchi, T. Yoshimori, and S. Akira. 2009. 'Atg9a controls dsDNA-driven dynamic translocation of STING and the innate immune response', *Proc Natl Acad Sci U S A*, 106: 20842-6.

Sarraf, S. A., H. V. Shah, G. Kanfer, A. M. Pickrell, L. A. Holtzclaw, M. E. Ward, and R. J. Youle. 2020. 'Loss of TAX1BP1-Directed Autophagy Results in Protein Aggregate Accumulation in the Brain', *Mol Cell*, 80: 779-95 e10.

Sarraf, S. A., D. P. Sideris, N. Giagtzoglou, L. Ni, M. W. Kankel, A. Sen, L. E. Bochicchio, C. H. Huang, S. C. Nussenzweig, S. H. Worley, P. D. Morton, S. Artavanis-Tsakonas, R. J. Youle, and A. M. Pickrell. 2019. 'PINK1/Parkin Influences Cell Cycle by Sequestering TBK1 at Damaged Mitochondria, Inhibiting Mitosis', *Cell Rep*, 29: 225-35 e5.

Sasai, M., H. Oshiumi, M. Matsumoto, N. Inoue, F. Fujita, M. Nakanishi, and T. Seya. 2005. 'Cutting Edge: NF-kappaB-activating kinase-associated protein 1 participates in TLR3/Toll-IL-1 homology domain-containing adapter molecule-1-mediated IFN regulatory factor 3 activation', *J Immunol*, 174: 27-30.

Sasai, M., M. Shingai, K. Funami, M. Yoneyama, T. Fujita, M. Matsumoto, and T. Seya. 2006. 'NAK-associated protein 1 participates in both the TLR3 and the cytoplasmic pathways in type I IFN induction', *J Immunol*, 177: 8676-83.

Savitski, M. M., M. Wilhelm, H. Hahne, B. Kuster, and M. Bantscheff. 2015. 'A Scalable Approach for Protein False Discovery Rate Estimation in Large Proteomic Data Sets', *Mol Cell Proteomics*, 14: 2394-404.

Schneider, I., and J. Ellenberg. 2019. 'Mysteries in embryonic development: How can errors arise so frequently at the beginning of mammalian life?', *PLoS Biol*, 17: e3000173.

Schweppe, D. K., J. K. Eng, Q. Yu, D. Bailey, R. Rad, J. Navarrete-Perea, E. L. Huttlin, B. K. Erickson, J. A. Paulo, and S. P. Gygi. 2020. 'Full-Featured, Real-Time Database Searching Platform Enables Fast and Accurate Multiplexed Quantitative Proteomics', *J Proteome Res*, 19: 2026-34.

Schweppe, D. K., S. Prasad, M. W. Belford, J. Navarrete-Perea, D. J. Bailey, R. Huguet, M. P. Jedrychowski, R. Rad, G. McAlister, S. E. Abbatiello, E. R. Woulters, V. Zabrouskov, J.

J. Dunyach, J. A. Paulo, and S. P. Gygi. 2019. 'Characterization and Optimization of Multiplexed Quantitative Analyses Using High-Field Asymmetric-Waveform Ion Mobility Mass Spectrometry', *Anal Chem*, 91: 4010-16.

Schweppe, D. K., S. F. Rusin, S. P. Gygi, and J. A. Paulo. 2020. 'Optimized Workflow for Multiplexed Phosphorylation Analysis of TMT-Labeled Peptides Using High-Field Asymmetric Waveform Ion Mobility Spectrometry', *J Proteome Res*, 19: 554-60.

Seki, A., J. A. Coppinger, C. Y. Jang, J. R. Yates, and G. Fang. 2008. 'Bora and the kinase Aurora a cooperatively activate the kinase Plk1 and control mitotic entry', *Science*, 320: 1655-8.

Shapiro, R. S., and K. V. Anderson. 2006. 'Drosophila Ik2, a member of the I kappa B kinase family, is required for mRNA localization during oogenesis', *Development*, 133: 1467-75.

Sharma, S., B. R. tenOever, N. Grandvaux, G. P. Zhou, R. Lin, and J. Hiscott. 2003. 'Triggering the interferon antiviral response through an IKK-related pathway', *Science*, 300: 1148-51.

Shu, C., B. Sankaran, C. T. Chaton, A. B. Herr, A. Mishra, J. Peng, and P. Li. 2013. 'Structural insights into the functions of TBK1 in innate antimicrobial immunity', *Structure*, 21: 1137-48.

Singh, V., M. Ram, R. Kumar, R. Prasad, B. K. Roy, and K. K. Singh. 2017. 'Phosphorylation: Implications in Cancer', *Protein J*, 36: 1-6.

Steigemann, P., C. Wurzenberger, M. H. Schmitz, M. Held, J. Guizetti, S. Maar, and D. W. Gerlich. 2009. 'Aurora B-mediated abscission checkpoint protects against tetraploidization', *Cell*, 136: 473-84.

Sternsdorf, T., K. Jensen, D. Zuchner, and H. Will. 1997. 'Cellular localization, expression, and structure of the nuclear dot protein 52', *J Cell Biol*, 138: 435-48.

Stolz, A., A. Ernst, and I. Dikic. 2014. 'Cargo recognition and trafficking in selective autophagy', *Nat Cell Biol*, 16: 495-501.

Strnad, P., K. Zatloukal, C. Stumptner, H. Kulaksiz, and H. Denk. 2008. 'Mallory-Denk-bodies: lessons from keratin-containing hepatic inclusion bodies', *Biochim Biophys Acta*, 1782: 764-74.

Tanaka, Y., and Z. J. Chen. 2012. 'STING specifies IRF3 phosphorylation by TBK1 in the cytosolic DNA signaling pathway', *Sci Signal*, 5: ra20.

Taylor, J. H. 1960. 'Nucleic acid synthesis in relation to the cell division cycle', *Ann N Y Acad Sci*, 90: 409-21.

Thurston, T. L., K. B. Boyle, M. Allen, B. J. Ravenhill, M. Karpiyevich, S. Bloor, A. Kaul, J. Noad, A. Foeglein, S. A. Matthews, D. Komander, M. Bycroft, and F. Randow. 2016. 'Recruitment of TBK1 to cytosol-invading Salmonella induces WIPI2-dependent antibacterial autophagy', *EMBO J*, 35: 1779-92.

Thurston, T. L., G. Ryzhakov, S. Bloor, N. von Muhlinen, and F. Randow. 2009. 'The TBK1 adaptor and autophagy receptor NDP52 restricts the proliferation of ubiquitin-coated bacteria', *Nat Immunol*, 10: 1215-21.

Tojima, Y., A. Fujimoto, M. Delhase, Y. Chen, S. Hatakeyama, K. Nakayama, Y. Kaneko, Y. Nimura, N. Motoyama, K. Ikeda, M. Karin, and M. Nakanishi. 2000. 'NAK is an IkappaB kinase-activating kinase', *Nature*, 404: 778-82.

Tumbarello, D. A., P. T. Manna, M. Allen, M. Bycroft, S. D. Arden, J. Kendrick-Jones, and F. Buss. 2015. 'The Autophagy Receptor TAX1BP1 and the Molecular Motor Myosin VI Are Required for Clearance of Salmonella Typhimurium by Autophagy', *PLoS Pathog*, 11: e1005174.

Tyanova, S., T. Temu, P. Sinitcyn, A. Carlson, M. Y. Hein, T. Geiger, M. Mann, and J. Cox. 2016. 'The Perseus computational platform for comprehensive analysis of (prote)omics data', *Nat Methods*, 13: 731-40.

Uhlen, M., C. Zhang, S. Lee, E. Sjostedt, L. Fagerberg, G. Bidkhori, R. Benfeitas, M. Arif, Z. Liu, F. Edfors, K. Sanli, K. von Feilitzen, P. Oksvold, E. Lundberg, S. Hober, P. Nilsson, J. Mattsson, J. M. Schwenk, H. Brunnstrom, B. Glimelius, T. Sjoblom, P. H. Edqvist, D. Djureinovic, P. Micke, C. Lindskog, A. Mardinoglu, and F. Ponten. 2017. 'A pathology atlas of the human cancer transcriptome', *Science*, 357.

Vargas, J. N. S., C. Wang, E. Bunker, L. Hao, D. Maric, G. Schiavo, F. Randow, and R. J. Youle. 2019. 'Spatiotemporal Control of ULK1 Activation by NDP52 and TBK1 during Selective Autophagy', *Mol Cell*, 74: 347-62 e6.

Verstrepen, L., K. Verhelst, I. Carpentier, and R. Beyaert. 2011. 'TAX1BP1, a ubiquitin-binding adaptor protein in innate immunity and beyond', *Trends Biochem Sci*, 36: 347-54.

Wang, Y., F. Yang, M. A. Gritsenko, Y. Wang, T. Clauss, T. Liu, Y. Shen, M. E. Monroe, D. Lopez-Ferrer, T. Reno, R. J. Moore, R. L. Klemke, D. G. Camp, 2nd, and R. D. Smith. 2011. 'Reversed-phase chromatography with multiple fraction concatenation strategy for proteome profiling of human MCF10A cells', *Proteomics*, 11: 2019-26.

Wei, C., Y. Cao, X. Yang, Z. Zheng, K. Guan, Q. Wang, Y. Tai, Y. Zhang, S. Ma, Y. Cao, X. Ge, C. Xu, J. Li, H. Yan, Y. Ling, T. Song, L. Zhu, B. Zhang, Q. Xu, C. Hu, X. W. Bian, X. He, and H. Zhong. 2014. 'Elevated expression of TANK-binding kinase 1 enhances tamoxifen resistance in breast cancer', *Proc Natl Acad Sci U S A*, 111: E601-10.

Weidberg, H., and Z. Elazar. 2011. 'TBK1 mediates crosstalk between the innate immune response and autophagy', *Sci Signal*, 4: pe39.

Wild, P., H. Farhan, D. G. McEwan, S. Wagner, V. V. Rogov, N. R. Brady, B. Richter, J. Korac, O. Waidmann, C. Choudhary, V. Dotsch, D. Bumann, and I. Dikic. 2011. 'Phosphorylation of the autophagy receptor optineurin restricts Salmonella growth', *Science*, 333: 228-33.

Wong, Y. C., and E. L. Holzbaur. 2014. 'Optineurin is an autophagy receptor for damaged mitochondria in parkin-mediated mitophagy that is disrupted by an ALS-linked mutation', *Proc Natl Acad Sci U S A*, 111: E4439-48.

Wu, T., E. Hu, S. Xu, M. Chen, P. Guo, Z. Dai, T. Feng, L. Zhou, W. Tang, L. Zhan, X. Fu, S. Liu, X. Bo, and G. Yu. 2021. 'clusterProfiler 4.0: A universal enrichment tool for interpreting omics data', *Innovation (N Y)*, 2: 100141.

Yamamoto, H., S. Kakuta, T. M. Watanabe, A. Kitamura, T. Sekito, C. Kondo-Kakuta, R. Ichikawa, M. Kinjo, and Y. Ohsumi. 2012. 'Atg9 vesicles are an important membrane source during early steps of autophagosome formation', *J Cell Biol*, 198: 219-33.

Yamamoto, T., M. Ebisuya, F. Ashida, K. Okamoto, S. Yonehara, and E. Nishida. 2006. 'Continuous ERK activation downregulates antiproliferative genes throughout G1 phase to allow cell-cycle progression', *Curr Biol*, 16: 1171-82.

Yamano, K., C. Wang, S. A. Sarraf, C. Munch, R. Kikuchi, N. N. Noda, Y. Hizukuri, M. T. Kanemaki, W. Harper, K. Tanaka, N. Matsuda, and R. J. Youle. 2018. 'Endosomal Rab cycles regulate Parkin-mediated mitophagy', *Elife*, 7.

Yim, W. W., H. Yamamoto, and N. Mizushima. 2022. 'A pulse-chasable reporter processing assay for mammalian autophagic flux with HaloTag', *Elife*, 11.

Young, A. R., E. Y. Chan, X. W. Hu, R. Kochl, S. G. Crawshaw, S. High, D. W. Hailey, J. Lippincott-Schwartz, and S. A. Tooze. 2006. 'Starvation and ULK1-dependent cycling of mammalian Atg9 between the TGN and endosomes', *J Cell Sci*, 119: 3888-900.

Zatloukal, K., C. Stumptner, A. Fuchsbichler, H. Heid, M. Schnoelzer, L. Kenner, R. Kleinert, M. Prinz, A. Aguzzi, and H. Denk. 2002. 'p62 Is a common component of cytoplasmic inclusions in protein aggregation diseases', *Am J Pathol*, 160: 255-63.

Zeng, P. H., and W. J. Yin. 2023. 'The cGAS/STING signaling pathway: a cross-talk of infection, senescence and tumors', *Cell Cycle*, 22: 38-56.

Zhang, C., G. Shang, X. Gui, X. Zhang, X. C. Bai, and Z. J. Chen. 2019. 'Structural basis of STING binding with and phosphorylation by TBK1', *Nature*, 567: 394-98.

Zhang, Y., X. Wang, H. Yang, H. Liu, Y. Lu, L. Han, and G. Liu. 2013. 'Kinase AKT controls innate immune cell development and function', *Immunology*, 140: 143-52.

Zhong, L., M. M. Hu, L. J. Bian, Y. Liu, Q. Chen, and H. B. Shu. 2020. 'Phosphorylation of cGAS by CDK1 impairs self-DNA sensing in mitosis', *Cell Discov*, 6: 26.

Zhu, L., Y. Li, X. Xie, X. Zhou, M. Gu, Z. Jie, C. J. Ko, T. Gao, B. E. Hernandez, X. Cheng, and S. C. Sun. 2019. 'TBKBP1 and TBK1 form a growth factor signalling axis mediating immunosuppression and tumourigenesis', *Nat Cell Biol*, 21: 1604-14.

Zhu, L., X. Xie, L. Zhang, H. Wang, Z. Jie, X. Zhou, J. Shi, S. Zhao, B. Zhang, X. Cheng, and S. C. Sun. 2018. 'TBK-binding protein 1 regulates IL-15-induced autophagy and NKT cell survival', *Nat Commun*, 9: 2812.